OPTICAL AND OPTO–ELECTRONIC INVESTIGATIONS OF SEMICONDUCTOR DEFECTS AND HETEROSTRUCTURES

Thesis by

Tuviah Ehud Schlesinger

in Partial Fulfillment of the Requirements

for the Degree of

Doctor of Philosophy

California Institute of Technology

Pasadena, California

1986

(Submitted June 12, 1985)

To My Parents

ACKNOWLEDGEMENTS

I would like to thank Professor T. C. McGill for the opportunity to have been a member of his unique research group at Caltech. I have learned a great deal from him and he has provided me with guidance, excellent laboratory facilities, and many research ideas. I would like to thank him for reading my papers as well as this thesis. I have profited also from the insight and physical intuition of Dr. D. L. Smith. I would also like to thank Vere Snell, she is as excellent a secretary as one could ever hope to meet.

I am grateful to Drs. R. S. Bauer and R. D. Burnham of Xerox Palo Alto Research Center for providing the GaAs/AlAs heterostructures used in this work. I would also like to thank Drs. O. J. Marsh and J. P. Baukus of Hughes Research Laboratories for providing the Si samples used in this work. For financial support I gratefully acknowledge the Natural Sciences and Engineering Research Council of Canada, G T E Corporation, the California Institute of Technology, and the Office of Naval Research.

I would like to acknowledge Drs. G. S. Mitchard and A. T. Hunter for getting me started in the lab. I would also like to thank Drs. R. M. Feenstra, R. T. Collins, and C. Mailhiot for all the discussions we have had in the course of my work. I have profited also from my many discussions with Dr. A. Zur and Bob Hauenstein both in the lab and over dinner. I have also benefited from discussions with A. R. Bonnefoi, M. B. Johnson, R. H. Miles, T. K. Woodward and particularly S. R. Hetzler.

Finally my deepest gratitude goes to my parents and sister for their constant support and encouragement.

ABSTRACT

This thesis basically consists of two parts. In the first part is discussed photoluminescence experiments performed on p-type silicon doped with B, In, or Tl. These substitiutional dopants were believed to form complexes with interstitial Fe and thought to be the source of some very intense luminescence in the silicon. Also presented are the results of photoluminescence experiments performed on luminescence features which were thought to be due to an isolated Fe complex observe in n-type Si:P. These spectra generally consisted of one or two sharp no-phonon lines followed by a subsidiary peak approximately 9 - 10 meV below the no-phonon line which was identified as a phonon replica of the no-phonon line. This phonon mode was thought to be a local vibrational mode of the Fe. Isotope shift experiments were performed on these luminescence features by diffusing ^{54}Fe and ^{56}Fe into the silicon samples to see whether a change in the phonon energy or a shift in the no-phonon line could be observed (as predicted by theory) and thus more conclusively identify the center. No isotope shift was observed in the case of any of the Fe related centers studied. Similar experiments which were performed on luminescence features attributed to (Cu,Cu) pairs in silicon (using ^{65}Cu and ^{63}Cu) are also described in the first part of this thesis. An isotope shift of the no-phonon line and a change in the characteristic 7 meV phonon mode, seen in this spectrum, were observed. This confirmed the identification of these luminescence features as being due to the presence of Cu. Also this result confirmed that the lack of a shift in the Fe case was real. Possible explanations for the null result in the Fe case are discussed.

The second part of this thesis consists of optical investigations of GaAs/AlAs heterostructures. In these experiments the transport of electrons past a thin (50 Å to 200 Å) AlAs barrier sandwiched between thick GaAs cladding layers was studied by measuring the voltage developed across these structures as a function of the wavelength of light illuminating the sample. Calculations to

model the optical absorption in these structures were also carried out. Based on the data and the calculations the following explanation for the observed photovoltages was proposed. Electrons, in the degenerately doped GaAs, are optically excited by free carrier absorption to energies greater than that presented by the AlAs barrier and flow from the illuminated side of the AlAs barrier to the back side of the barrier. The driving force for this flow would be the difference in the concentration of optically excited electrons on either side of the barrier. This difference results from the light intensity difference on either side of the barrier as modeled by the calculations. These experiments were conducted for samples with different AlAs layer thicknesses, GaAs layer thicknesses and dopings, and at various temperatures. Further work involved applying a constant dc bias to the structure while measuring the photovoltage spectrum. This, it was found, increased the photovoltage signal (by several orders of magnitude in some cases) and caused some shifts in the spectrum to slightly longer wavelengths. These effects were explained in terms of charge redistribution in the sample, that is, accumulation and depletion on either side of the barrier and the effective band gap narrowing in the GaAs due to the large electric fields that these dc biases can create in the depleted areas of the GaAs.

Parts of this thesis have been or will be published under the following titles:

Chapter 2:

Role of Fe in New Luminescence Lines in Si:Tl and Si:In,

T. E. Schlesinger and T. C. McGill, *Phys. Rev.*, **B25**, 7850(1982).

Isotope Shifts For the P, Q, R Lines in Indium-Doped Silicon,

T. E. Schlesinger, R. J. Hauenstein, R. M. Feenstra, and
T. C. McGill, *Solid State Commun.*, **46**, 321(1983).

Isotope-Shift Experiments on Luminescence Attributed to (Fe,B) Pairs in Si,

T. E. Schlesinger and T. C. McGill, *Phys. Rev.*, **B28**, 3643(1983).

Isotope-Shifts of the P, Q, R Lines in Indium-Doped Silicon,

T. E. Schlesinger and T. C. McGill
Proceedings of the Symposium on Defects in Silicon,
Published by the Electrochemical Society, **83-9**, 512(1983).

Chapter 3:

Photovoltaic Investigation of GaAs/AlAs Heterostructures,

T. E. Schlesinger, R. T. Collins, T. C. McGill, and R. D. Burnham,
Appl. Phys. Lett., **45**, 686(1984).

Photovoltaic Investigation of GaAs/AlAs Heterostructures,

T. E. Schlesinger, R. T. Collins, T. C. McGill, and R. D. Burnham,
to appear in *Superlattices and Microstructures.*

Optical Investigations of Electron Transport Through GaAs/AlAs Heterostructures,

T. E. Schlesinger, R. T. Collins, T. C. McGill, and R. D. Burnham, to appear in *Journal of Applied Physics.*

Photoresponse of GaAs/AlAs Heterostructures Under External Bias,

T. E. Schlesinger, A. Zur, T. C. McGill, and R. D. Burnham, to appear in *Journal of Vacuum Science and Technology.*

CONTENTS

CHAPTER 1

Photoluminescence Studies of Defects in Silicon and Photovoltaic Investigations of GaAs/AlAs Heterostructures

1.1 INTRODUCTION

This thesis discusses the results of experiments which were used to study defects in semiconductors and the optical properties of semiconducting structures. The defects studied were those centers in silicon believed to involve Fe and Cu. The semiconducting structures investigated were heterostructures consisting of a thin layer (50 Å − 250 Å) of AlAs sandwiched between cladding layers of GaAs. In both cases optical techniques were used to probe these materials. The Fe and Cu related centers were probed using photoluminescence while the GaAs/AlAs heterostrucutures were studied using photoresponse techniques. In either case an optical excitation was used to probe the semiconductor.

When any semiconductor is illuminated a number of optical absorption processes may take place. Three of these, which are most important to the work discussed in this thesis are shown in Figure 1.1. Presented in this figure is (a) direct interband absorption, (b) indirect interband absorption, and (c) free carrier absorption. By free carrier is meant a carrier which is free to move in a band and this will be discussed in more detail later. Both indirect transitions and free carrier absorption require that the electron make a transition to a higher energy state with a different $\vec{k}$. Thus, to conserve momentum an additional interaction is required. This interaction can take the form of a phonon. The optical absorption process then becomes a three-body interaction and is generally weaker than the direct interband transition which does not involve a phonon. Interband transitions create electron hole pairs while free carrier absorption does not. The absorption coefficient, α, is defined as the relative rate of decrease in light intensity, I, along its propagation path[1]

$$\alpha = \frac{1}{I}\frac{dI}{dx}.$$

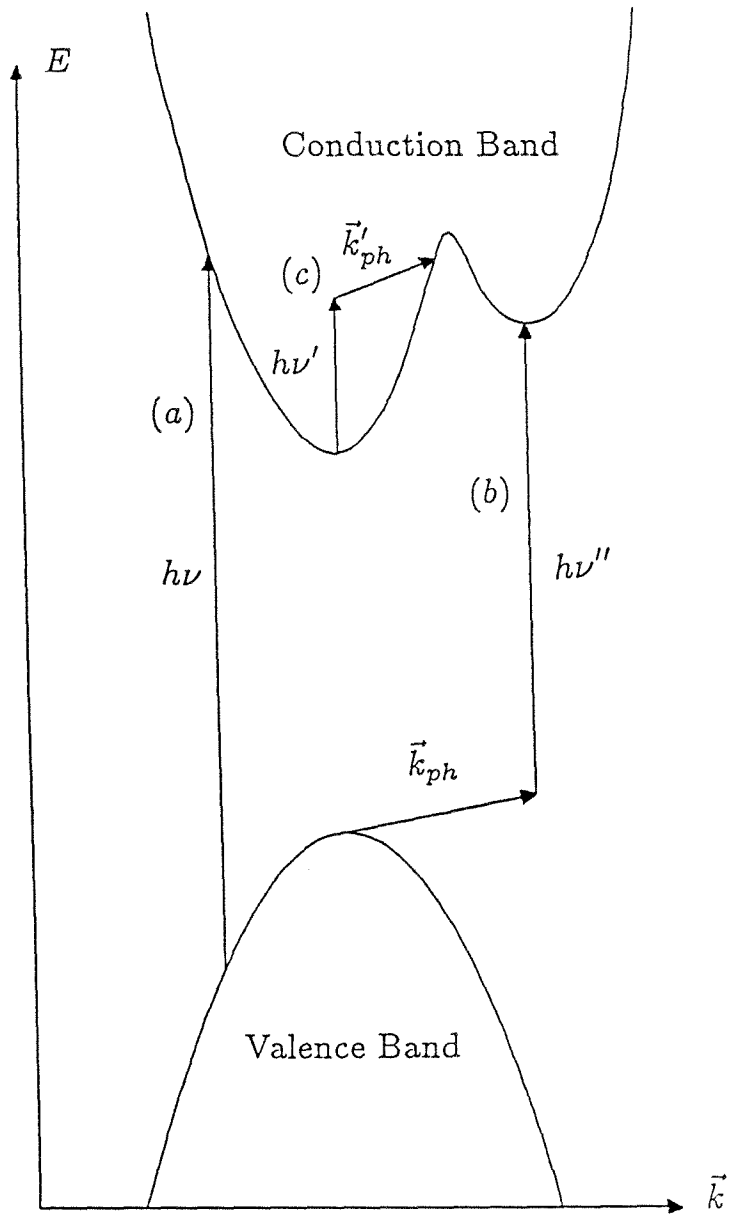

Figure 1.1: Optical absorption processes in a semiconductor. (a) direct interband, (b) indirect interband, (c) free carrier absorption. Processes (b) and (c) are generally weaker as they involve a phonon to conserve momentum.

1.2 Fe AND Cu DEEP LEVELS

Shallow level impurities are those which are used generally to alter the conductivity of a semiconductor in a controlled manner in order to produce working devices. In fact, it is the ability to control their conductivity over many orders of magnitude by the introduction of small amounts of impurities[2] which makes semiconductors of such overwhelming technological importance. There are impurities that bind their valence electrons more strongly than shallow level impurities. These are called deep level impurities and are not as well understood as shallow level impurities since they cannot be treated in a simple hydrogenic model. Since these impurities bind their valence electrons more tightly they also cause the electrons to be more localized around the impurity atom. Thus, the electron is no longer subjected to the average bulk properties of the crystal and one is forced to consider the local properties of the impurity in order to understand these defects.[3]

The transition metals form deep levels in silicon. The transition metals are those elements in the periodic table in which d-orbitals are being filled with electrons. The choice was made to study centers related to the particular transition metals Fe and Cu for a number of reasons. Since both Fe and Cu diffuse into silicon as interstitial impurities they are fast diffusers and thus are often found to contaminate silicon. Fe in particular is a contaminant which is easily introduced into silicon unintentionally during high-temperature processing. This contamination can result from a wafer being brought into contact with metal implements containing Fe.[4] Since both Fe and Cu form deep levels in silicon they provide states through which electrons and holes may recombine and thus decrease carrier lifetimes. This decrease in the carrier lifetimes may be a desirable or undesirable effect depending on the particular device one is attempting to produce. It would be desirable, for example, if the device were a fast switch in which one wanted to create carriers (ON) and have them recom-

bine as quickly as possible (OFF). It would be undesirable if the device were a photovoltaic cell where carrier recombination decreases the efficiency of the device. Therefore, the understanding of these transition metal impurities is of technological importance.

1.3 PHOTOLUMINESCENCE

It is the recombination of the electron-hole pairs created by the optical excitation which produces the luminescence that is studied in photoluminescence spectroscopy. However, before the electron and hole recombine a number of processes can take place. Firstly, the electron and hole will each relax to the band edges by the emission of phonons. Since they are oppositely charged they may then bind to each other, thus forming a free exciton, or they may bind to an impurity center, thus forming an impurity-bound exciton. The energy of the photon emitted when they recombine will depend on the intial states of the electron and hole. When the electron and hole recombine part of the energy of the recombination may go into a phonon. This phonon could be a momentum-conserving phonon if the electron and hole have different $\vec{k}$, analogously to the case of absorption discussed above, or this phonon could be a local vibrational mode of the impurity to which the electron and hole are bound. The local vibrational mode is not a momentum conserving phonon.

There were luminescence features observed in silicon which were thought to be due to defects involving Fe and Cu.[5] The defect centers studied were those thought to consist of (Fe,B), (Fe,In), and (Fe, Tl) pairs, an isolated Fe complex, and (Cu,Cu) pairs. Evidence as to the identification of these luminescence features is presented and discussed. Some of the luminescence features identified as being related to Fe were some of the most intense luminescences seen in silicon. Intense luminescence of this sort can be used to monitor minute quantities of

transition metals in the silicon. The decay lifetime of the electrons and holes recombining on these centers were more than 200μsec, all of which generated a great deal of interest in them.[6] Thus, it was possible to apply photoluminescence spectroscopy to the problem of transition metal impurities in silicon. It is not always possible to apply this technique to the study of semiconductor defects since not all defects provide radiative recombination centers for electron and holes.

These luminescence spectra generally consisted of one or two sharp no-phonon lines followed by peaks at lower energies which were identified as phonon-replicas of the no-phonon lines. These phonon replicas were thought to be local vibrational modes of the Fe and Cu and whose energy was about 9 - 10 meV in the Fe related spectra and 7 meV in the Cu case. The experiments consisted of intentionally diffusing, into the silicon, different isotopes of Fe or Cu and looking for changes in the phonon energies or shifts in the position of the no-phonon lines as a result of the change in mass of the impurity. The experiments, described in detail in Chapter 2 of this thesis, were aimed at determining conclusively that these luminescence features were indeed related to Fe and Cu. These experiments also had as their objective the identification of particular lines in the photoluminescence spectra as being due to vibrational modes of the Fe or Cu atom. In the case of the Fe-related centers no isotope shift was observed while in the case of the Cu-related center a very clear shift was observed. Possible explanations for these results are offered.

1.4 HETEROSTRUCTURES

1.4.1 Introduction

In the third chapter of this thesis photovoltaic experiments performed on GaAs/AlAs heterostructures are described. The experiment discussed here con-

sisted of illuminating a structure consisting of a thin layer of AlAs (50 Å to 250 Å thick) sandwiched between thicker layers of GaAs (a few microns thick) and measuring the resulting voltage developed across this structure as a function of the wavelength of the incident light. AlAs is an indirect material with the conduction band minimum occurring in the (100) direction at the X-point. There is also a local minimum in the (111) direction at the L-point which is higher than the X-point minimum. The Γ-point, zone center, is above both of these. GaAs is a direct material with the conduction band minimum occurring at the zone center, Γ-point. The band gap of AlAs is about 2.1 eV and that of GaAs is about 1.4 eV. This difference in band gaps leads to conduction and valence band offsets and therefore the AlAs provides an energy barrier for electron flow. Calculations are also presented which were used to model the optical absorption properties of such a structure. The results of the experiments are interpreted in terms of electron transport across this sort of single barrier structure. It is argued that electrons are optically excited within the conduction band of the GaAs by free carrier absorption since the GaAs was degenerately doped. These electrons then flow across the barrier presented by the offsets in the conduction bands of the GaAs and the AlAs. It is further argued on the basis of the model calculations that the driving force for the flow of the electrons is the difference in the concentration of optically excited electrons on either side of the barrier which results from the light intensity difference on either side of the barrier. Results of these experiments for various samples, at various temperatures, and with and without an applied external dc bias are presented. These results are discussed in terms of the optical and electrical properties of such a structure. A short discussion of the possible application of these structures as photosensitive devices is also presented in Chapter 3. In the Appendix at the end of this thesis are discussed a technical problem and its solution which was encountered while making the photoresponse measurement.

There is a great deal of current interest in heterostructures for a number of

reasons. As long as semiconductor physics and device technology were limited to bulk semiconductor materials, both the properties studied and the devices created were limited to the properties that naturally occurring semiconductors displayed. With the development of new growth techniques such as metalorganic chemical vapor deposition and molecular beam epitaxy, it became possible to grow reproducibly thin layers (as thin as 20 Å) of different semiconductors on top of each other.[7] These heterostructures afford the opportunity of studying fundamental quantum mechanical phenomena. Also it will be possible to exploit these effects to produce novel devices with the small dimensions promising very high speeds. As technology moves to these very small dimensions, two things happen. The first is that it becomes not only desirable but necessary to move from doped junctions to heterojunctions. A p-n junction, for example, formed by doping a bulk semiconductor has the property that electrically one has two different materials but chemically one has the same material. This enables one to form almost defect-free junctions. On the other hand, by creating heterostrucutes which may consist of layers of different matertials which have vastly different properties one is able to form structures whose electrical characteristics can change drastically over length scales of tens of angstroms. Alternating layers can be made up of semiconductors which have very different properties such as their band gaps, whether they are direct or indirect, and so on. Heterostructures have already been exploited to produce novel devices and structures in which fundamental physical phenomena have been studied. For example, quantum barrier structures have been used to study inelastic tunneling processes.[8] Quantum wells have been used to study resonant tunneling, an effect which has applications in microwave technology.[9] Quantum wells have also been used to produce laser structures.[10]

There are also problems unique to heterostructures. The physics of transport changes from diffusion and drift to coherent transport (i.e., the electrons are not scattered while moving across typical device dimensions). Coherent trans-

port of electrons is one of the aspects of these heterostructures which makes them of interest as discussed below. Another interesting problem is that of doping very thin layers. Suppose one were to create a heterostructure device which has an "active" region which is 50 Å thick. The device itself could be 1 μm on a side. The volume of such a layer would then be 5×10^{-15} cm^3. If the doping level in this layer were 10^{16} cm^{-3}, then one has only 50 impurity atoms doping this region. The fluctuations from one device to the next would be 7 atoms, simply because of the random distribution of impurities. It may be no longer meaningful to speak in terms of a bulk-doping level in such a region. Moreover, it may be that random fluctuations play an important role in determining the properties of such a device.

1.4.2 Motivation

The photoresponse experiments described in this thesis were carried out to advance the understanding of the optical and electrical properties of GaAs/AlAs heterostructures. There are a number of specific fundamental questions which could be addressed through experiments of this nature in general. It is hoped that eventually a direct optical determination of the band offsets between the AlAs and GaAs could be made by looking for cutoffs in the photovoltage spectra associated with this barrier. There is a question regarding which valley in the AlAs determines the energy barrier presented to an electron incident from the GaAs Γ valley. Calculations by C. Mailhiot et al.[11] have shown that for a barrier structure of this sort an electron incident from the GaAs couples most strongly through states in the AlAs of the same symmetry as the incident electron. For example, a Γ-point electron incident from the GaAs in the (111) direction onto the AlAs will be presented with an energy barrier determined by the Γ-point of the AlAs rather than the lower L-point valley. This is an important point which needs to be verified in the understanding of coherent transport of electrons. It

also has a possible technological application in terms of producing what may be referred to as an electron filter. One could use a structure such as this in order to allow only Γ-point electrons to propagate past such a barrier. This would be very useful since the Γ-point electrons are faster than the heavier L-point electrons. In principle, one could construct an electron filter as follows. Suppose one were to grow a single barrier structure where the barrier was $Ga_xAl_{1-x}As$ of a composition where the Γ-point was still lower in energy than the L-point. Then for a mixture of Γ and L electrons of an energy between these two values the Γ electrons would propagate past the barrier. The L electrons could only get past the barrier by tunnelling. Thus, one would mainly pass Γ electrons as desired.

There is yet another interesting effect related to the coherent transport of electrons past an energy barrier and that is electron interference effects. When an electron is incident on an energy barrier, then for energies greater than the barrier height the transmission coefficient for the electron through the barrier oscillates between one, and values less than one as a function of energy. These oscillations are predicted in the work of C. Mailhiot et al. and are of the same sort as those discussed in elementary quantum mechanics texts. It may be possible to observe these transmission coefficient oscillations as oscillations in the photovoltage spectra measured in experiments of the sort described in this thesis.

1.5 FREE CARRIERS

As mentioned above it is electrons present in the conduction band of the GaAs (free carriers) which are optically excited and flow across the AlAs barrier to produce the observed photovoltage. These electrons are present in the GaAs conduction band since it is degenerately doped n-type. One can understand degenerate doping in the following simple model. Consider the case of an n-

type impurity atom whose extra valence electron is in an orbital such that this electron sees only a screened positive charge due to the nucleus of plus one. This electron acts like that of a hydrogen atom but moves in a medium whose dielectric constant is that of the host crystal. The binding energy of this electron would then be, in this hydrogenic model[1]

$$E = \frac{m^*}{m\epsilon^2} 13.6 \quad \text{eV}$$

where m is the electron mass, m^* is the effective mass of the electron in the host crystal, ϵ is the dielectric constant of the host crystal, and 13.6 eV is the ionization energy of hydrogen. The orbital radius of this electron would be

$$a = \frac{\epsilon m}{m^*} a_0$$

where a_0 is the first Bohr orbit of hydrogen. In GaAs, for example, with $m^* = 0.067m$ and $\epsilon = 13.2$, this ionization energy would be 5 meV and $a \sim 100$ Å. This impurity level is thus very close to the conduction band minimum and so this dopant is referred to as a shallow level impurity. The thermal energy of a phonon at 300 K is $kT \sim 25$ meV and is thus sufficient to ionize this sort of impurity level. The orbit of such an electron extends over many lattice sites and at a concentration of a^{-3} the orbits begin to overlap. In practice, the wave function overlap occurs at lower doping levels. The overlap introduces an interaction between these electrons which causes the impurity level to be perturbed and at sufficiently high doping levels causes the formation of a band of impurity states. As the impurity concentration is increased the impurity band broadens and eventually merges with the nearest intrinsic band. For GaAs one would expect a doping level of about 10^{18} cm^{-3} to produce an impurity band. In the samples discussed in Chapter 3 the GaAs doping level was always above 5×10^{17} cm^{-3} which is, in practice, a sufficiently high doping level to place the Fermi level in the conduction band.

1.6 INTERFACE CONSIDERATIONS

1.6.1 Band Bending

In the photoresponse experiments described in Chapter 3 the AlAs layer provides an energy barrier to the flow of electrons across the structure. This energy barrier arises from the band offsets between the GaAs and the AlAs. Band offsets are the difference in the position of the valence bands and conduction bands of two different semiconductors grown one on the other. It is argued that it is the difference in the concentration of optically excited electrons on either side of the AlAs barrier which drives the flow of electrons across this barrier. In principle, band bending could also cause the flow of charge carriers. To understand what band offsets are, one must understand the difference (if any) between band offsets and band bending. Suppose one has a semiconductor in which the doping changes from p-type to n-type across some spatial region as shown in Figure 1.2. In each of these two regions the fermi level will be at a different position in the gap. This difference in the chemical potential exists due to the difference in concentration of electrons in each of the two regions. Now in Figure 1.2 (b) the two regions are brought into contact. Electrons tend to diffuse from the n-type region to the p-type region. As electrons move across the interface they leave behind, in the n-type region, ionized donors which are positive charges and produce, in the p-type region, ionized acceptors which are negative charges. Between these positive and negative charges there is set up an electric field and associated with this electric field is a potential gradient. In Figure 1.2 (c) equilibrium is achieved. The fermi levels in the two regions are aligned when the potential energy lost by an electron moving from the n to p region due to the difference in chemical potentials (not including electrostatic interactions) is equal to the potential energy gained by the electron in moving against the electrostatic potential due to the electric field. This electrostatic

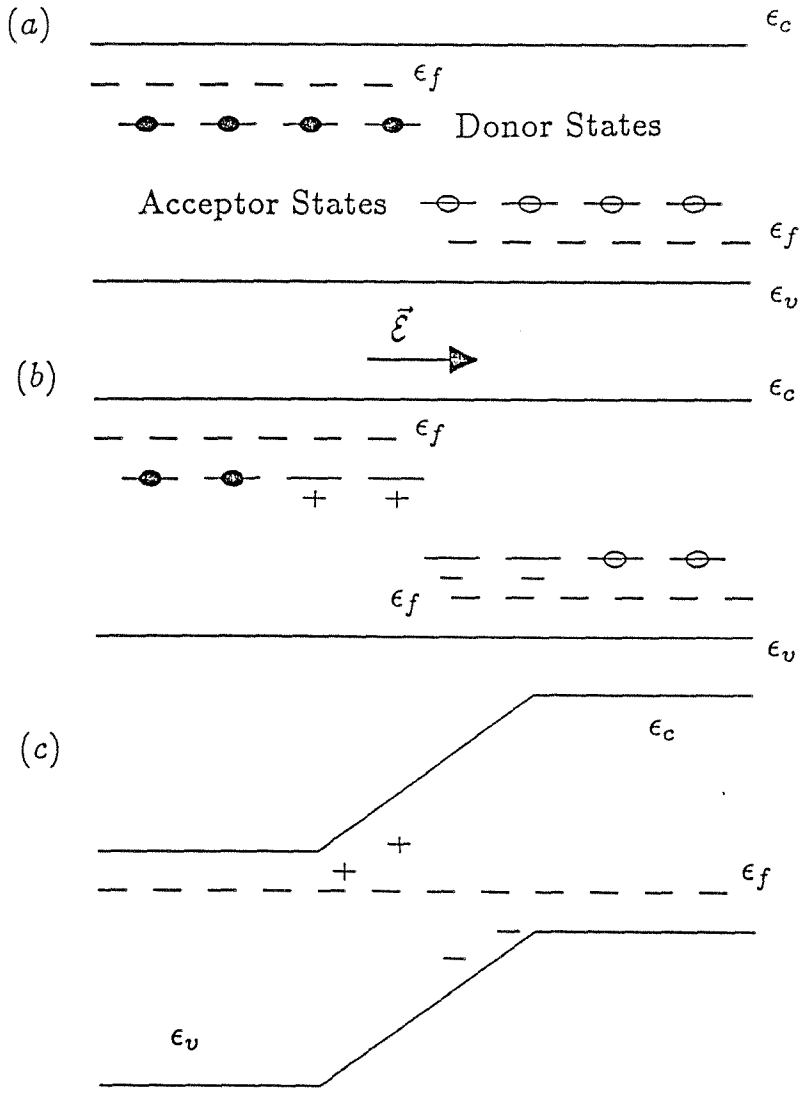

Figure 1.2: Schematic representation of the mechanism that produces the gradient in the electrostatic potential energy which aligns the fermi level across the interface of a p-n junction. (a) The two materials are not in contact. (b) The two materials are brought together and electrons flow across the interface. (c) Equilibrium is acheived.

potential difference that exists across the interface bends the bands across the interface. To calculate the exact shape of the band bending one would solve the Poisson equation. This requires knowledge of the charge distribution for which some approximation is usually made. This sort of band bending occurs over length scales on the order of a few hundred angstroms on either side of the interface. Of course, the amount of band bending will depend on the initial difference in the positions of the fermi levels, which is itself determined by the doping in the two semiconductors.

1.6.2 Band Offsets

Suppose that one were to grow a semiconductor, A, on another semiconductor, B, as shown in Figure 1.3 (a). These two semiconductors may have very different band gaps. Also initially their fermi levels may not be aligned. The difference in the positions of the fermi level is not just a result of the difference in the doping levels that may exist between the two semiconductors. There is always an arbitrary zero of energy assigned to the band structure of any semiconductor. In the case of a single semiconductor the top of the valence band is often taken to be the zero of energy. When two different semiconductors are brought together it becomes somewhat ambiguous to choose a consistent zero of energy. For example, one might think that the vacuum level (the energy required to remove an electron from the semiconductor and take it to infinity) is a good choice for a zero of energy. The vacuum level is, however, an ill-defined term. The energy required to remove an electron from any semiconductor through one surface may be different than the energy required to remove the same electron through another surface. This difference could result from different surface dipole layers that one may have to pass through and which could be different for different surfaces of the semiconductor.

The lack of knowledge of how the fermi levels will be aligned relative to each

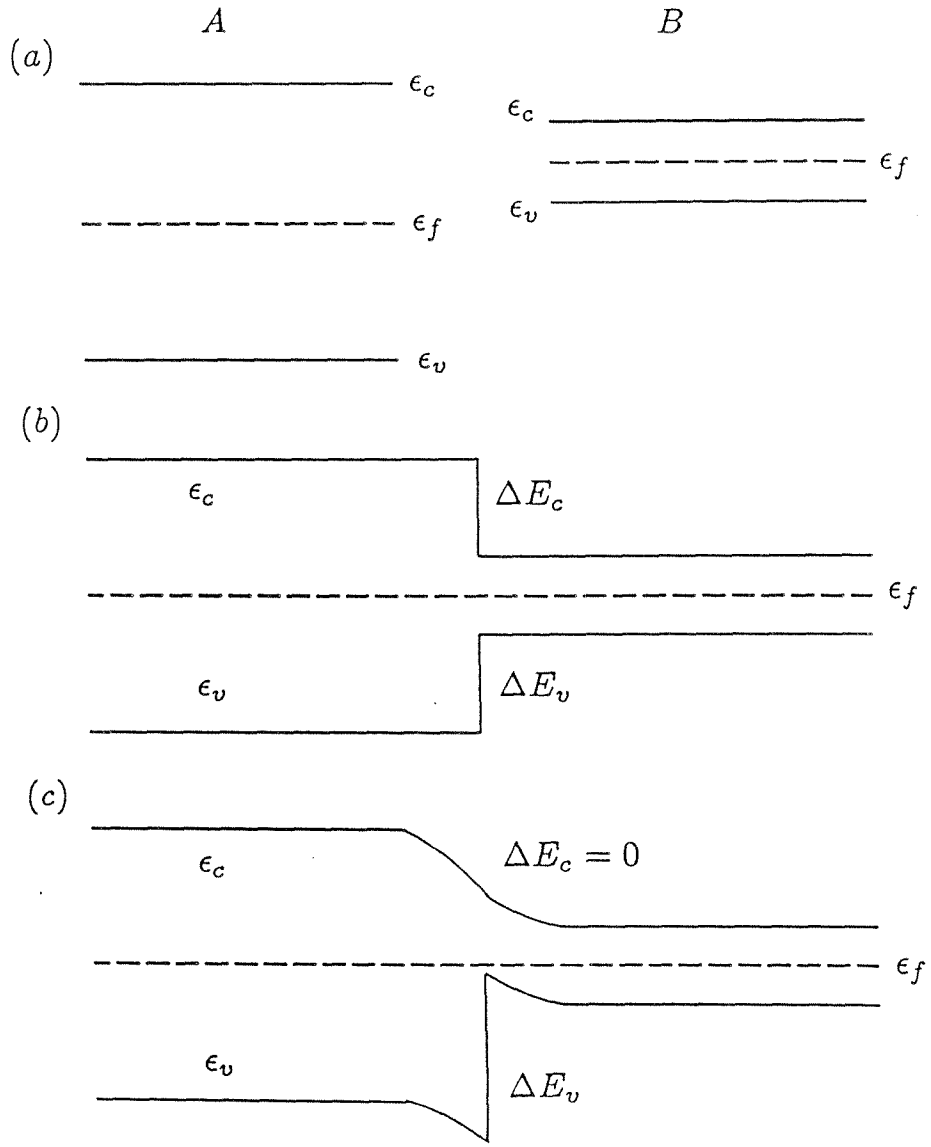

Figure 1.3: In this figure is shown how the offset in the conduction band and valence band of two different semiconductors could depend on the amount of energy difference that is taken up in band bending.

other means that it is very difficult to know *a priori* what will be the conduction band and valence band offsets, that is to say, what fraction of the band gap difference will go into a conduction band offset and what fraction will go into a valence band offset. Any band offset is a jump in potential energy. These jumps in energy occur over distances of about 10 Å and it is this short length scale which distinguishes a band offset from band bending. However, the ambiguity in the zero of energy is not the only reason that it is difficult to know what the band offsets will be. One might believe that the band bending in the two different materials could affect the band offsets.

In practice there are always donor and acceptor states in any semiconducting material. These states could charge and cause band bending as discussed above. Different amounts of band bending could lead to very different conduction and valence band offsets. This is shown in Figures 1.3 (b) and (c). In Figure 1.3 (b) is presented the unlikely situation in which no band bending takes place and thus the conduction band offset is ΔE_c and the valence band offset is ΔE_v. In Figure 1.3 (c) a situation is shown where band bending has created a situation where the valence band offset has been made zero. It is believed, though not proven, that the amount of band offset in the conduction and valence bands is an intrinsic property of any two materials which are brought together.[12] That is, regardless of the doping levels the fraction of the band gap difference that goes into the conduction band offset and the fraction of the energy gap difference that goes into the the valence band offset is always the same. The role of interface states and dipole layers in affecting band offsets is a topic of much current research.[13,14]

REFERENCES

1. J. I. Pankove, *Optical Processes in Semiconductors* (Dover Publications Inc., New York), 1975.

2. S. M. Sze, *Physics of Semiconductor Devices* (John Wiley and Sons, New York), 1981.

3. O. Madelung, *Introduction to Solid-State Theory* (Springer-Verlag, Berlin), 1978.

4. K. Graff and H. Pieper, *J. Electrochem. Soc.* **3**, 669 (1981).

5. R. Sauer and J. Weber, *Physica* **116B**, 195 (1983).

6. G. S. Mitchard, S. A. Lyon, K. R. Elliot, and T. C. McGill , *Solid State Comm.* **29**, 425 (1979).

7. A. C. Gossard, *Treatise on Materials Science and Technology* (Academic Press, New York), 1978.

8. R. T. Collins, J. Lambe, T. C. McGill, and R. D. Burnham, *Appl. Phys. Lett.* **44**, 523 (1984).

9. A. R. Bonnefoi, R. T. Collins, T. C. McGill, R. D. Burnham, and F. A. Ponce, *Appl. Phys. Lett.* **46**, 285 (1985).

10. D. R. Scifres, C. Lindstroem, R. D. Burnham, W. Streifer, and T. L. Paoli, *Electron. Lett.* **19**, 170 (1983).

11. C. Mailhiot, D. L. Smith, and T. C. McGill, *J. Vac. Sci. Technol.* **B1(3)**, 637 (1983).

12. P. Chiardia, A. D. Katnani, H. W. Sang., Jr., and R. S. Bauer , *Phys. Rev. Lett.* **52**, 1233 (1984).

13. A. Zur and T. C. McGill, *J. Vac. Sci. Technol.* **B2(3)**, 440 (1984).

14. A. Zur, T. C. McGill, and D. L. Smith, *Surface Sci.* **13**, 456 (1983).

CHAPTER 2

Isotope Shift Experiments on Transition Metal Impurities in Silicon

2.1 INTRODUCTION

Photoluminescence is the light (luminescence) emitted by a semiconducting material as a result of some optical excitation[1] (i.e., being illuminated by some optical source, usually a laser). By studying the luminescence as a function of wavelength one gains an understanding of the processes taking place in the semiconductor. From this one can then infer the nature of the bulk properties of the semiconductor, or the nature of defects in the semiconductor. Defects may include extended defects, such as grain boundaries, or point defects, such as a vacancy in the lattice. Point defects may also include single impurity atoms replacing a host atom in the lattice (substitutional impurity), or an impurity atom sitting at an interstitial site of the lattice (interstitial impurity), and these point defects may cluster together. There are, of course, many other types of defects. To study any bulk or defect property of a semiconductor using photoluminescence spectroscopy some light emitting process must take place as a result of the band structure of the semiconductor or the presence of the defect. This is not always the case, so while photoluminescence spectroscopy is a useful method to investigate semiconductor properties it is only one of many investigative techniques.

In this chapter is discussed the application of photoluminescence spectroscopy to the study of some deep level defects in silicon. A deep level defect is one which creates an electronic level deep in the energy gap of the semiconductor.[2] In general the distinction between a deep level and a shallow level is not absolute. A shallow level binds an electron (or hole) weakly and so the electron (or hole) is spread out over many lattice sites while a deep level binds an electron (or hole) strongly, thus localizing it near the impurity itself. For this reason deep level defects are not as well understood as shallow level defects. In trying to understand the electronic properties of a shallow level defect, one may view its properties as resulting from the average properties of the semiconductor. In

the case of a deep level one is forced to consider the local electronic nature of the defect perturbed by the semiconductor.

The defects studied in this chapter are those which have been previously identified as being (Fe,B), (Fe,In), (Fe, Tl), and (Cu,Cu) pairs as well as an isolated Fe complex. In the case of the (Fe,In) and (Fe,Tl) pairs experimental results are presented showing the enhancement of the luminescence attributed to these defects upon the introduction of iron to the silicon. Then for the (Fe,B), (Fe,In), (Cu,Cu) pairs and the isolated Fe complex the results of isotope shift experiments are presented. The nature of these experiments is discussed below. Deep level transient spectroscopy (DLTS) was also employed as a diagnostic tool in order to check for the presence of iron-related deep levels in the silicon before and after some of the processing to which the sample was subjected.

2.2 PHONON MODES AND ISOTOPE SHIFTS

2.2.1 Photoluminescence Spectra

As stated above photoluminescence can result from various processes taking place in a semiconductor. In general, if the energy of the photons of the optical excitation source is greater than the band gap of the semiconductor, then electrons and holes are created in the semiconductor which recombine and emit light. This emitted light is the luminescence which is studied. Before the electron and hole recombine they may form other complexes (e.g., excitons) or bind to different impurity centers in the semiconductor (e.g., impurity-bound excitons).[1] When they subsequently recombine, the wavelength of the emitted light will depend on their initial states. Further, this recombination process may involve not only the electron and hole but may also involve the production of a phonon with some of the energy of the recombination going into this phonon. Consider silicon which is indirect. One may have an electron and hole bound to

an impurity center, thus forming a bound exciton. The electron would be near the conduction band minimum and the hole near the valence band maximum in $\vec{k}$-space. In the recombination process a phonon would be emitted to conserve the difference in $\vec{k}$. Impurity states deep in the gap bind the electron and hole more tightly, thus localizing them in real space which in turn delocalizes the electron and hole in $\vec{k}$-space, since the wave function of the electron or hole in real space and $\vec{k}$-space are related through Fourier transforms. This means that the states of the electron and hole involve some $\vec{k}$ which are the same. Thus, there is some probability that the electron and hole recombine without the emission of a phonon and some probability that the electron and hole recombine with the emission of a phonon. A recombination which does not involve a phonon gives rise to a no-phonon line in the spectrum, while a recomination which does involve a phonon gives rise to a phonon replica of the no-phonon line at a slightly lower energy, since the momentum conserving phonon carries off with it some energy.[1] The recombination rate for the transitions involving or not involving the phonon in the final state would be determined by Fermi's Golden Rule.

The phonon produced in the recombination of the electron and hole need not always be a momentum-conserving phonon. Sometimes the recombination process may excite a vibrational mode of the impurity center to which the electron and hole were bound.[2] This vibrational mode is called a local phonon mode since the vibration itself is localized on and around the impurity center (i.e., the amplitude of vibration may decrease exponentially as one moves away from the impurity). This is in contrast to a momentum-conserving phonon which involves a vibrational excitation of the entire crystal lattice. Thus, a typical photoluminescence spectrum may consist of lines which are due to electron-hole recombinations which involve no phonons, the excitation of a momentum conserving phonon, or the excitation of a local phonon.

2.2.2 Isotope Shifts

Suppose one has a luminescence spectrum that consists of a luminescence peak which is due to a no-phonon recombination of an electron and hole bound to an impurity atom and a phonon replica of this no-phonon line which involves the excitation of a local vibration of the impurity atom. The frequency of the vibration of the impurity atom, ω, is related to its mass, m, by

$$\omega \sim \sqrt{\frac{k}{m}},$$

where k is the spring constant connecting the impurity atom to the crystal lattice. If one makes an isotopic substitution of the impurity atom, thus changing the mass of the impurity atom, then frequency of vibration of the local vibration is also changed by

$$\frac{\Delta\omega}{\omega} = -\frac{1}{2}\frac{\Delta m}{m} \tag{1}$$

and this change in frequency would be reflected in the photoluminescence spectrum by a change in the relative spacing of the no-phonon line and the phonon replica due to the change in energy of the local vibrational mode. It has been assumed that the spring constant does not change as a result of the isotopic substitution of the impurity atom. This is a reasonable assumption since the spring constant is a result of the chemical nature of the impurity atom.

In performing an isotopic substitution of an impurity atom this is not the only source of shifts in the luminescence spectrum. The no-phonon line also shifts and the reason for this can be explained as follows.[3] There is a certain zero-point energy of the impurity atom in the crystal lattice. This zero-point energy is given by

$$E_0 = \frac{1}{2}\hbar\omega_0 = \frac{1}{2}\hbar\sqrt{\frac{k}{m}}.$$

When the electron or hole bound to the impurity atom is in an excited state it causes the impurity atom to be less tightly bound to the the crystal lattice,

so it reduces the spring constant k connecting the impurity atom to the crystal lattice to k'. When the electron and hole bound to the impurity atom recombine there is an increase in the zero-point energy of the impurity atom given by

$$\Delta E_0 = \frac{1}{2}\frac{\hbar}{\sqrt{m}}(\sqrt{k} - \sqrt{k'}).$$

Now if one makes an isotopic substitution of the impurity atom, then this increase in the zero-point energy is smaller for the heavier isotope. Since less of the energy of the recombination has to go into increasing this zero-point energy, then the no-phonon line in the luminescence spectrum for the isotope with the heavier mass will occur at higher energies. One would expect that, since $\Delta E_0 \sim \frac{1}{\sqrt{m}}$, this shift in the position of the no-phonon line would be of the same magnitude as the change in the phonon energy.

Both the discussion of the change in phonon energy and the change in the position of the no-phonon line presented here are oversimplified. They assume that only motion of the impurity atom is important and that the crystal lattice remains perfectly rigid. In the case of deep levels where the electrons and holes are bound tightly to the impurity atom and are thus localized on it, this sort of discussion can give reasonable estimates for the magnitude of the shifts one should expect.

2.3 EXPERIMENTAL APPARATUS

The experimental apparatus used to take the photoluminescence data is pictured schematically in Figure 2.1. The optical excitation source used was either a Spectra Physics model 166 argon-ion laser or a Coherent model CR 3000 K krypton-ion laser operated in C W mode. Either of these lasers provided above band gap excitation of the silicon. The samples were mounted in a Janis model 10-DT variable temperature dewar and the luminescence was collected from the edge of the sample and directed onto the entrance slits of a SPEX model 1269

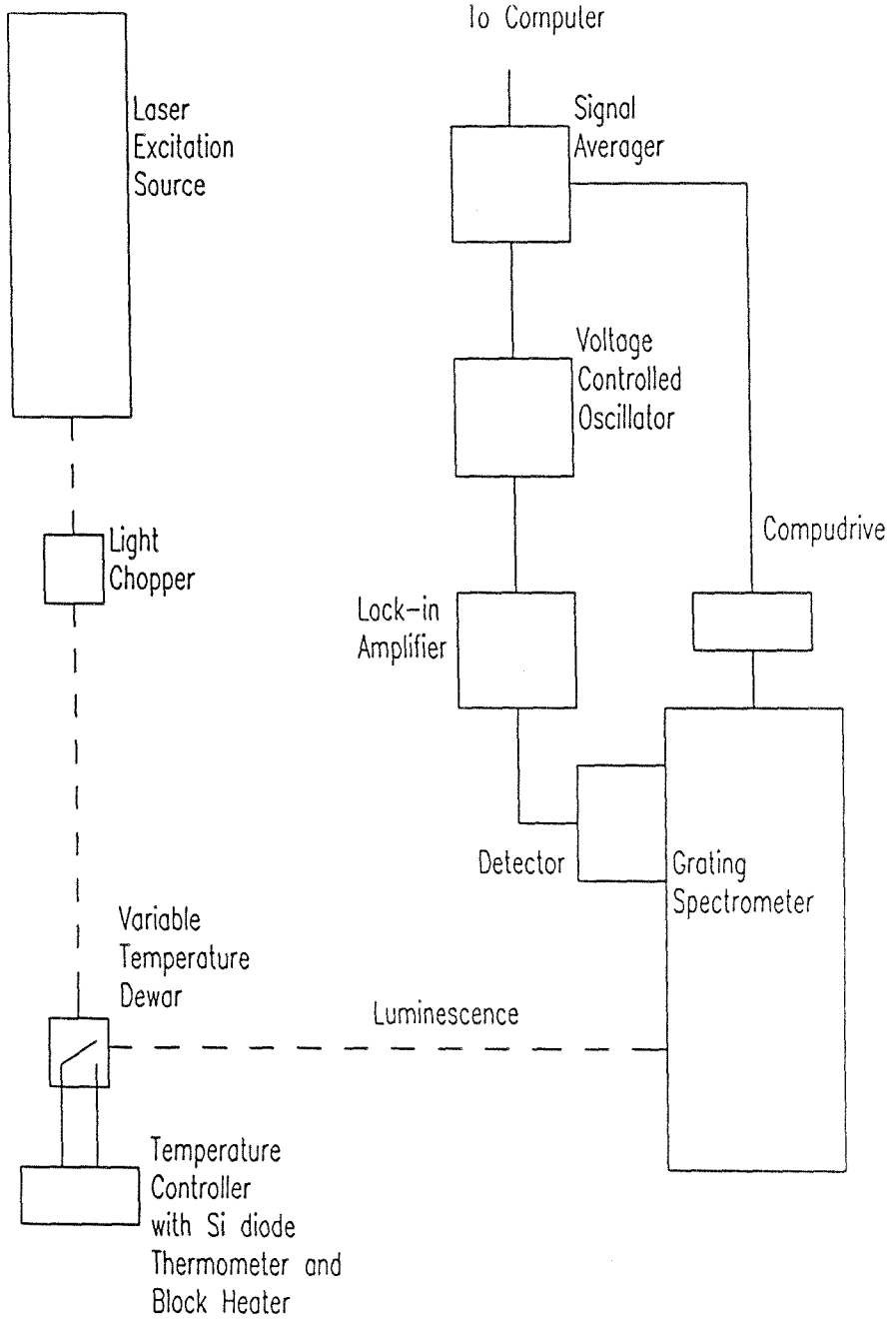

Figure 2.1: Schematic diagram of the experimental apparatus used to conduct the photoluminescence experiments.

or 1404 spectrometer. The model 1269 spectrometer was driven by a SPEX model CD2 compudrive which was interfaced to the Nicolet signal averager so that multiple scans of a spectrum could be taken and thus improve the signal-to-noise ratio. In some cases the detector used to measure the luminescence was an RCA model 7102 photomultiplier with an S-1 response and cooled to liquid nitrogen temperatures. When this photomultiplier was used, the individual pulses from the photomultiplier were shaped and amplified and then counted by a Nuclear Data model 60 A multichannel analyzer or a Nicolet model 1170 signal averager. Two other solid state detectors were employed and these were a North Coast model EO-817 Ge detector or a Barnes Engineering series A-100 InAs detector. When using these solid state detectors the laser excitation source was chopped at about 400 Hz and the signal was then measured with a PAR model 124A lock-in amplifier. This signal was digitized using a voltage-controlled oscillator and then counted as in the case of the photomultiplier. There was a problem unique to the Ge detector and this was the presence of spurious spikes in the luminescence spectra. These were eliminated by using a signal processor, Model 829B (supplied by the vendor) which detected these fast-rising pulses, eliminated them, and then integrating the spectrum over the small region where they occur.

2.4 SAMPLE PREPARATION

The samples used in this study were silicon grown by the Czochralski and float zone methods. In particular, the p-type and n-type silicon used in the various measurements which are described in this chapter are summarized in Table 2.1.

Iron was introduced into the samples as follows. The surface of the silicon was first cleaned using a chemical etch (3:1:0.4 HNO_3: CH_3COOH : HF), followed by a rinse in acetone and methanol. Iron was then evaporated onto

Sample	Growth Technique*	Dopant	Concentration $\times 10^{16}$ cm^{-3}	Vendor
1	CZ	B	0.6**	Monsanto
C112.2	CZ	In	24.0	Hughes
Z038	FZ	In	2.8	Hughes
Z20404	FZ	In	0.32	Hughes
B001	CZ	Tl	3.0	Hughes
2	CZ	P	0.06**	Wacker
C028	CZ	Bi	2.0	Hughes

* CZ: Czochrolski grown, FZ: Float zone

** Derived from resistivity using $\frac{1}{\rho} = qn\mu$, with $\mu = 1350 \frac{\text{cm}^2}{V\,sec}$.

Table 2.1: Characteristics of silicon samples used in this work.

the surface of the silicon from a tungsten filament in a vacuum at about 10^{-6} torr. The iron was then diffused into the sample by annealing at about 1100 °C for 1 h in an inert He atmosphere followed by a rapid quench in distilled water. This anneal was carried out in a quartz tube furnace, Lindberg model 59344. This rapid quench is very important in order to ensure that the iron does not precipitate out of the silicon. The solid solubility of iron at 1100 °C is about 10^{16} cm^{-3} and the diffusion coefficient, D, is about 5×10^{-6} cm^2 sec^{-1}.[4] In one hour then one would expect the iron to diffuse into the silicon a distance $2\sqrt{Dt} = 0.3$ cm. The concentration of iron can, in fact be found from the empirical formula[5]

$$[\mathrm{Fe}] = 5.0 \times 10^{22} \exp(7.3 - \frac{2.87 \text{ eV}}{kT}).$$

Thus, one expects that the above procedure would result in an iron concentration of about 2×10^{15} cm^{-3} which is somewhat less than that predicted by the solid solubility. Copper was also introduced into the silicon samples in this way though in this case the anneal was carried out at a temperature of 850 °C. For copper the solid solubility at 850 °C is about 5×10^{16} cm^{-3} and the diffusion coefficient is about 5×10^{-4} cm^2 sec^{-1}.[4]

For the isotope shift experiments two isotopes of iron were used, ^{56}Fe (99.93% enriched) and ^{54}Fe (97.08% enriched). These isotopes were obtained from Oak Ridge National Laboratories as oxide (Fe_2O_3). The oxide was subsequently reduced at 700 °C for one hour in an atmosphere consisting of 12% H_2 with the balance made up of He. Two isotopes of copper were used in these experiments and these were ^{65}Cu (99.70% enriched) and ^{63}Cu (99.89% enriched). These were also obtained as oxide, CuO, and subsequently reduced as above but at 650 °C.

When making DLTS measurements on some of the p-type samples Al circular pads were evaporated onto the surface of the silicon from a tungsten filament in a vacuum system at about 10^{-6} torr. Indium ohmic contacts were made to the

back of the silicon also by evaporation but in a vacuum of 10^{-3} torr. These Al pads provided the Schottky barriers which are required for the DLTS technique.

It is important when performing the photoluminescence or DLTS experiments that the region probed is less than that into which iron or copper was introduced. In the case of the photoluminescence the critical parameter is the depth to which the laser excitation penetrates. This is usually taken to be the distance which attenuates the laser intensity by a factor of $\frac{1}{e}$. For an excitation source of about 2 eV, α (the absorption coefficient) for silicon is about 10^3 cm^{-1} so the $\frac{1}{e}$ distance is about 10^{-3} cm. To this one must add the carrier diffusion length and this is given by[4]

$$\sqrt{D\tau} \quad \text{where} \quad D = \frac{kT\mu}{q}$$

and τ is the minority carrier lifetime. Thus, this diffusion length turns out to be less than 4×10^{-2} cm, well within the region into which iron or copper would have been diffused.

In DLTS the critical parameter is the width of the depletion region, W, which for a Schottky barrier can be approximated by[4]

$$W = \sqrt{\frac{2\epsilon}{qN}(V_{bi} + V)}$$

where ϵ is the dielectric constant of the semiconductor, V_{bi} is the built in voltage or the Schottky barrier height, N is the charge in the depletion region, q is the electron charge, and V is the applied bias. For Al Schottky barriers on p-type silicon $V_{bi} = 0.58$V and typically for the samples studied here $V = 3$V, $N = 10^{16}$ cm^{-3}. This gives a depletion width on the order of 10^{-4} cm. In both cases the iron or copper would have diffused much farther into the silicon than the region probed.

2.5 EXPERIMENTAL RESULTS

2.5.1 Isoelectronic Centers

In Figure 2.2 is presented the luminescence seen in Si:B, Si:In, and Si:Tl which have been attributed to an Fe-acceptor pair[6-9]. This Fe-acceptor pair would consist of an interstitial iron donor paired with the substitutional acceptor atom. These Fe-acceptor pairs are referred to as isoelectronic centers. A consequence of a center's being isoelectronic in nature is that no auger process is involved in the recombination. In each case the spectrum presented is that seen after iron diffusion at 1100 °C. In the topmost panel of Figure 2.2 the spectrum for Si:B is presented using the labeling scheme of Sauer and Weber[6] to identify the prominent peaks at the high energy end of the spectrum. The peak labeled FeB_1^0 has been identified as a no-phonon line. The doublet labeled FeB_1^1 and FeB_0^1 has been identified as phonon replicas, with FeB_1^1 being the replica of FeB_1^0 and FeB_0^1 being the replica of FeB_0^0 (not visible in this spectrum at 4.2 K). This phonon mode is of about 9.8 meV. In the central panel of Figure 2.2 is presented the luminescence spectrum of Si:In, using the labeling scheme of Mitchard et al.[10] The line labeled P has been identified as a no-phonon line with the line labeled R being its phonon replica. This phonon mode is of about 9.0 meV. The symmetry of the P line center has been determined to be of an axial $< 100 >$ configuration consisting of at least two atoms.[11] (Fe,In) pairs are known to have such a symmetry in silicon. Indium is a large atom and so distorts the nearest interstitial site in the $< 111 >$ direction that the interstitial iron moves to the next nearest interstitial site in the $< 100 >$ direction. This symmetry of the P line center is a strong piece of evidence for its identification as being due to the presence of iron. In the bottom panel of Figure 2.2 is presented the luminescence spectrum of Si:Tl using the labeling scheme of Thewalt et al.[12] The line labeled A has been identified as a no-phonon transition with the B, C,

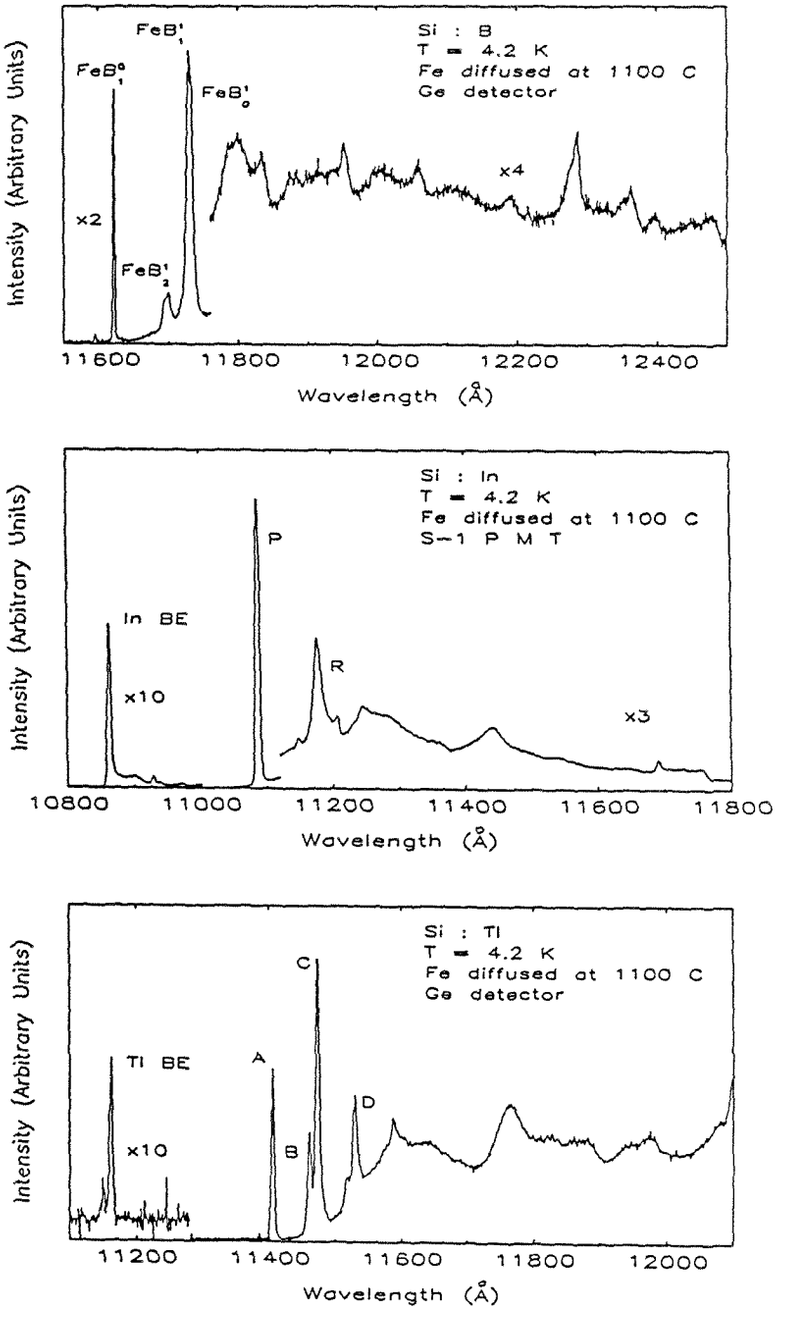

Figure 2.2: Photoluminescence spectra for silicon doped with B, In, and Tl (from the top to bottom) showing the luminescence identified as being due to Fe acceptor pairs. In each case these spectra were obtained after Fe diffusion at 1100 °C.

D lines being phonon replicas. The phonon mode associated with the D line is of about 10.5 meV. Moderate heating of the sample (or even a period of a few days at room temperature) results in a reduction of the luminescence intensity. This indicates that these luminescence centers involve a mobile constituent and, again, this makes iron a likely possibility.

In each case the phonon mode has been attributed to a local vibrational mode of the iron atom. A phonon mode of 9.0 meV is not a bulk momentum conserving phonon and so could be a vibrational mode of either the iron or the acceptor atom. The acceptor atom is a substitutional impurity and is bound strongly (large k) to the crystal lattice; it is unlikely therefore to have such a low energy mode. Since the iron atom is an interstitial dopant when introduced by diffusion, it is bound with smaller k to the crystal lattice and so is more likely to have such a low energy mode. Further, in the case of thalium and indium, iron is the lighter atom and so again is more likely to have such a low energy mode.

2.5.2 The Role of Iron

A further piece of evidence as to the identification of the center responsible for these luminescence spectra was the enhancement of the luminescence intensity upon the deliberate introduction of iron into the samples. In Figure 2.3 is presented the spectrum of Si:Tl before (upper panel) and after (lower panel) iron diffusion. The spectra were taken at 4.2 K, using the Ge detector. The spectrum in the top half of Figure 2.3 is plotted on a different arbitrary intensity scale than that in the lower panel. The large peak in the top panel is the thalium-bound exciton line and the smaller peaks at lower energies are probably due to donor-acceptor luminescence resulting from the unintentional presence of phospherous in the samples. In the bottom panel is presented the spectrum of Si:Tl after iron diffusion at 1100 °C. The thalium-bound exciton

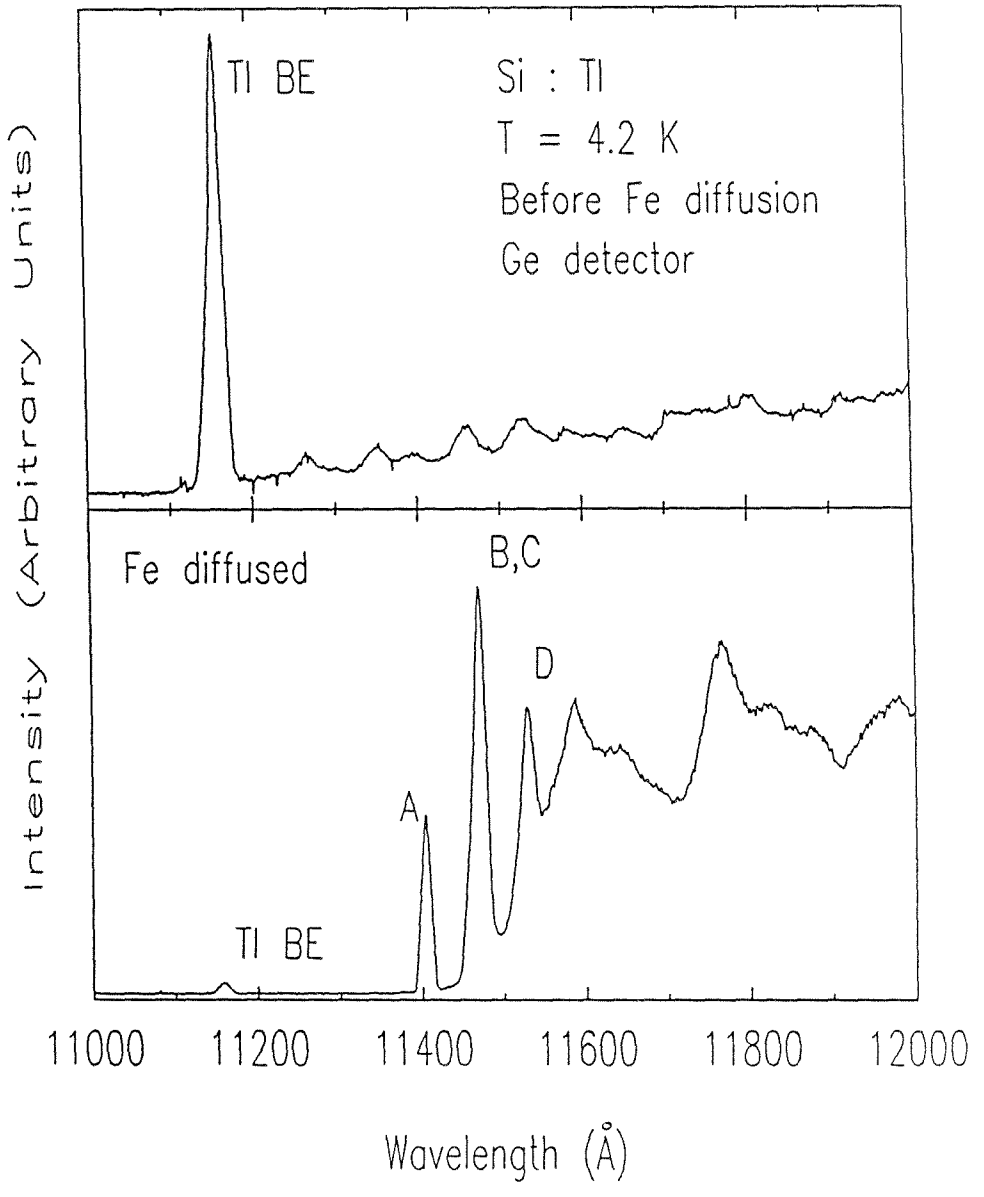

Figure 2.3: Photoluminescence spectra of Si:Tl before Fe diffusion (top panel) and after Fe diffusion (bottom panel). Note the magnitude of the A, B, C, D lines relative to the thalium-bound exciton line which may be regarded as being of constant intensity in the two spectra.

line appears in both the top and bottom panel and is of constant intensity and thus can be used to compare the relative intensities of the other luminescence lines in the spectra. These spectra show that, after the diffusion of iron, the A, C, D lines in Si:Tl are increased in intensity from not being observable in the spectra before diffusion to dominating the spectrum after diffusion. When some care was taken not to contaminate the samples and when they were subjected to the same cleaning and annealing procedure without iron this luminescence did appear. The luminescence was, however, more that an order of magnitude less intense relative to the thalium-bound exciton line than in the samples into which iron was diffused. The appearance of the luminescence is attributed to the presence of iron in the as-grown material or to slight contamination during the processing. This result is consistent with the work of Mitchard et al.[10] in Si:In in which the P, Q, R luminescence was observed without intentionally introducing iron into their samples.

In Figure 2.4 is presented the spectrum of Si:In before and after iron diffusion. The spectra were taken at 4.2 K but with the photomultiplier. In this figure is presented the spectrum for the untreated sample in the upper panel and that for the sample which had been iron diffused in the lower panel. The spectra show that after the diffusion of iron the P, Q, R lines in Si:In are increased in intensity from being barely observable to dominating the spectra. It has been observed in the case of Si:In, in particular, that the luminescence can be diminished by annealing the samples at high temperatures (1100 °C) and allowing them to cool slowly. This can be attributed to iron precipitating out of the samples.

Both the above results seem to help verify the identification of the luminescence centers as being iron-related. However, experiments such as this, while being very suggestive, must be viewed with some caution. While the intensities of the lines did increase substantially with the introduction of iron the annealing process could be responsible for the introduction of other impurities or vacancies

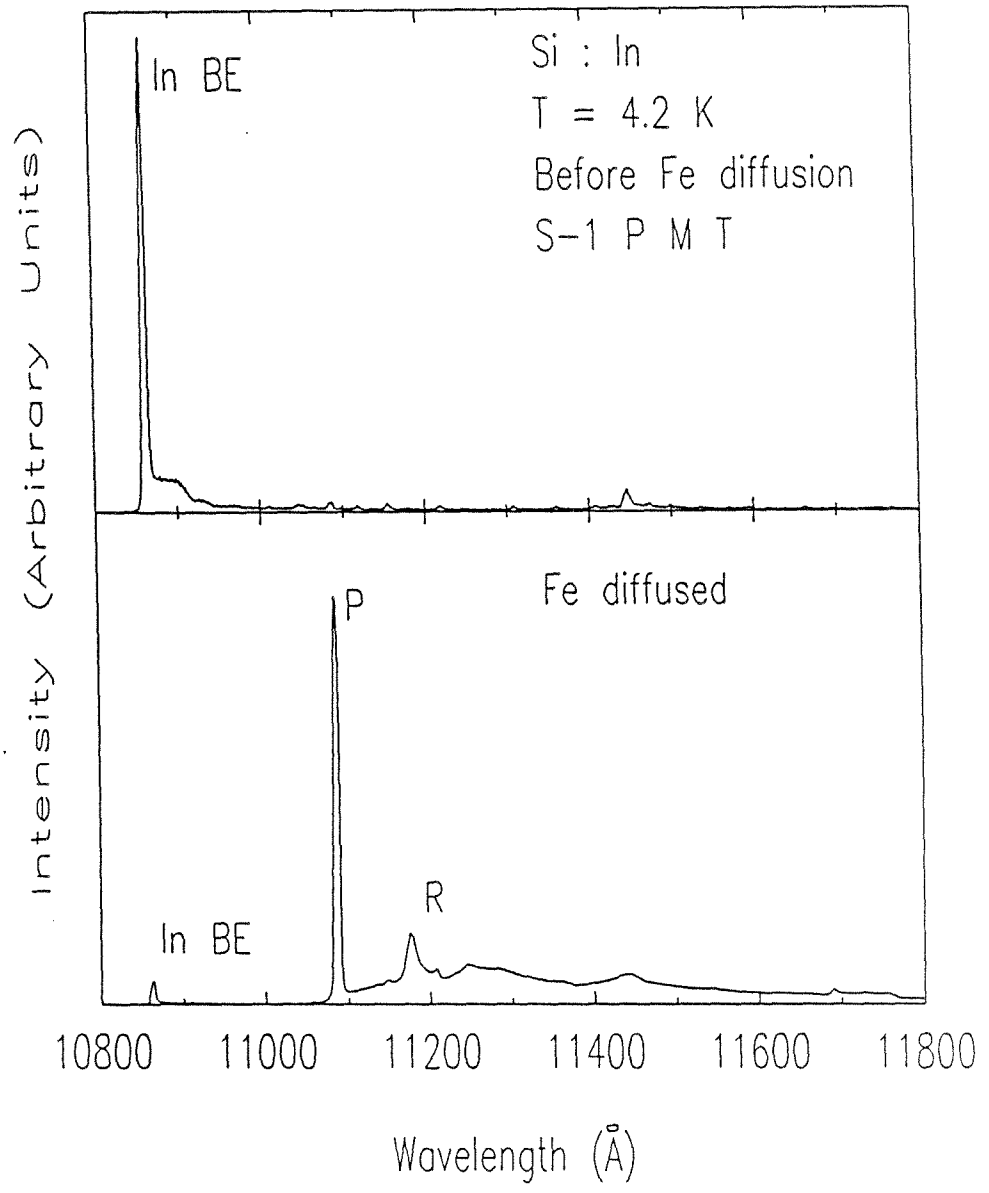

Figure 2.4: Photoluminescence spectra of Si:In before Fe diffusion (top panel) and after Fe diffusion (bottom panel). Note the magnitude of the P and R lines relative to the indium-bound exciton line which may be regarded as being of constant intensity in the two spectra.

into the samples which might play a role in these centers. Therfore, in order to identify these centers with more certainty, isotope shift experiments were performed and these are described below.

2.5.3 Isotope Shift Experiments on (Fe,B) and (Fe,In) Pairs

As discussed above, both in the case of the luminescence attributed to (Fe,B) and (Fe,In) pairs, prominent lines had been identified as being no-phonon recombinations followed by phonon replicas of these no-phonon lines. Isotope shift experiments were performed on these luminescence features. This was accomplished by diffusing two different isotopes of iron, ^{54}Fe and ^{56}Fe, into two different pieces of either boron or indium doped silicon and then measuring the absolute positions of the no-phonon lines and the first phonon replicas. In the case of (Fe,B) the no-phonon line is FeB_1^0 and the phonon replicas are the lines labeled FeB_0^1 and FeB_1^1. For the case of (Fe,In) the no-phonon line is that labeled P, and the phonon replica is that labeled R. The results for the (Fe,B) luminescence is presented in Figure 2.5. In the left-hand side of the figure is presented the no-phonon line, FeB_1^0, for both isotopes, and, in the right-hand side of the figure are presented the phonon replicas, FeB_1^1 and FeB_0^1, presented for both isotopes. The spectra shown in these figures are the result of extensive signal averaging. It is clear that there is no observable shift in the peak postion to at least 0.3 Å. From equation (1) one would have expected a change in the phonon energy of about 0.16 meV (2 Å at these wavelengths) and a similar shift in the position of then no-phonon line. In Figure 2.6 is presented the results for the (Fe,In) luminescence. The no-phonon line, P, is presented in the left-hand side of the figure and the phonon replica, R, is presented in the right-hand side of the figure. Again, no shift in the no-phonon line or change in the phonon energy is observed to at least 0.2 Å. In the case of the R line in particular the width of the peak is the same and a broad feature at about 11,192 Å has been

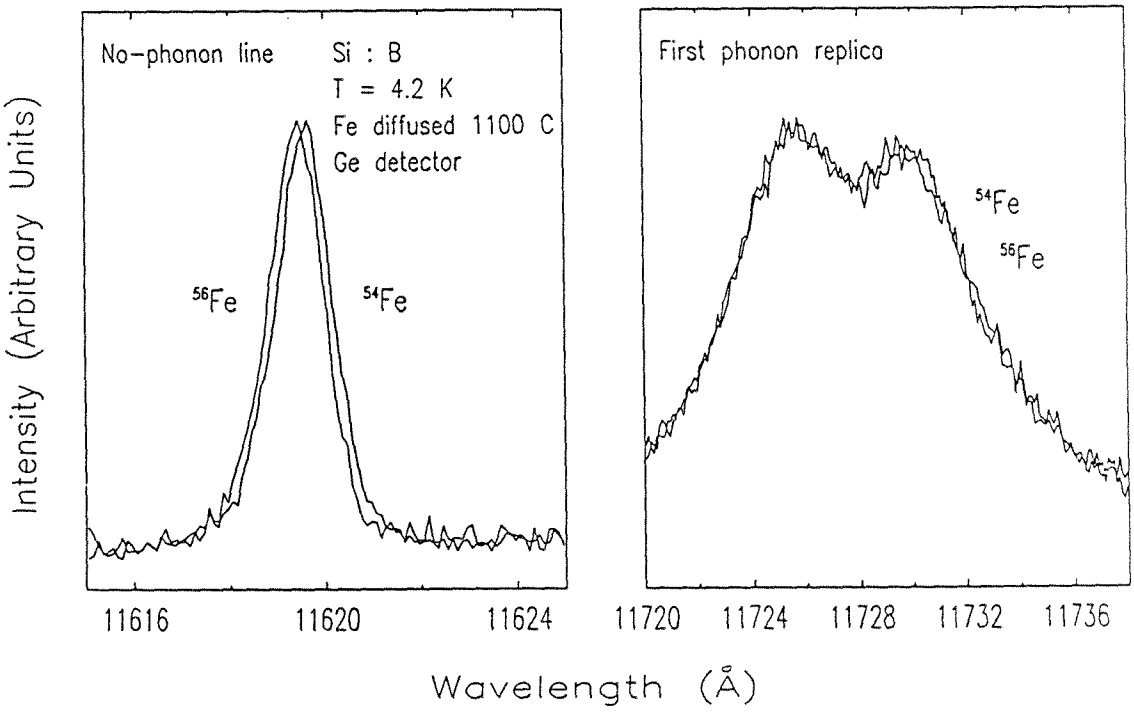

Figure 2.5: Results of the isotope shift experiments performed on Si:B presented for ^{54}Fe and ^{56}Fe. The left-hand side of the figure showing the no-phonon line and the right-hand side of the figure showing the phonon replica.

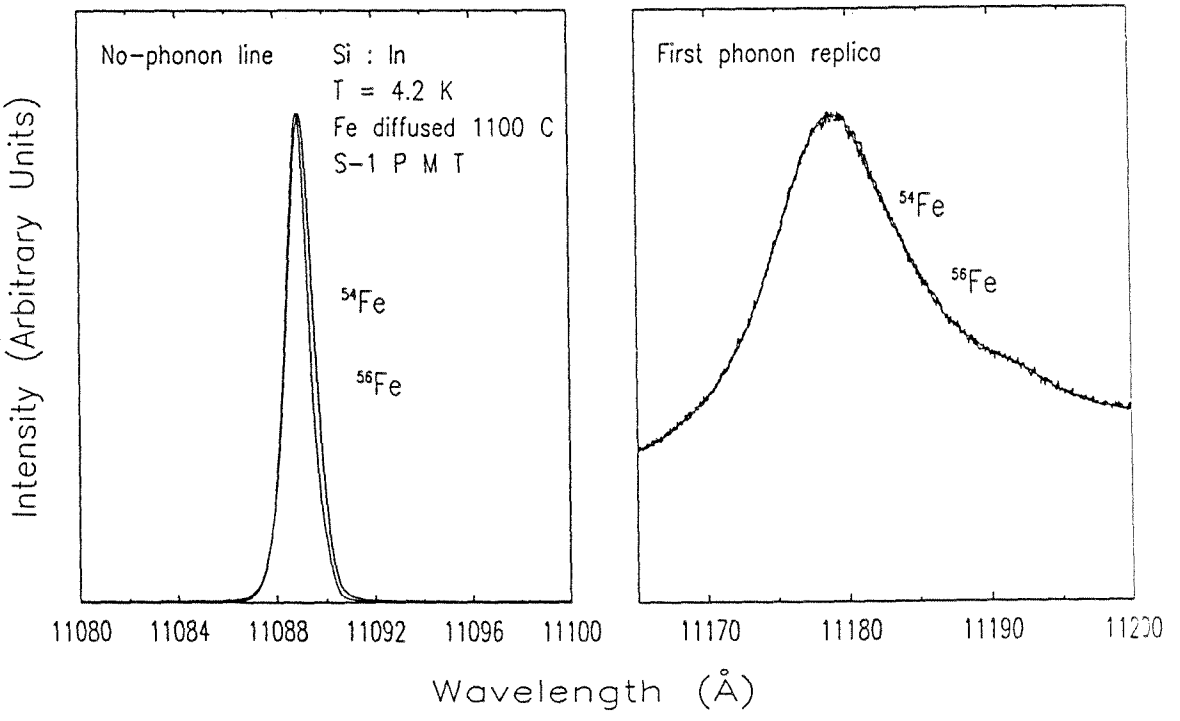

Figure 2.6: Results of the isotope shift experiments performed on Si:In for ^{54}Fe and ^{56}Fe. The left-hand side of the figure showing the no-phonon line and the right-hand side of the figure showing the phonon replica.

reproduced. In this case the change in phonon energy or shift in the postion of the no-phonon line should have resulted in shifts of the order of 2 Å also. Small and not reproducible shifts in the peak position and line widths are observed. These are on the order of 0.02 meV to 0.03 meV and could be the result of the limitations in the repeatability of the apparatus or could be accounted for as follows. Masking tape was used to mount the samples onto a sample holder in the dewar. It is possible that stress introduced into the samples when cooling them to 4.2 K produces these slight variations in the spectra. To illustrate the magnitude that such effects can attain, one can describe the motion of the electronic levels E, with strain ϵ, by a deformation potential c. If the strain is produced by the difference in the thermal expansion coefficient of the masking tape and the silicon, then

$$\Delta E = ac\beta\Delta T$$

where β is the volume expansivity, ΔT is the temperature change, and a is a numerical coefficient describing the nonuniformity and difference in the thermal expansivities. If one takes $c = 1$ eV, $\beta = 10^{-5}$ K^{-1} and $\Delta T = 300$ K, then $c\beta\Delta T = 2$ meV. Hence, our shifts of a few hundreths of an meV could be accounted for by a coefficient a as small as 10^{-3}.

The lack of an observed isotope shift is very surprising and calls into question the identification of these lines. Further experiments were performed as outlined below.

2.5.4 Isotope Shift Experiments on Isolated Iron Centers

In Figure 2.7 is presented the spectrum of n-type silicon after iron diffusion. The luminescence features seen in this spectrum have been attributed to an isolated iron complex.[8] The line at about 1.687 μm actually consists of two no-phonon lines followed by phonon replicas at about 1.704 μm and 1.709 μm. The phonon energy here is about 9.4 meV and is also thought to be a local

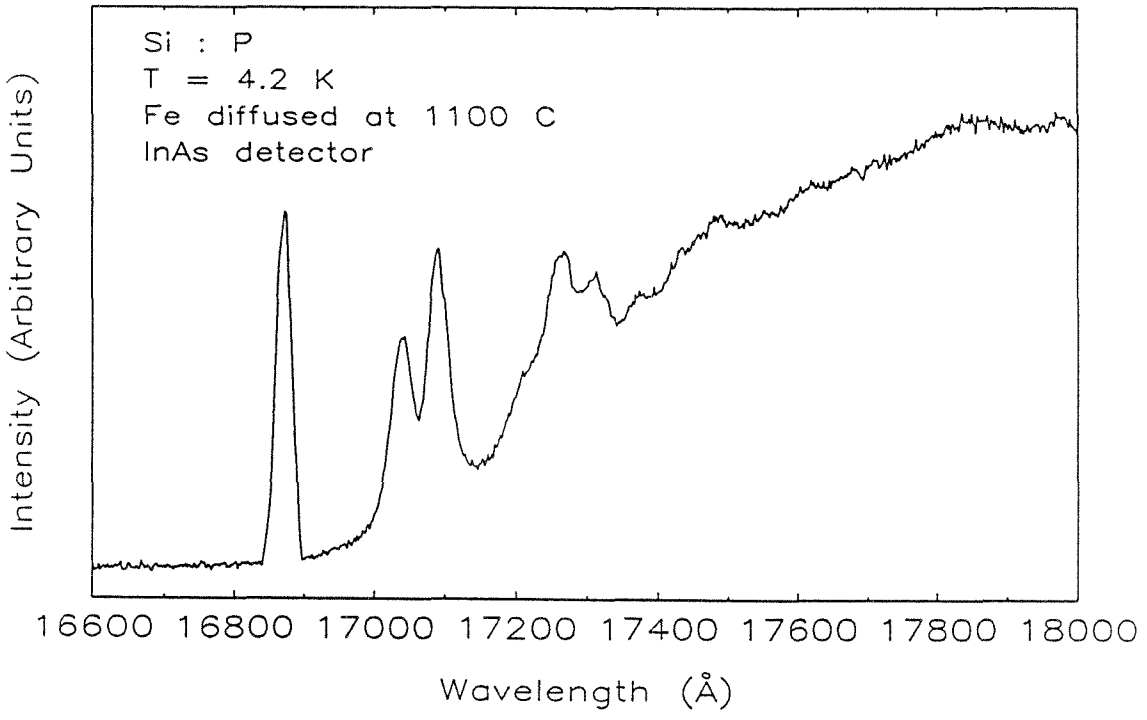

Figure 2.7: Photoluminescence spectrum of Si:P after diffusion of Fe at 1100 °C. The line at about 16870 Å actually consists of two no-phonon lines followed by phonon replicas at about 17040 Å and 17090 Å.

vibrational mode of the iron. The broad luminescence peaks at about 0.7 eV and has been attributed to a transition of an electron to the interstitial iron level since iron has a donor level 0.4 eV above the valence band maximum in silicon. Isotope shift experiments were performed on samples displaying this luminescence by carefully measuring the position of the no-phonon lines and phonon replicas after diffusion with ^{56}Fe and ^{54}Fe. The results are presented in Figure 2.8 with the no-phonon lines presented on the left-hand side of the figure and the phonon replicas presented on the right-hand side of the figure. One can see once again the lack of any substantial change in either the position of the no-phonon lines or the phonon energy to at least 0.03 meV. The predicted change in phonon energy, 0.16 meV, would correspond to a shift of about 4 Å at these wavelengths.

One possible explanation for the lack of an observed isotope shift in the cases presented above is that the as-grown samples were so contaminated with iron that the introduction of isotopically pure iron did not significantly alter the iron distribution in the samples. To investigate this possibility DLTS was employed to look for iron-related deep levels in the samples before and after processing.

2.5.5 DLTS Experiments

DLTS is a technique used to detect the presence of electrically active deep levels in semiconductors and to determine such properties about them as the concentration in which they are present in the semiconductor, their energy in the gap, and their capture cross section. The technique is discussed in much detail elsewhere [13]. For the present purpose DLTS was employed to determine whether in the samples of Si used here there was significant iron contamination before any processing and whether the technique for introducing iron into these samples was in fact doing so. In figure 2.9 are presented the results of some of the

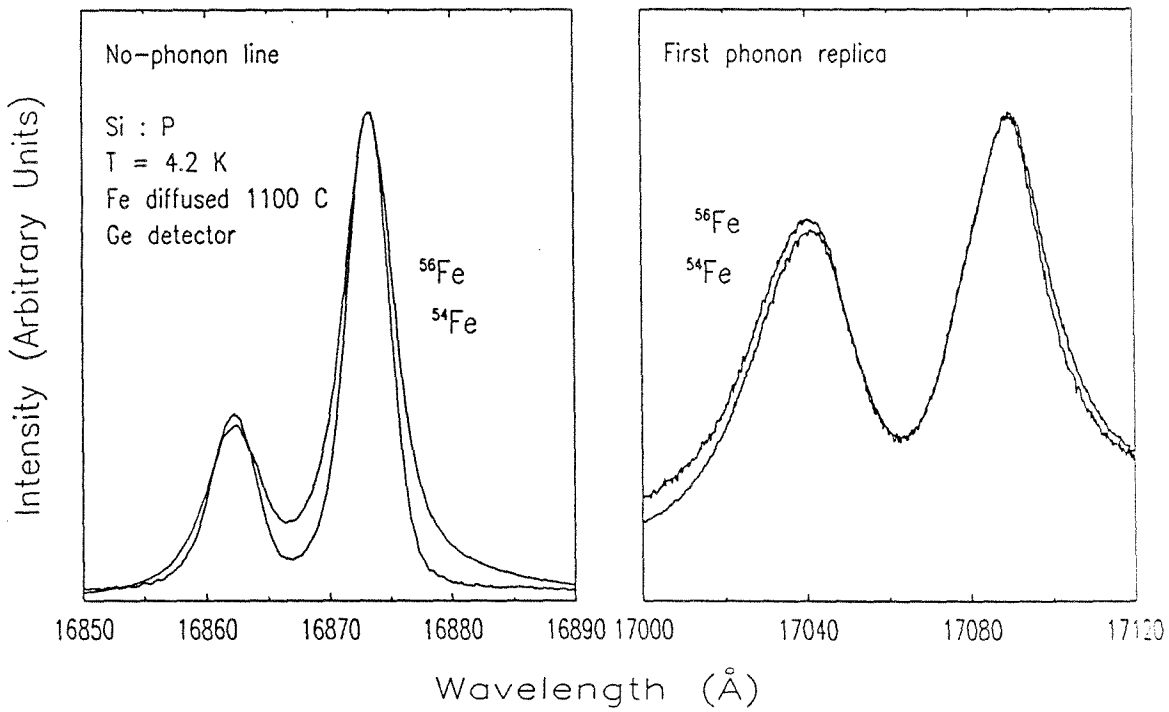

Figure 2.8: Results of the isotope shift experiments performed on Si:P for ^{54}Fe and ^{56}Fe. The left-hand side of the figure showing the no-phonon lines and the right-hand side of the figure showing the phonon replicas.

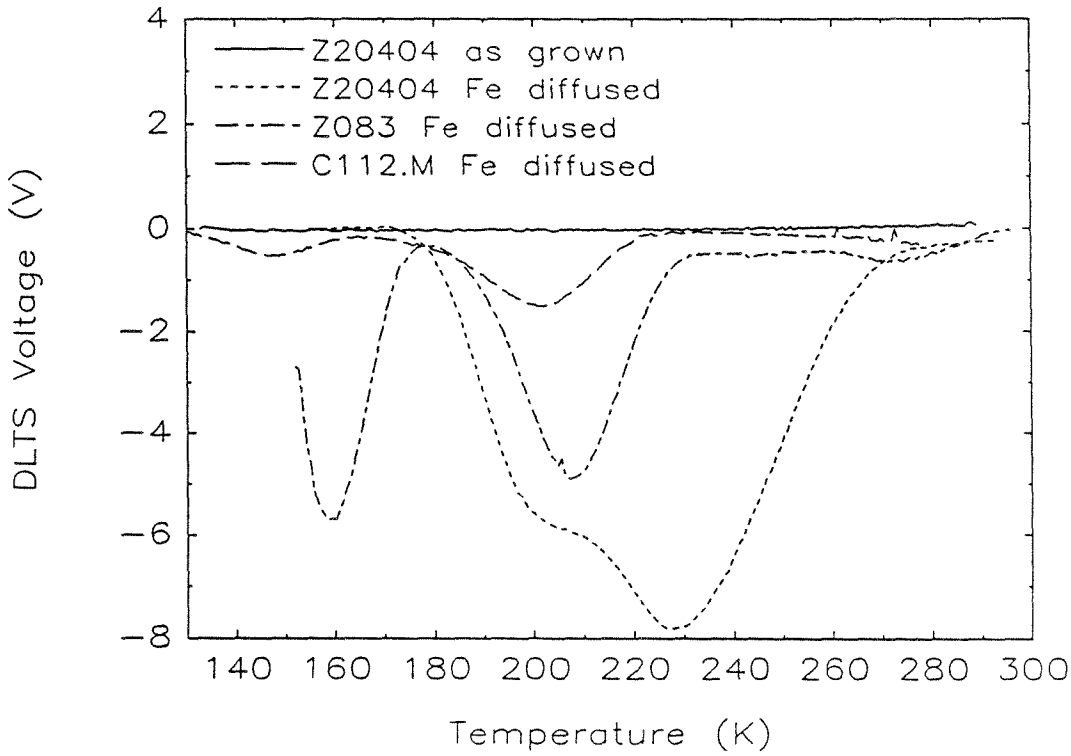

Figure 2.9: DLTS spectra of as-grown and iron-diffused Si:In samples as labeled. The peaks shown have been previously identified as being related to iron centers.

DLTS measurements that were made. The voltage on the vertical axis represents a change of capacitance which can be converted into trap concentration. One can see that in the as-grown samples and those annealed at 1100 °C, but without iron no deep levels are seen. In fact, in all those samples studied before an anneal or after an anneal without iron no deep levels were observed. This places an upper limit on the iron concentration in these samples of 10^{13} cm^{-3}. In those samples that did have iron deliberately introduced, one sees deep levels which have been previously identified as being related to iron[14]. These indicate an iron concentration which can be estimated from[13]

$$N_d = 2N_s \frac{\Delta C}{C}$$

where N_d is the concentration of the deep level, N_s is the concentration of the shallow dopant in the sample, C is the capacitance of the schottky barrier at the applied reverse bias, and ΔC is the change in that capacitance represented by the DLTS peak. For the prominent peak at about 200 K in the spectrum of Z083, for example, this yields a concentration of about 10^{14} cm^{-3}. One must remember that this is the concentration of the particular level associated with this peak so that this number should not be regarded as necessarily being the total iron concentration. It is therefore reasonable that this number is less than the iron concentration expected. It would seem, however, that one can conclude that the diffusion process employed here does increase the iron concentration significantly and that this is probably not the source of the lack of an isotope shift presented above.

2.5.6 Copper in Silicon

In Figure 2.10 is presented the specturm of n-type silicon showing luminescence lines which have been attributed to (Cu,Cu) pairs labeled using the scheme of Sauer and Weber.[6] These luminescence features do not depend on the particular n-type dopant, the line labeled Cu_0^0 being a no-phonon line and the line labeled

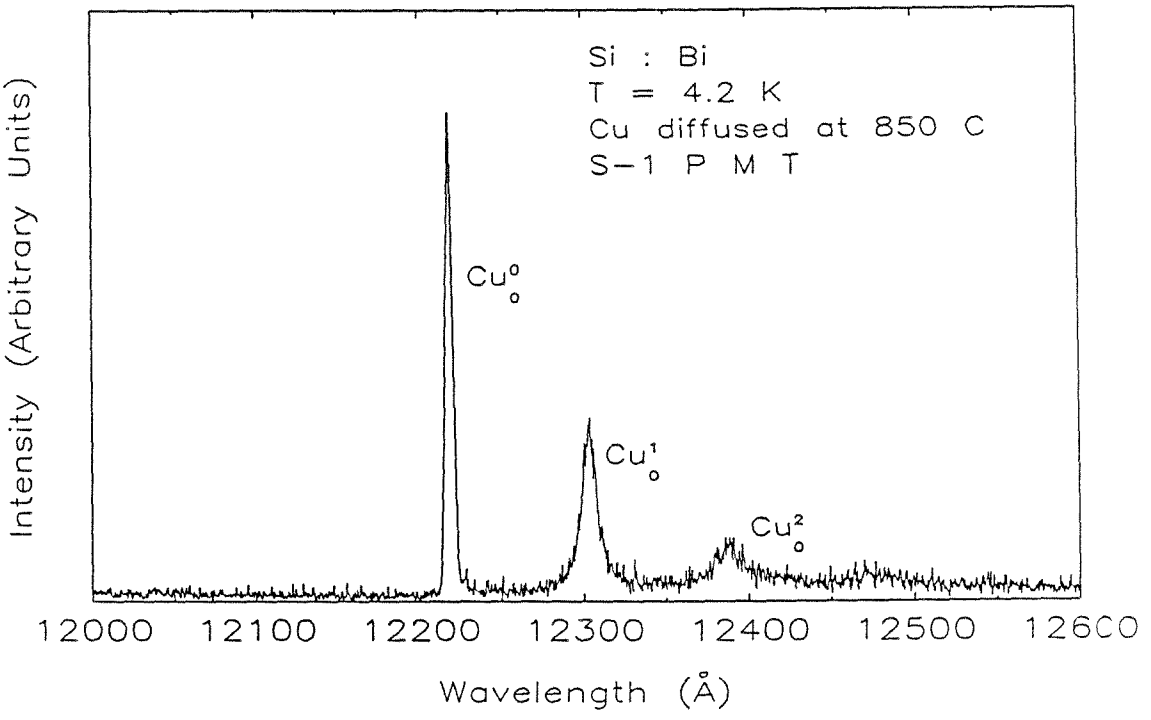

Figure 2.10: Photoluminescence spectrum of Si:Bi after Cu diffusion at 800 °C. The highest energy line was identified as a no-phonon line followed by phonon replicas. This luminescence did not depend on the particular n-type dopant.

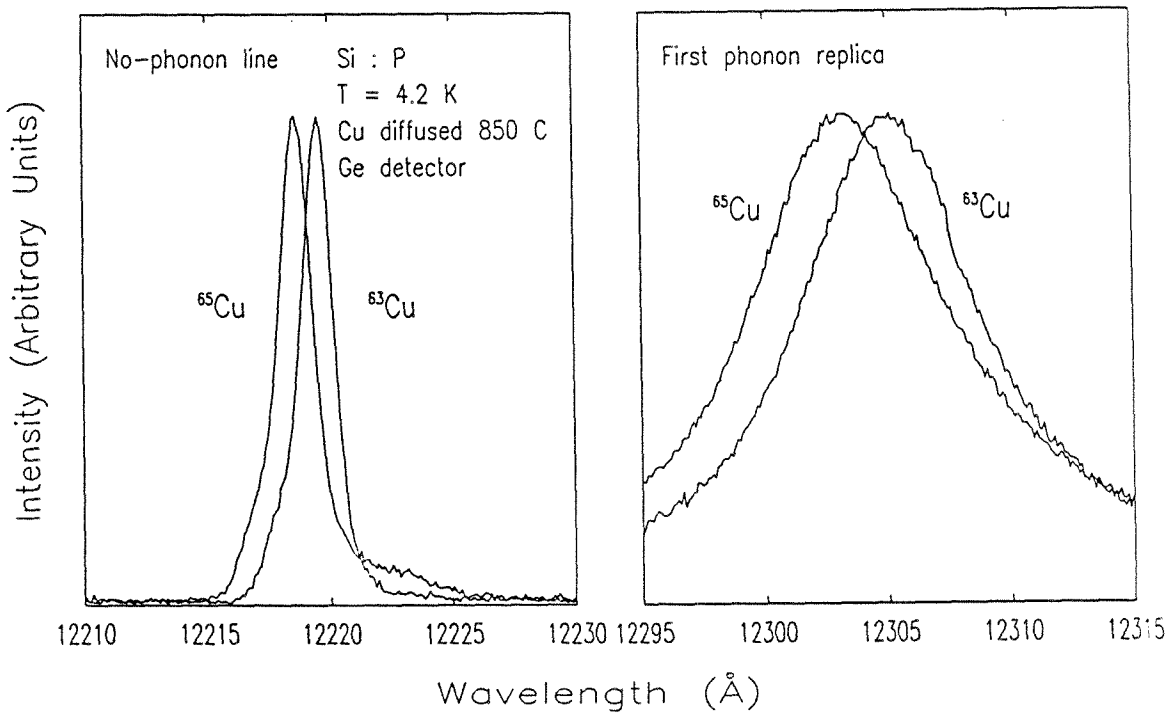

Figure 2.11: Results of the isotope shift experiments performed on the luminescence attributed to Cu, presented for ^{65}Cu and ^{63}Cu. The left-hand side of the figure showing the no-phonon line and the right-hand side showing the first phonon replica.

Cu_0^1 being a 7.0 meV phonon replica of the no-phonon line. Isotope shift experiments were performed on these luminescence features by diffusion of ^{65}Cu and ^{63}Cu into two different pieces of the Si:Bi. The results of this experiment are presented in Figure 2.11, with the no-phonon line presented in on the left-hand side of the figure and the first phonon replica presented on the right-hand side of the figure. In this figure one sees a clear shift in the positions of the no-phonon line and phonon replica. The shift of the no-phonon line is about 0.0726 meV with the line for the heavier isotope shifted to higher energies as predicted. The shift in the position of the phonon replica is of about 0.1506 meV. Thus, the phonon energies for ^{65}Cu and ^{63}Cu are 6.98 meV and 7.05 meV, respectively. This change in the phonon energy of 0.07 meV is in good agreement with the expected change in the phonon energy of about 0.11 meV. Also, as expected, the change in the position of the no-phonon line is of the same magnitude as the change in the phonon energy.

This result, then, confirms that the luminescence show in Figure 2.10 is indeed related to copper, that in particular the line labeled Cu_0^1 is a phonon replica of Cu_0^0, and that this phonon mode is a local vibrational mode of the copper atom. Further, this also helps to confirm the null results in the case of the luminescences which are supposed to involve iron. That is to say, that the experiment is sufficiently sensitive to have observed any isotope shift in those systems, had one been present.

2.6 DISCUSSION

The experiments above, related to iron, seem to display a contradiction. On the one hand, the deliberate introduction of iron into the samples enhances the luminescence features which are attributed to the presence of iron. On the other hand, the isotope shift experiments failed to display the expected shift in the line positions or phonon energies. One can propose a number of possible

resolutions to this seeming contradiction. The first is that these luminescence features are not, in fact, related to iron. The enhancement, then, would be the result of the annealling and quench process which may introduce other defects, such as vacancies, into the silicon. Indeed, as mentioned earlier, in some samples, an anneal with no iron also enhanced the luminescence somewhat. This latter effect may, however, be the result of the unintentional introduction of iron into the silicon from such sources as the furnace tube at high temperatures. Iron is a fast diffuser in silicon at 1100 °C and is a very common contaminant. This center is a very efficient radiative recombination center and as few as 10^{12} cm^{-3} could be the source of this luminescence. Thus, very little iron contamination could enhance the luminescent intensity.

Another possibility is that while iron is involved in the center, the defect is more complicated than a simple iron interstitial atom paired with a substitutional acceptor atom. In the case of the (Fe,B) pairs there has recently been some work investigating and proposing just this sort of possibility[15]. The lack of a change in the phonon energy as a function of the isotope of iron introduced into the sample could have a number of explanations. One possibility is that the observed 9 - 10 meV phonon mode is not an iron phonon mode. Indeed, the magnitude of the changes in the phonon energies which have been predicted above are for iron motion alone. The large acceptor atoms (In, Tl) as well as the small acceptor B deform the silicon lattice and destroy its tetrahedral symmetry. This distortion of the lattice could lead to low energy phonon modes that involve substantial motion of the atoms around the iron and thus no isotope shift would be expected.

2.7 CONCLUSIONS

In this chapter results of photoluminescence experiments which were aimed at trying to identify the nature of some isoelectronic centers in silicon were

presented. The deliberate introduction of iron into the Si:In and Si:Tl samples enhanced the luminescence features which were thought to be an iron interstitial atom paired with a the substitutional acceptor atom. However, isotope shift experiments failed to show a change in peak positions or phonon energies that might be expected in the case of (Fe,B), (Fe,In), or in the isolated iron complex. DLTS experiments showed that the silicon samples were initially free of iron contamination to a concentration of 10^{13} cm^{-3}. These experiments also showed that the diffusion and quench process did increase the iron concentration by at least an order of magnitude.

These experiments cast doubt on the identification of these isoelectronic centers as being a simple iron interstitial paired with the substitutional acceptor atom. Further, these experiments would indicate that the 9-10 meV phonon mode seen in these spectra cannot be a vibrational mode that involves primarily motion of the iron atom.

Isotope shift experiments performed on a luminescence spectrum seen in n-type silicon and attributed to (Cu,Cu) pairs displayed shifts in line postions and changes in phonon energies. This positively identified the nature of these lines and the fact that copper is the major constituent of the center. The experiments on the copper center also helped to verify the null results in the case of the iron related centers.

REFERENCES

1. J. I. Pankove, *Optical Processes in Semiconductors* (Dover Publications Inc., New York, 1975).

2. O. Madelung, *Introduction to Solid State Theory* (Springer-Verlag, Berlin, 1978).

3. V. Heine and C. H. Henry, *Phys. Rev.* **B25**, 3795 (1975).

4. S. M. Sze, *Physics of Semiconductor Devices* (John Wiley and Sons, New York, 1981).

5. K. Graff and H. Pieper, *J. Electrochemical Soc.* **188**, 669 (1981).

6. R. Sauer and J. Weber, *Physica* **116B**, 195 (1983).

7. T. E. Schlesinger and T. C. McGill, *Phys. Rev.* **B25**, 7850 (1982).

8. J. Weber and P. Wagner, *J. Phys. Soc. Jpn.* **49**, 263 (1980).

9. J. Weber, R. Sauer, and P. Wagner, *J. Lumin.* **24/25**, 155 (1981).

10. G. S. Mitchard, S. A. Lyon, K. R. Elliot, and T. C. McGill, *Solid State Commun.* **29**, 425 (1979).

11. J. Weber, R. Sauer, and P. Wagner, *Proceedings of the International Conference on Luminescence*, Berlin, edited by I. Broser (North-Holland, Amsterdam, 1981).

12. M. L. W. Thewalt, U. O. Ziemelis, and R. R. Parsons, *Phys. Rev.* **B24**, 3655 (1981).

13. R. T. Collins, Doctoral Thesis, California Institute of Technology, 1985.

14. K. Wunstel and P. Wagner, *Solid State Commun.* **40**, 797 (1981).

15. H. D. Mohring, J. Weber, and R. Sauer, *Phys. Rev.* **B30**, 894 (1984).

CHAPTER 3

Photovoltaic Investigations of GaAs/AlAs Heterostructures

3.1 INTRODUCTION

Heterostructures consisting of layers of GaAs, AlAs, and $Al_xGa_{1-x}As$ are of great scientific interest and promise to be of great technological importance as well.[1-3] GaAs and AlAs have lattice constants which are the same to within a few tenths of a percent. They are thus said to be lattice-matched. Related to this is the fact that they may be grown in epitaxial layers on each other free of strain and defects due to misfits. Since these layers may be extremely thin, the heterostructures grown of these materials allow one to observe fundamental quantum mechanical phenomena such as resonant and inelastic tunneling.[4,3] It is of interest to study these phenomena in their own right and, since these processes happen over extremely short distances (as little as 20 Å) and fast times, they may be exploited for new high speed electrical and optical devices. However, to understand these heterostructures one needs to investigate some of the basic electrical and optical properties of these structures.

In this chapter is discussed the application of photoresponse techniques to the study of a simple GaAs/AlAs heterostructure. The heterostructure studied consisted of a thin layer of AlAs (50 Å to 250 Å thick) sandwiched between degenerately doped layers of GaAs. Photoresponse is a technique in which the structure to be studied is illuminated by light. The light may excite charge carriers in the structure. These charge carriers may drift or diffuse through the structure and thus create a current or voltage. The optical excitation and subsequent movement of these charge carriers depend on the optical and electrical properties of the structure being studied. By measuring these currents or voltages one can gain insight into the nature of these structures. Generally, one studies the currents or voltages as a function of the wavelength of the incident light. Different wavlengths correspond to different photon energies, and thus one might expect different optical excitations to be possible at different wavelengths. Also one may study these heterostructures as one alters their optical and elec-

trical properties by either varying layer thicknesses, dopings, alloy compositions or by applying external biases to the structure.

The experimental techniques used as well as calculations which were performed are described in detail in the following sections. It is shown how electrons may be optically excited in this structure and a mechanism involving the transport of these electrons past the AlAs barrier is proposed. It is the movement of these electrons which results in the photovoltage which is studied. It is shown how the nature of the photoresponse spectrum depends on the optical properties of the structure. The effects of doping, temperature, layer thickness, and applied biases on the photoresponse spectrum are discussed. A short description of photodetectors is presented, defining such quantities as figures of merit; the use of the structures studied as photodetectors is also discussed.

3.2 EXPERIMENTAL METHOD

3.2.1 Sample Preparation

The samples used in this study were grown by a metalorganic chemical vapor deposition technique (MOCVD)[5,6], with all the AlAs barriers doped p-type with Mg[7,8] at 1×10^{18} cm^{-3} while the GaAs was doped n-type with Se. The substrates on which these structures were grown were (100)-oriented GaAs wafers doped at about 3×10^{18} cm^{-3} with Si. In this chapter, results from measurements on a number of samples will be discussed. The source materials and MOCVD reactor design are described in detail in the references quoted above. The characteristics of these samples are summarized in Table 3.1. For these doping levels, the AlAs barrier is fully depleted.

In Figure 3.1 is presented a schematic cross-sectional view of the sample geometry which is discussed below. The thickness of the top layer (illuminated side) of GaAs varied from 0.5 μm thick to 4.4 μm thick, depending on the sam-

Sample	Growth No.	Barrier Thickness (Å)	GaAs Doping Se ($\times 10^{18}$ cm^{-3})
1	H115	160	5.0
2	H125	50	3.0
3	H135	110	5.0
4[a]	H144	240	3.0
5[b]	H151	160	3.0
6	H428	175	0.5

[a] GaAs doping gradually dropped to 2.0×10^{18} cm^{-3} in front of the AlAs barrier.

[b] GaAs doping 1.2×10^{18} cm^{-3}1 μm either side of the AlAs barrier.

Table 3.1: GaAs/AlAs heterostructure sample characteristics used in the experiments described in this chapter.

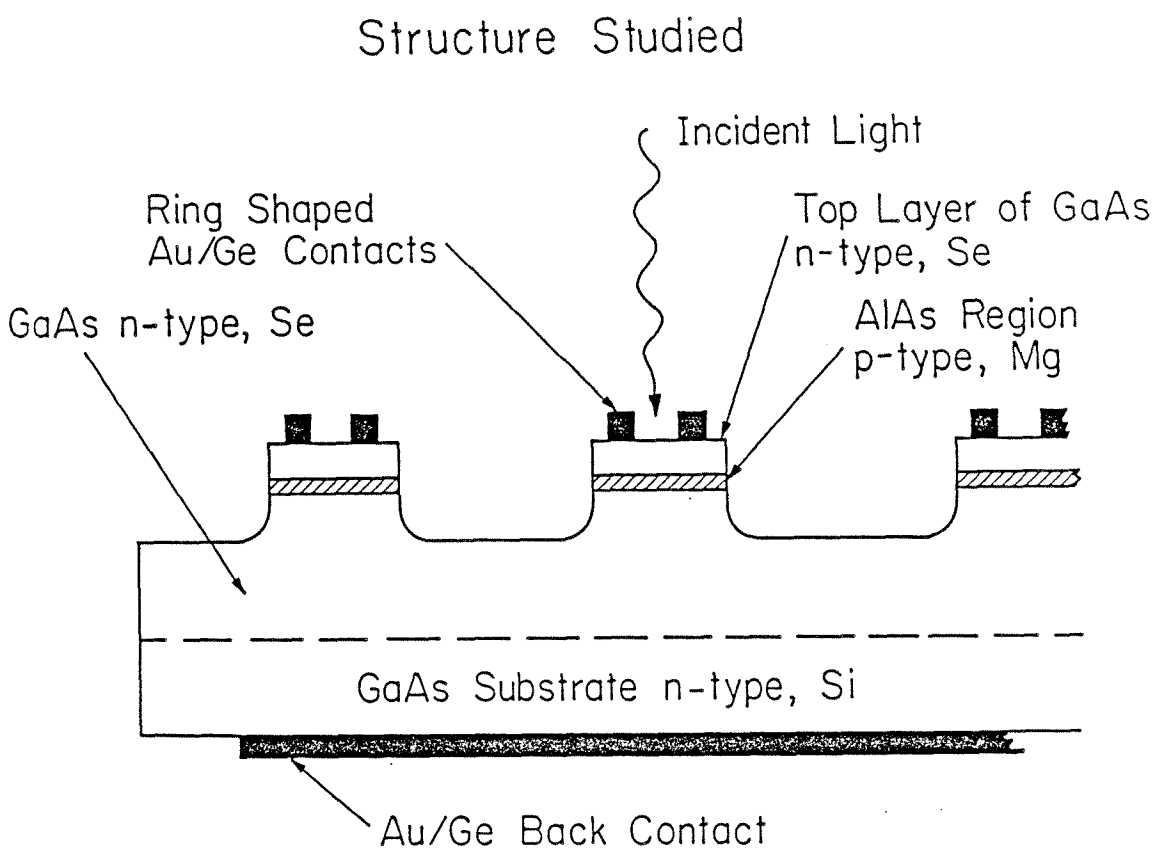

Figure 3.1: Schematic cross-sectional view of the structure studied. The mesas were approximately 350 μm in diameter and 10 μm high. The ring-shaped top contacts had an inner diameter of about 120 μm. The experiment consisted of measuring the voltage between the top and bottom contacts as a function of the wavelength of the incident light.

ple, while the bottom layer was substantially thicker. Ohmic contacts were made to the samples by evaporation from a tungsten filament, a eutectic mixture of a Au/Ge (12% Au and 78% Ge by weight) alloy followed by a 20 second anneal at 420 °C.[9,10] The evaporation was made in a vacuum of about 10^{-6} torr. The samples were annealed on a tungsten filament strip heater in a flowing forming gas (12% H_2, 88% He) atmosphere. Photolithographic techniques were employed to make ring-shaped contacts to the top surface of the samples to allow light to penetrate into the GaAs through the center of the rings. The steps in the photolithography consisted of laying down a layer of positive photoresist on the top layer of GaAs and then exposing and developing this so as to create annular shaped holes in the photoresist layer, after the metalization acetone was used to lift off the Au/Ge everywhere except where it had adhered to the GaAs surface. A second layer of photoresist was then laid down, exposed and developed to leave pads of photoresist slightly larger than and on top of the Au/Ge rings. These pads defined the mesas which were then etched to electrically isolate the individual contacts from each other. The rings had an outer diameter of about 300 μm and an inner diameter of about 120 μm while the mesas were about 350 μm in diameter. The mesas were created by etching with a GaAs etch (4:1:1, H_2SO_4:H_2O_2:H_2O) to a depth of about 10 μm. A Au/Ge ohmic contact was evaporated onto the substrate surface of the sample. The samples were then mounted on transistor headers using silver paint; wire bonds were made to the Au/Ge top contacts.

3.2.2 Experimental Apparatus

The experimental apparatus used to conduct the photoresponse experiments is pictured schematically in Figure 3.2. The light source used was a 1200 W tungsten filament lamp whose output could be adjusted with a variable voltage source. The light from this lamp was collected by a pair of lenses and

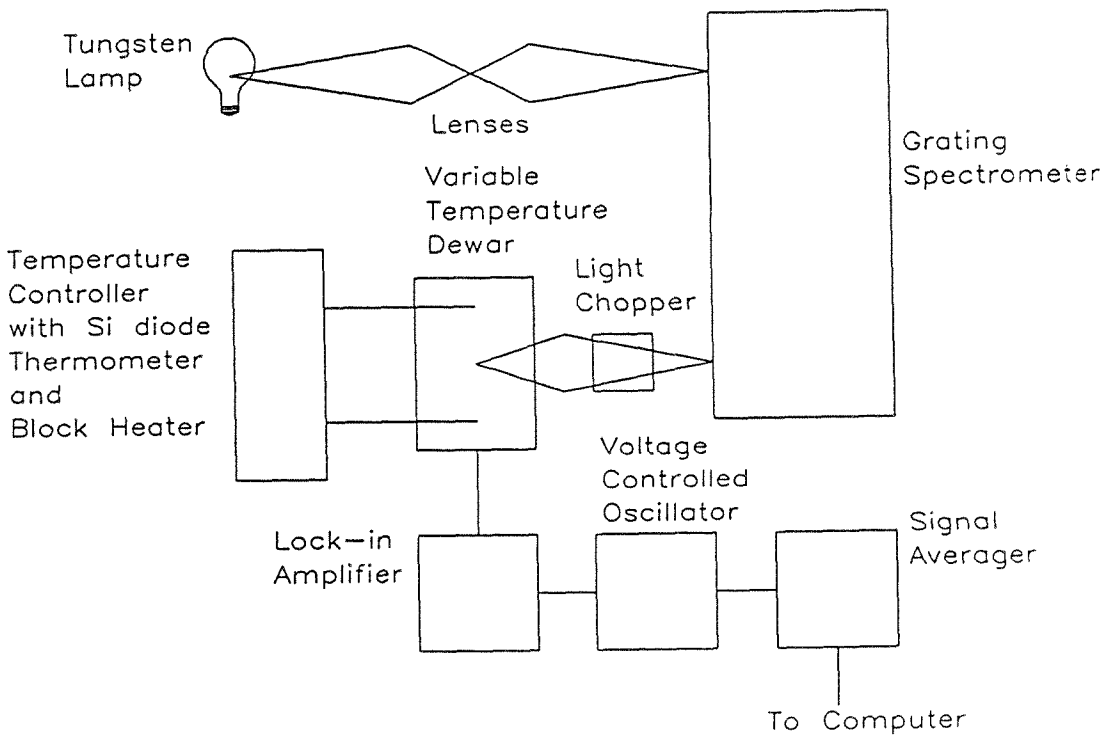

Figure 3.2: Schematic diagram of the experimental apparatus used to conduct the photoresponse experiments discussed in this chapter.

directed through the entrance slits of a single-pass grating spectrometer, (SPEX model 1269). An iris was also used in conjunction with the lenses to create an external optical system of the same f-number as the spectrometer. The wavelength of the light could thus be selected by scanning the spectrometer. The light exiting from the spectrometer was generally chopped at about 270 Hz and was then focussed onto a particular device to be studied. The transistor headers on which the samples were mounted could themselves be mounted inside a variable temperature dewar (Janis model DT 11), and thus the samples could be cooled to any temperature desired from room temperature to 4.2 K. The photovoltage was then measured as a fuction of wavelength using a lock-in amplifier. The signal from this instrument was digitized using a voltage controlled oscillator, and the photovoltage spectrum stored on a signal averager (Nicolet model NIC 1170). This, then, is an open circuit measurement of the voltage across the sample. One could also make a closed circuit measurement of the current through the sample by using a current preamlifier before the lock-in amplifier. If it was desired to know the sign of the voltage, the light incident on the sample was not chopped and the signal was measured using a voltmeter.

3.2.3 Applied External Bias

In Figure 3.3 is presented the circuit used to apply external dc biases to the samples. The sample is represented as a current source i_s with a resistor in parallel r_s, the sample resistance at the applied voltage. It is $v_s = i_s r_s$, which is the photovoltage one wishes to measure with the lock-in amplifier. The lock-in amplifier is represented by R_l (this would be 100 MegΩ). The dc power supply provides a dc voltage, V, and we have a resistor in series with it, R; the need for this resistor will become apparent. In general, the lock-in amplifier will only measure some fraction of the photovoltage as this is the only voltage which is at the same frequency and in phase with the incident light. The question, then,

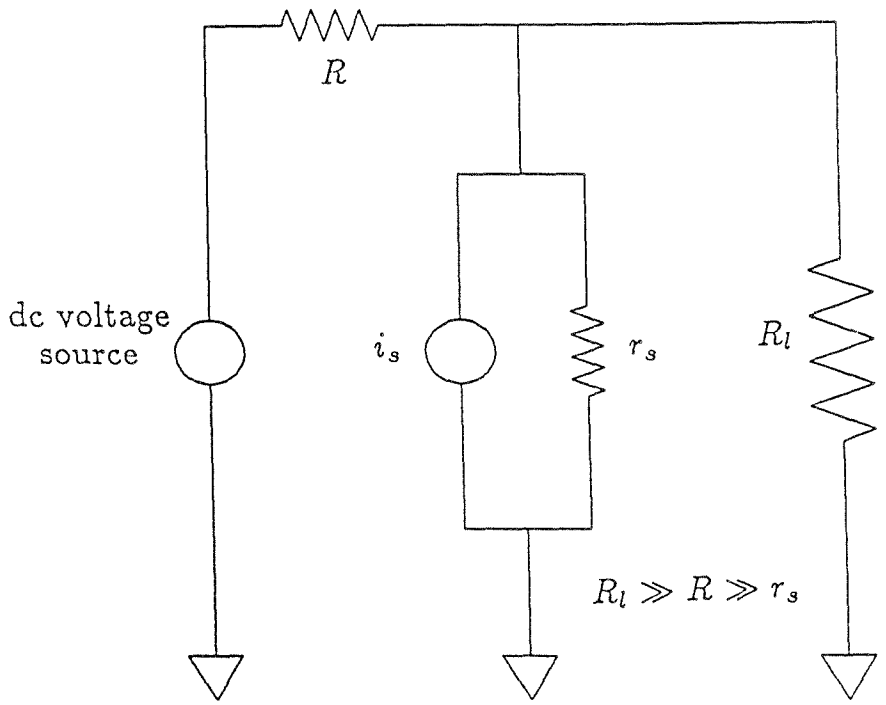

Figure 3.3: Circuit employed to apply external dc biases to the samples. The sample is represented by the current source, i_s, and resistance, r_s. The lock-in amplifier is R_l and R is a resistor whose value is intermediate to R_l and r_s.

is: What is the dc voltage that is dropped across the sample and what is the magnitude of the voltage that the lock-in amplifier measures ?

The dc power supply puts out a voltage V. Since r_s and R_l are in parallel one has $R_{\|} = \frac{r_s R_l}{r_s + R_l}$, and the current flowing through the sample is $\frac{V}{R+R_{\|}}$. The voltage dropped across the sample is

$$\frac{V}{R + R_{\|}} R_{\|}.$$

In principle, if $R = 0$ then we drop the full V across the sample. From the point of view of the current source i_s the three resistances are in parallel and so the photovoltage that is measured across the lock-in amplifier is

$$i_s \left(\frac{R R_l r_s}{R_l r_s + R r_s + R_l R} \right),$$

which is $i_s r_s$ when $R_l, R \gg r_s$. One sees that, although making R as small as possible causes a greater fraction of V to be dropped across the sample, one must at the same time have $R \gg r_s$ so that the lock-in will measure the full photovoltage. In summary then, one uses $R_l \gg R \gg r_s$ in order that a reasonable dc voltage (0.5 V to 2.0 V) is dropped across the sample while at the same time allowing the lock-in amplifier to measure the full photovoltage.

3.3 THEORETICAL MODEL

To model the absorption of the light in these structures, the following calculations were carried out. Consider a one-dimensional model where one has a layer of GaAs, a layer of AlAs, and a semi-infinite layer of GaAs. Light impinges on the first layer of GaAs from a vacuum at normal incidence. It is assumed that no attenuation of the light takes place in the AlAs. In the GaAs, however, the attenuation of the light is modeled, using a coefficient of absorption, α, which was obtained by fitting and extrapolating the curves published by H.C. Casey et al.[11] for heavily doped n-type GaAs at room temperature. Constant values

for the index of refraction of GaAs and AlAs of 3.4 and 3.1, respectively, were used.[12] For an electromagnetic wave incident onto the interface between two dielectric media, the boundary conditions at the interface are the continuity of the tangential components of the electric and magnetic fields, $\vec{E}$, and $\vec{H}$, respectively. If one has a wave propagating in the $\hat{z}$ direction normal to the interface, then the electric field is given by,

$$\vec{E} = E_0 \exp[i(\omega t - kz)]\hat{x}$$

where

$$k = \frac{\omega n}{c} - \frac{i\alpha}{2}$$

and where n is the real part of the index of refraction and α is the absorption coefficient. From Maxwell's equation

$$\nabla \times \vec{E} + \mu \frac{\partial \vec{H}}{\partial t} = 0$$

it is obtained that

$$\vec{H} = \frac{k}{\mu\omega} E_0 \exp[i(\omega t - kz)]\hat{y}.$$

Thus, for non-magnetic materials the continuity of the tangential component of $\vec{H}$ is equivalent to the continuity of $\frac{\partial \vec{E}}{\partial z}$. In matching these boundary conditions at the interface one must take into account the total electric field due to the incident, reflected, and transmitted waves in any region. Thus, the boundary conditions at an interface, z_0, can be expressed as

$$\begin{pmatrix} E_{2t} \\ E_{2r} \end{pmatrix} = \frac{1}{2B} \begin{pmatrix} (B+A)e^{(B-A)z_0} & (B-A)e^{(B+A)z_0} \\ (B-A)e^{-(B+A)z_0} & (B+A)e^{-(B-A)z_0} \end{pmatrix} \begin{pmatrix} E_{1t} \\ E_{1r} \end{pmatrix}$$

where E_{2t} and E_{2r} are, respectively, the transmitted and reflected waves in the region past the interface and E_{1t} and E_{1r} are the incident and reflected waves in the region before the interface and where

$$A = \frac{i\omega n_1}{c} + \frac{\alpha_1}{2}$$

and

$$B = \frac{i\omega n_2}{c} + \frac{\alpha_2}{2}.$$

Subscripts 1 and 2 refer to the regions before and after the interface, respectively. One also has the boundary conditions that in the very first region $E_t = 1$, and in the very last region, $E_r = 0$. By employing this transfer matrix technique to solve for the electric field throughout the model structure one can, in principle, extend the calculation to as many layers as one wishes. The light intensity was then calculated as the square of the electric field throughout the model structure and was then integrated in the region of GaAs in front of the AlAs barrier and in an equal region behind the AlAs barrier to obtain the total light intensity in each of the two regions. The exact results obtained from these calculations depend somewhat on the size of the regions on either side of the AlAs barrier one chooses to integrate over; however, this does not affect the qualitative nature of the results. The integration also included an integration over the phase of the electric field to account for the incoherence of the light. The total light intensity behind the AlAs barrier was then subtracted from the total in front of the AlAs and this difference was plotted as a function of wavelength. The calculations assume that the absorption properties of the GaAs are those of bulk GaAs at the same doping levels. This is not completely true at the GaAs/AlAs interface where the band bending can drastically alter the free carrier concentration, and thus, the absorption properties of the GaAs layers. The number of optically excited carriers is proportional to the light intensity; thus this calculation helps one understand from where charge carriers are originating.

3.4 EXPERIMENTAL RESULTS

3.4.1 Photovoltage Spectrum

In Figure 3.4 is presented the photovoltage spectrum for Sample 4 at room temperature. The two spectra presented in this figure correspond to two different thicknesses of the top layer of the GaAs. In both cases one should note that there is a substantial signal at wavelengths which correspond to energies less than the band gap of the GaAs (1.424 eV or 8700 Å at room temperature). Also, the sign of the voltage is consistent with electrons moving from the front to the back of the AlAs barrier. The heavy doping causes the band gap to shrink,[13] but it also pushes the Fermi level into the conduction band of the GaAs. For degenerate GaAs the position of the Fermi level above the conduction band minimum can be estimated from

$$\epsilon_f - \epsilon_c = \left(\frac{3N_d\hbar^3\pi^2}{2\sqrt{2}}\right)^{\frac{2}{3}} \frac{1}{m^*}$$

where m^* is the electron effective mass and N_d is the concentration of donors. To obtain this expression it has been assumed that for the degenerately doped GaAs the donor electrons are all in the conduction band. For a doping level of 3×10^{18} cm^{-3} in the GaAs, it is estimated that the Fermi level is 110 meV above the conduction band minimum. The net effect of the band gap shrinkage and the movement of the Fermi level into the conduction band of the GaAs is a net increase in the energy required to take an electron from the valence band into the conduction band. Thus, the energy required to produce holes in this structure would be greater than the band gap of the GaAs. This implies that the photovoltage is not the result of the movement of holes in the GaAs. At wavelengths which might correspond to energies that could promote an electron from the valence band into the conduction band and thus also create a hole, band bending at the GaAs/AlAs interface would cause electron and hole movement which would create a voltage opposite in sign to the one that is observed.

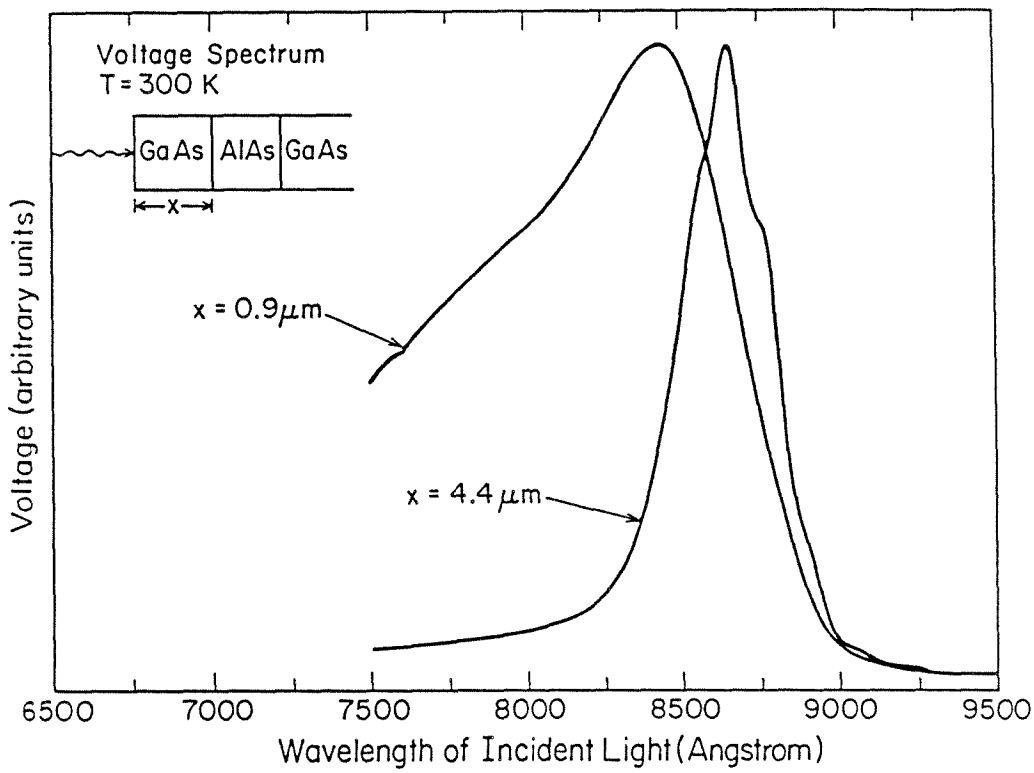

Figure 3.4: Photovoltage spectra taken at room temperature for Sample 4. The AlAs layer was 240 Å thick and the GaAs layers were doped at 3×10^{18} cm^{-3}. The thicknesses of the top layer of GaAs were 4.4 μm and 0.9 μm as indicated.

In Figure 3.5 is presented the dependence of the magnitude of the signal on the incident power for Sample 1. This measurement was made at 6 K and at 7900 Å. As can be seen the curve is quite linear; thus the number of optically excited charge carriers is proportional to the light intensity. On the basis of these observations it was concluded that electrons promoted from the occupied states in the conduction band of the GaAs by free-carrier absorption to energies greater than the GaAs/AlAs conduction band offset flow past this barrier and produce the observed voltages. The difference in light intensity in front of and behind the AlAs barrier creates a difference in the concentration of optically excited electrons on either side of the AlAs barrier. It is this difference in the concentration of optically excited electrons which drives the electron flow from the front to the back of the AlAs barrier and which thus produces the measured photovoltage. Since the number of electrons excited in the conduction band due to free-carrier absorption is proportional to the light intensity, one would expect that the measured photovoltage spectrum would have the same shape as the calculated difference in the light intensity in front of and behind the AlAs barrier.

To explain the general shape of these spectra one may refer to Figure 3.6 which schematically shows the band structure and absorption processes in a sample. The two absorption processes are free-carrier absorption (A) for which the coefficient of absorption is α_A and band-to-band absorption (B) for which the coefficient of absorption is α_B; since free-carrier absorption involves a phonon and direct interband absorption does not, $\alpha_A \ll \alpha_B$. At long wavelengths where the energy of a photon is insufficient to promote an electron from the valence band over the Fermi level, the much weaker free-carrier absorption dominates and there is not a substantial difference between the light intensity in front of and behind the AlAs barrier. There is, thus, a correspondingly small difference in the number of electrons promoted in the conduction band of the GaAs, and one expects to measure a samll signal. At short wavelengths where band-to-band

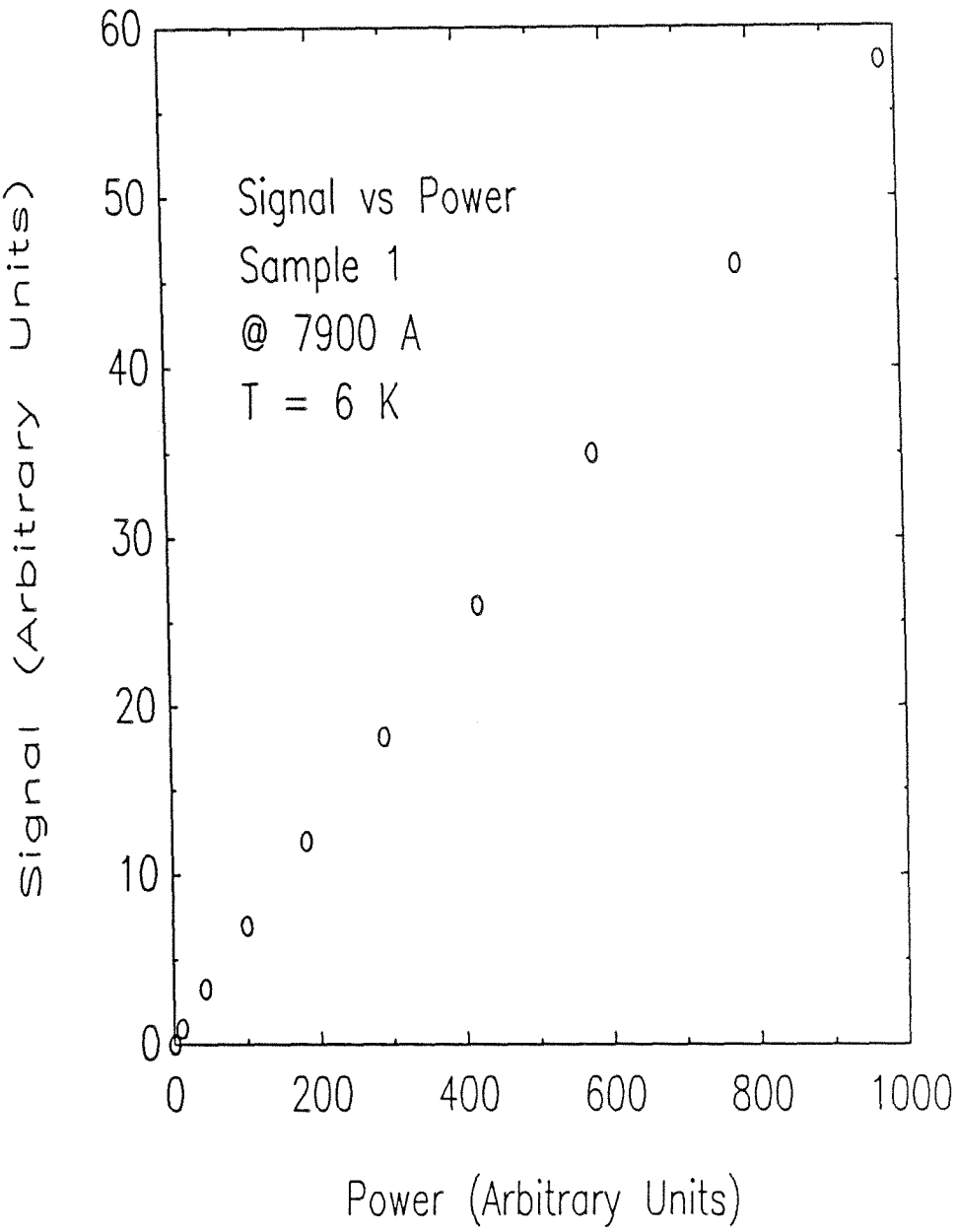

Figure 3.5: Photovoltage signal strength as a function of incident optical power. The very linear dependence implies that the number of electrons involved in producing the photovoltage is proportional to the number of incident photons.

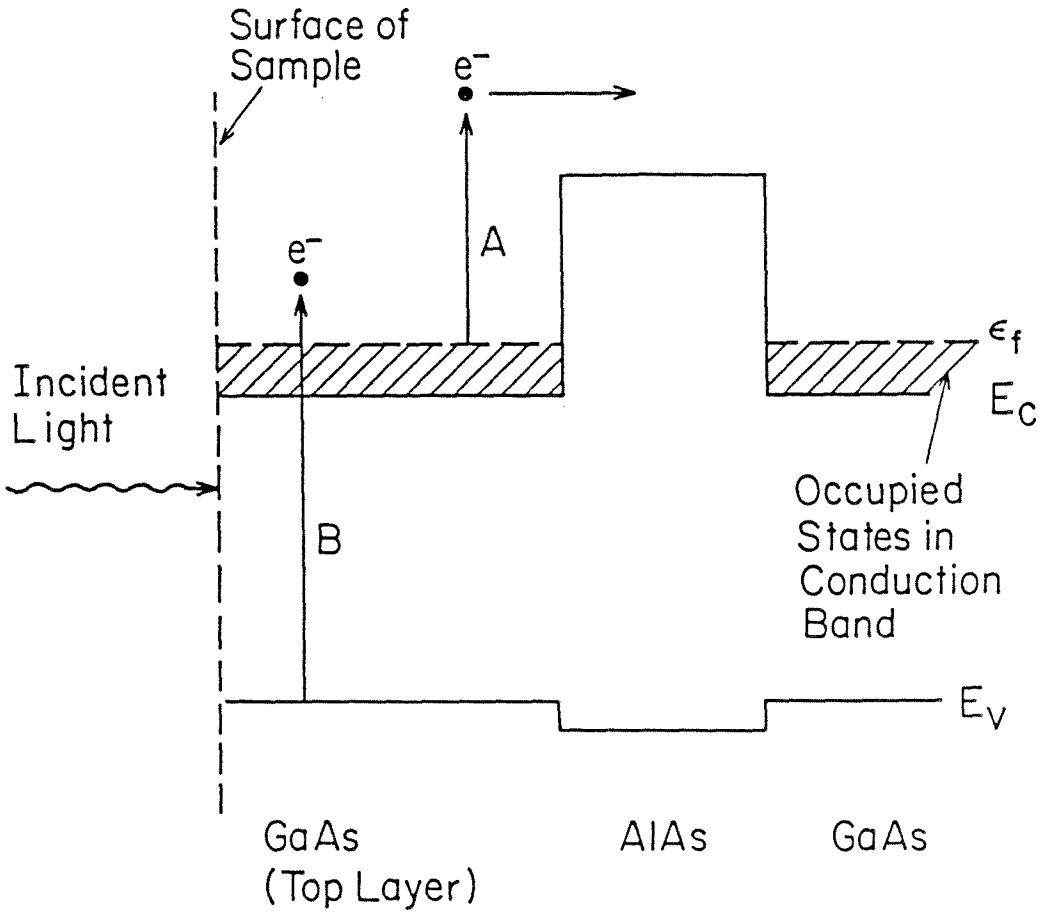

Figure 3.6: Schematic diagram of the conduction band (E_c) and valence band (E_v) edges of the GaAs/AlAs heterostructure showing the Fermi level (ϵ_f) in the conduction band. Indicated in the figure are free-carrier (A) and band-to-band (B) absorption of light by electrons.

absorption is very strong, the light is attenuated very quickly near the surface of the sample, and the difference in light intensity in front of and behind the AlAs barrier is very small, and, again, one expects to measure a small signal. Between these two extremes, one has some wavelength at which the difference in light intensity (and, hence, the concentration of electrons promoted in the conduction band of the GaAs) is a maximum, and one expects to see a maximum signal. One thus has a spectrum with a peak whose position is mainly determined by the optical properties of the sample. To explain the difference in the spectra when there is a thick top layer (5 μm) and thin top layer (1 μm), consider the following. For a sample with a top layer thickness of 5 μm at wavelengths where process B cannot occur (the energy of the light is insufficient to promote carriers from the valence band over the Fermi level), the light intensity is proportional to $e^{-5\alpha_A}$. At shorter wavelengths where process B can occur, the intensity of the light is proportional to $e^{-5\alpha_B}$. Consider the same sample with a thin top layer of 1 μm. The enhancement in the light intensity at wavelengths where process A dominates is proportional to

$$e^{-1\alpha_A}/e^{-5\alpha_A} = e^{4\alpha_A},$$

but at wavelengths where process B dominates (on the short wavelength tail of the spectrum), the enhancement in the intensity of light is proportional to

$$e^{-1\alpha_B}/e^{-5\alpha_B} = e^{4\alpha_B},$$

but since $\alpha_A \ll \alpha_B$, then $e^{4\alpha_B} \gg e^{4\alpha_A}$, and the enhancement in the intensity of the light is much greater at the shorter wavelength tail of the spectrum. Since the number of electrons promoted by process A is proportional to the light intensity, one would expect the voltage signal to be most enhanced at the short wavelength tail of the spectrum. Thus, a spectrum for a sample with a thick top layer will change qualitatively in the way it does in Figure 3.4 when the top layer is made thinner.

In Figure 3.7 are presented the results of the predicted spectrum for a sample with a doping level of 3.3×10^{18} cm^{-3} in the GaAs, which has a 240 Å thick layer of AlAs and which had a top layer thickness of 4.4 μm and 0.9 μm as labeled. This predicted spectrum is the result of the calculations which were described in Section 3.3. It can be seen that since the absorption coefficient data contain in it the effects of band-to-band and free-carrier absorption, the qualitative nature of the spectrum is correctly predicted. One can note, however, that the peak position (in the case of the thick top layer) and the turnoff wavelength (in the case of the thin top layer) are not exactly predicted by the calculations though they are in fairly good agreement. These positions depend very much on the doping of the sample used in the experiment. In the calculations these positions depend on the behavior of the coefficient of absorption, α, which in turn depends on the doping and which differs from the actual doping of the samples. In the calculations, a constant doping profile was assumed while in the actual samples the doping in the GaAs is a function of position. However in general one can see that both the qualitative and quantitative descriptions of the photovoltage spectrum are in good agreement with the actual spectrum. The origin of the undulations seen on the experimental spectra will be discussed below.

3.4.2 Long Wavelength Edge

The difference in light intensity in front of and behind the AlAs barrier creates a difference in the concenration of optically excited electrons on either side of the AlAs barrier. It is this difference in the concentration of optically excited electrons which drives the electron flow from the front to the back of the AlAs barrier and which, in turn, produces the voltage that is measured. Calculations by C. Mailhot et al.[14] have shown that it is the Γ-point offset between the AlAs and the GaAs which determines the energy barrier presented

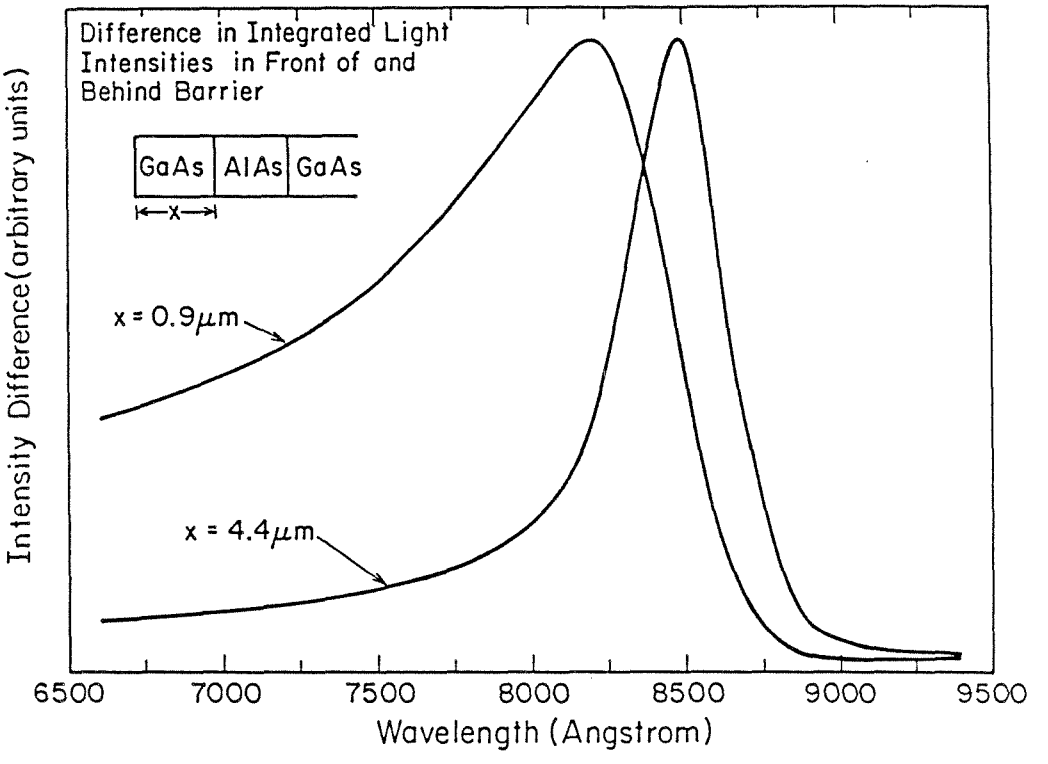

Figure 3.7: Calculated difference in the integrated light intensities in front of and behind the AlAs barrier as a function of wavelength. The coefficient of absorption, α, used in the calculation was for a GaAs n-type doping of 3.3×10^{18} cm^{-3} at room temperature. The results are presented for a top layer thickness of 4.4 μm and 0.9 μm as indicated in the figure.

to an electron in the GaAs. This is significant since these samples were grown in the < 100 > direction, and one might expect that it is the lower X-point of the AlAs which determines the barrier. The energy required to take an electron over this barrier is less than the full conduction band offset due to the fact that the Fermi level is above the conduction band minimum but is increased by the effects of band gap shrinkage in the GaAs due to the heavy doping, and is also affected by band banding in these structures. The energy required to promote an electron over this barrier also depends on the relative change in the band gaps of GaAs and AlAs as the temperature is varied. There is a controversy regarding the value of the conduction-band energy-gap discontinuity between the GaAs and the AlAs.[15] At room temperature if the offset is 60% of the total energy-gap discontinuity, the barrier presented to an electron would be about 0.95 eV. One may then ask why no appreciable signal is measured at long wavelengths that still correspond to energies greater than this barrier ? One does not observe a photovoltage when there is no difference in the number of optically excited electrons in front of and behind the AlAs barrier. Thus, there is an observable signal as long as there is a difference in the light intensity in front of and behind the AlAs barrier. The wavelength at which there ceases to be such a difference may correspond to an energy that is substantially greater than the barrier presented to an electron due to the conduction band offset between the AlAs and the GaAs. Thus, the cut-off in the spectrum presented in Figure 3.4 at long and at short wavelengths is determined by the optical properties of the structure and not the by conduction-band offset.

3.4.3 Temperature Dependence

In Figure 3.8 is presented the photovoltage spectrum for Sample 1 with a 4.0 μm thick top layer of GaAs at various temperatures. As can be seen, the peak of the photovoltage spectrum shifts to longer wavelengths for increasing

temperature. It is band-to-band and free-carrier absorption which determines the nature of the optical absorption in the GaAs and which, in turn, determines the peak position. Thus, as temperature increases, since the band gap of the GaAs decreases, the shift of the peak position to longer wavelengths is a reflection of the shift to lower energies of the band-to-band absorption edge. The band gap of GaAs, as a function of temperature, can be approximated by[16]

$$E_g = 1.519 - 5.405 \times 10^{-4} T^2/(204 + T) \text{ eV}.$$

To see whether the shift in the peak position follows the change in the band gap, one proceeds as follows. The half-maximum position on the shorter wavelength edge of the peak is chosen as an indication of the peak position. One can then plot the change in peak position referenced to its position at 6 K versus the change in the band gap referenced to its value at 6 K. If then the shift in the peak position is indeed a reflection of the change in the band gap, this plot would be a straight line with unit slope passing through the origin of such a plot. In Figure 3.9 is presented this plot. It can be seen that there is the behavior that one would expect, though the band gap tends to initially change slightly faster that the peak position. This difference between the movement in the peak position and the change in the band gap results from two sources. The first is the inaccuracy in assigning a value to the peak position at different temperatures especially at the lower temperatures where the changes are smaller. The second is the fact that as the temperature is increased, the electron distribution in the conduction band of the GaAs is thermally broadened. This also affects the position of the fundamental absorption edege in the GaAs and hence the peak position. This effect has not been taken into account in the plot presented in Figure 3.9. One can, however, conclude that the shift in the position of the peak in the photovoltage spectrum is a reflection of the change in the band gap of the GaAs. Thus again, one sees how the optical properties of the structure can determine the nature of the photovoltage signal. This being the case one might

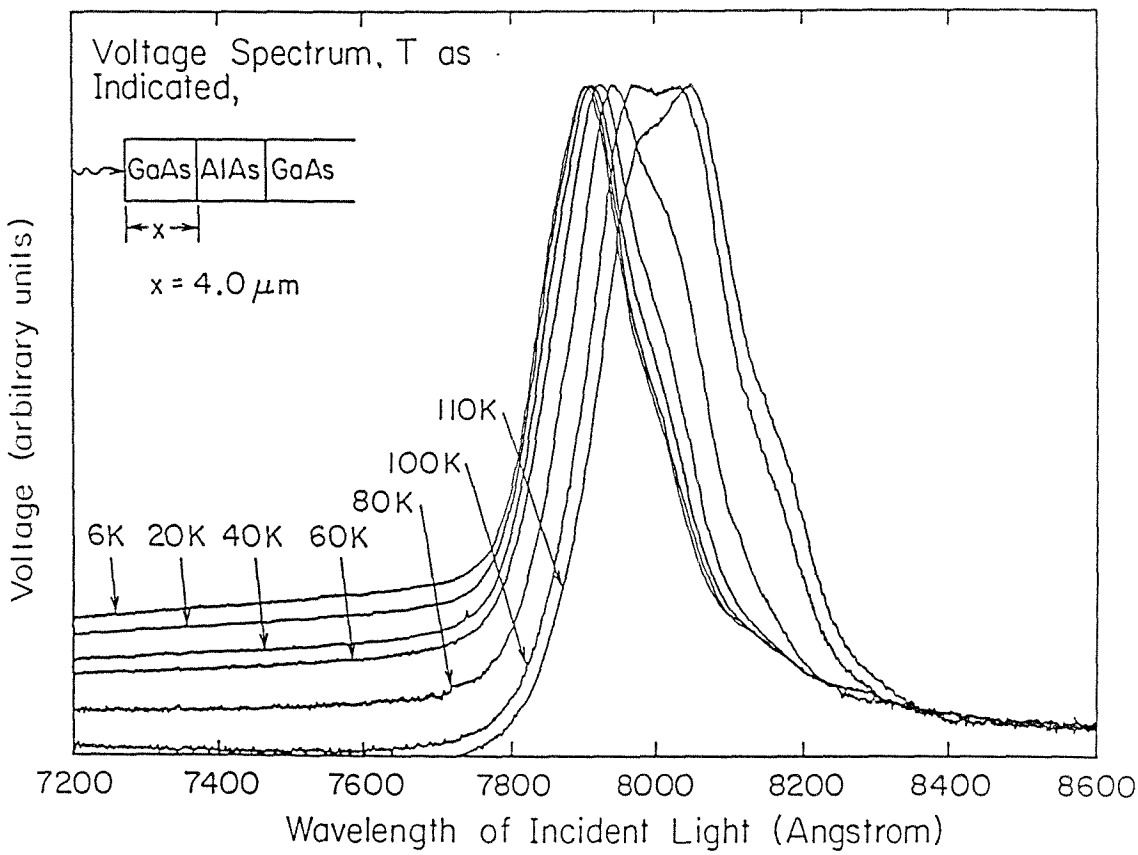

Figure 3.8: Photovoltage spectrum for Sample 1 at the temperatures indicated. The GaAs layers were doped n-type at 5×10^{18} cm-3 with the top layer of GaAs 4.0 μm thick and the AlAs layer 160 Å thick.

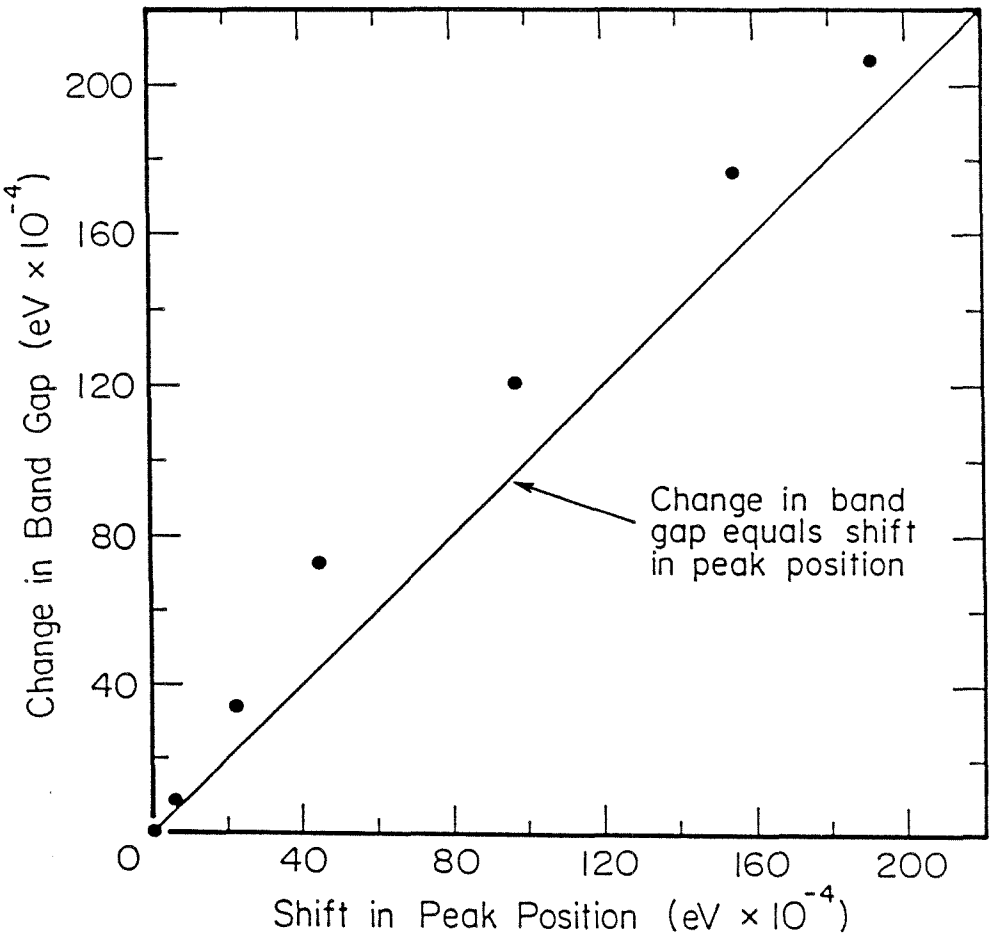

Figure 3.9: Change in the band gap versus the shift in the peak position in the photovoltage specturm of Sample 1 as a function of temperature. The straight line indicates the values for the change in the band gap equal to the shift in the peak position.

expect that the doping in the GaAs would affect the photovoltage spectrum and this is discussed below.

3.4.4 Doping Dependence

The effects of the doping in the GaAs on the photovoltage spectrum were studied by looking at four different samples of varying AlAs layer thicknesses and GaAs dopings. In Figure 3.10 are presented the photovoltage spectra for these four different samples at 80 K. While it is clear that there are differences in the spectra from sample to sample, one can nonetheless identify and explain the relative peak positions. One can see that in Figure 3.10 the peak positions for Samples 5 and 4 are the same though shifted to longer wavelengths than the photovoltage spectra of Samples 3 and 1. In Figure 3.11 are presented the results of the calculations for the light intensity difference in front of and behind the AlAs layer corresponding to various dopings in GaAs regions as idicated. These curves would correspond to spectra obtained at room temperature since the behavior of α was taken from data obtained at room temperature. The restriction to carrying out these calculations at room temperature and for these particular doping levels in the GaAs results from the fact that the only data available for the behavior of α in heavily doped GaAs are those which were obtained from Reference 11. In the calculations, the AlAs and GaAs layer thicknesses were kept constant. This was done in order to isolate the effects of the doping level on the photovoltage spectrum. One can see that the peak positions shift to shorter wavelengths as the doping in the GaAs is increased. The difference in the peak position is about 180 Å when the doping level is changed from 3.3×10^{18} cm^{-3} to 6.7×10^{18} cm^{-3} in the GaAs. Since these calculations were performed for data corresponding to room temperature and the experiment at 80 K, one would expect the absolute positions of the peaks in the experiment to be at shorter wavlengths than in the calculations, but

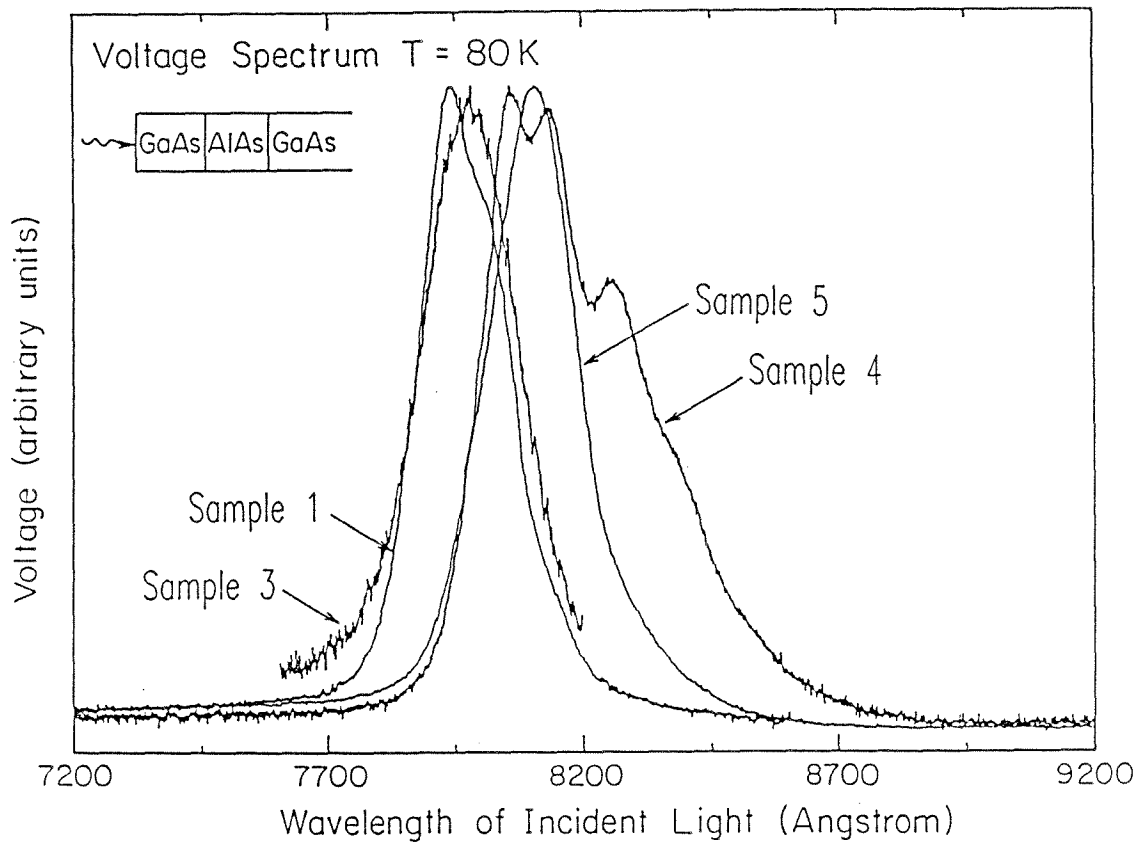

Figure 3.10: Photovoltage spectra for Samples 1, 3, 4, and 5 at 80 K, illustrating the relative peak positions. The band gap of GaAs at 80 K is about 1.51 eV (corresponding to about 8230 Å); Samples 4 and 5 show signal at wavelengths corresponding to energies below this value.

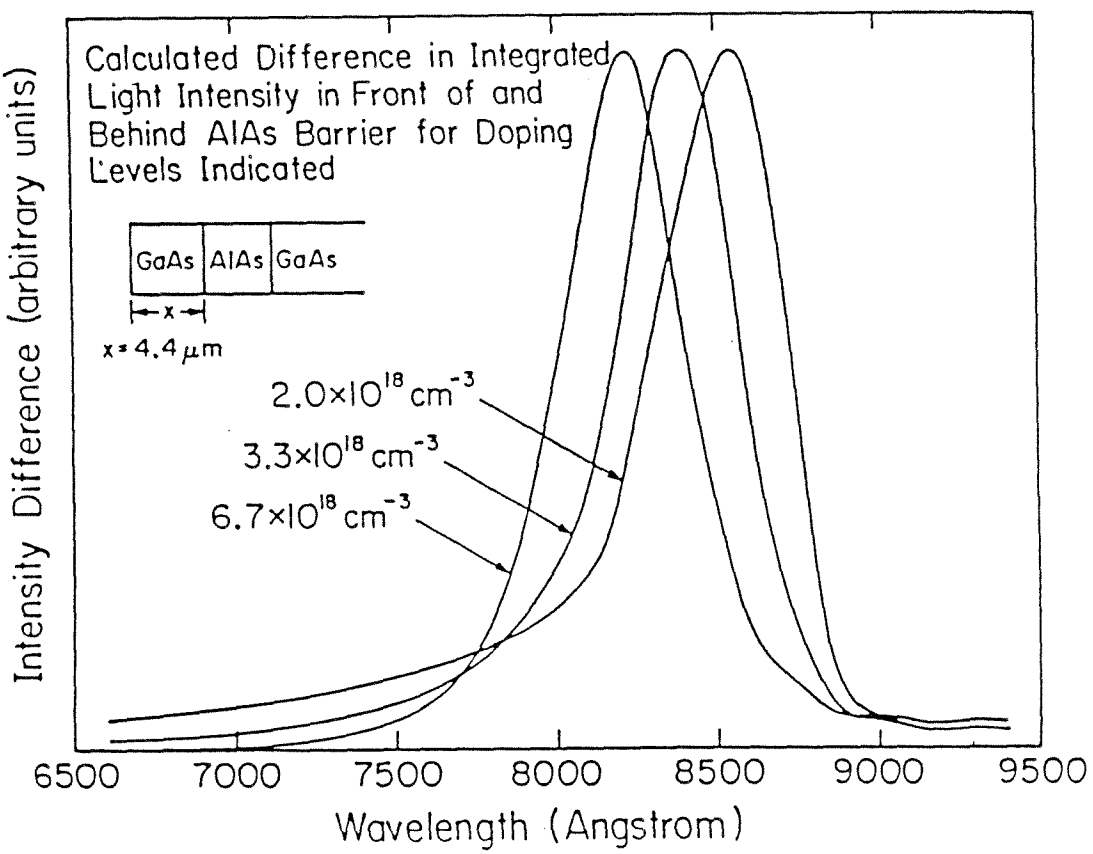

Figure 3.11: Calculated difference in the integrated light intensities in front of and behind the AlAs barrier as a function of wavelength. The model in all three cases was for a top layer of GaAs which was 4.4 μm thick and and AlAs layer thickness of 240 Å. The coefficient of absorption, α, used in the calculation was for a GaAs n-type doping of 2×10^{18} cm^{-3}, 3.3×10^{18} cm^{-3}, and 6.7×10^{18} cm^{-3} as indicated in the figure.

one would expect the relative peak positions for similar differences in doping levels to be the same. One can see that in Figure 3.10 the experimental peaks are at shorter wavelengths than the calculated peaks (Figure 3.11), due the temperature difference as expected. One should also note that the peaks in the spectra for Samples 3 and 1 which are both doped at 5×10^{18} cm^{-3} are at the same position and are at shorter wavelengths than the peaks in the photovoltage spectra for Samples 5 and 4. This is consistent with the fact that Samples 3 and 1 are more heavily doped in the GaAs region than Samples 5 and 4 which were doped at about 3×10^{18} cm^{-3}. The peaks for Samples 5 and 4 are also at the same position, and, this, too, is consistent with the fact that they have similar doping levels in the GaAs regions. The difference in the positions of the peaks in the experimental case is about 125 Å, and this is consistent with the predicted difference in the peak positions when one considers the fact that the difference in doping levels used in the calculations is larger than the difference in doping levels in the actual samples. Changing the AlAs layer thickness over the range found in these samples, while maintaining a constant doping level, does not result in such shifts in the peak positions.

3.4.5 Zero Bias Impedance

Larger voltages are generally observed for samples with larger zero-bias impedances. By zero-bias impedance is meant the slope of the voltage versus current curve at the origin. As samples are cooled from room temperature, their zero-bias impedances increase, and we observe that, in general, for a given sample, we measure a larger voltage at lower temperatures. Sample 3, for example, has a zero-bias impedance of about 37kΩ at 4.2 K, while Sample 4 has a zero-bias impedance which we can only estimate to be greater than 500MegΩ at room temperature. The experiment is an open circuit measurement of the voltage across the barrier. Hence, there is no net current through the barrier.

The light, which illuminates the samples at any given wavelength and for a given intensity, produces a constant number of electrons per unit time which can flow through the AlAs barrier and produce the photovoltage which is measured. This is asserted on the basis of the fact that the signal that is measured is proportional to the intensity of the illuminating light. As these electrons move to the back side of the barrier, a voltage is set up which tends to drive electrons from the back side to the front side of the barrier. In steady state these two currents must balance each other. The measured voltage is given by the sample impedance times the fixed current due to the light and is thus larger in samples with larger zero-bias impedances. Sample 4 is an exception to this trend, in that as it is cooled its zero-bias impedance increases as with all the samples, but the voltage we measure decreases. The above explanation breaks down, but currently there is not a a satisfactory explanation for this.

3.4.6 Capacitive and Resistive Impedance

In Figure 3.12 is presented a diagram of the circuit which was used to measure the capacitive and resistive impedance of the samples as a function of the wavelength of the incident light. Z is a complex impedance which in the case of the sample would be a capacitor and resistor in parallel. r is a small resistor such that $r \ll R_l$ where R_l is the lock-in amplifier. The ac voltage source provides a voltage at frequency $\frac{\omega}{2\pi}$. The current flowing through Z and r is

$$\frac{V}{Z+r} \simeq \frac{V}{Z} \quad \text{if} \quad |r| \ll |Z|.$$

The voltage measured by the lock-in amplifier is then $\frac{V}{Z}r$. Now if Z is a capacitor, then $Z = \frac{-i}{\omega C}$ and the phase associated with this voltage is purely imaginary. If Z is a resistor, then $Z = R$ and the phase of the voltage measured across the lock-in amplifier is purely real. By first replacing Z by a capacitor or a resistor one can calibrate the phase of the lock-in amplifier to pick off the voltage across r associated with the capacitive or resistive part of the impedance Z. Thus,

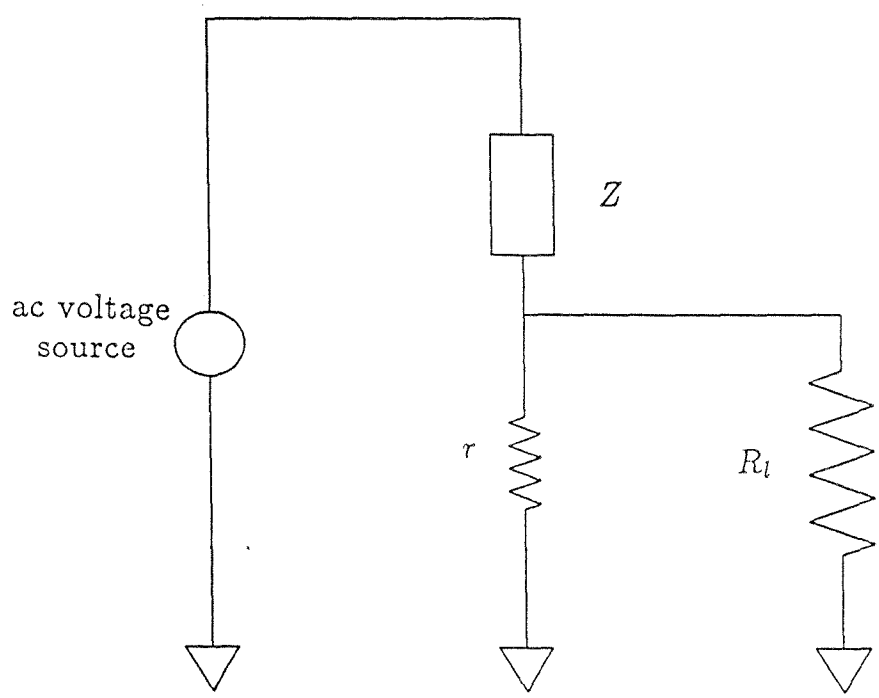

Figure 3.12: Circuit which was used to measure the capacitive and resistive impedances of a sample represented here by Z, as a function of the wavelength of the incident light. R_l is the lock-in amplifier and r is a small resistor.

when Z is replaced by the sample one can make a measurement of its resistive or capacitive impedance as a function of wavelength. The frequency of the voltage source is the frequency at which the measurement is made. Actually, as can be seen above one measures a voltage which is proportional to the reciprocal of Z.

In Figure 3.13 is presented a plot of the resistive and capacitive impedance of Sample 4. This measurement was made at 300 K and at 50 Hz. This frequency was chosen so that the magnitude of the resistive and capacitive impedance of the sample would be comparable. Typically, the capacitance of these samples was about 30 pf. One can see that the capacitve impedance of the sample is constant as a function of wavelength. The resistive impedance changes as a function of wavelength. In fact, the changes in the resistive impedance produce a spectrum which looks a great deal like the photovoltage spectrum of this sample. When a photovoltage is developed across the sample, this photovoltage biases the sample. When the sample is biased, its resistive impedance is the slope of the voltage versus current curve at that bias. These samples have their maximum resistive impedance at zero bias. Thus, when a photovoltage is developed across a sample, its resistive impedance decreases and the magnitude of the decrease in the resistive impedance is proportional to the magnitude of the photovoltage. One therefore would expect the resistive impedance of the samples to change as function of wavelength and produce a spectrum similar to the photovoltage spectrum. This change in the resistive impedance of the sample as a function of wavelength has implications for the photovoltage measurement which will be discussed below. The fact that the capacitive impedance is constant is an indication that deep levels are not playing a major role in the mechanism that creates the photovoltage.

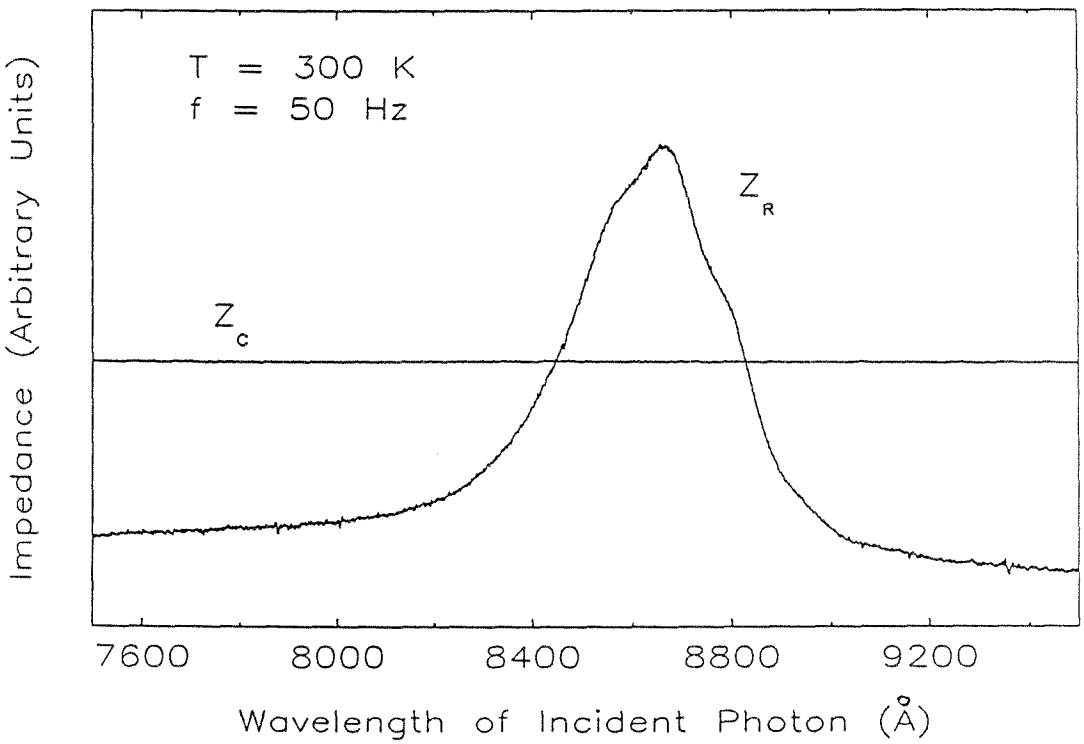

Figure 3.13: Resistive (Z_R) and capacitive (Z_C) impedances of Sample 4 as a function of the wavelength of the incident light at 300 K and 50 Hz. The capacitive impedance does not change while the resistive impedance changes in a manner similar to the photovoltage spectrum.

3.5 TRANSMISSION COEFFICIENT

In the experimental spectra presented above, one can see undulations which are not as marked but are nonetheless visible in the calculated spectra. These undulations are reproduced from device to device across a given wafer in terms of their amplitudes but not necessarily in terms of their positions. Possible origins for these undulations are discussed below. The origin of the observed voltages has been attributed to electrons flowing past the barrier presented by the AlAs layer. One might conclude then that the undulations are a reflection of the variation of the transmission coefficient of the electrons flowing past this finite potential barrier. For a one-dimensional potential barrier of height, V_0, and width $2a$, one can solve for the transmission coefficient, T, for an electron flowing past this barrier. This is done by considering only plane waves and solving the time independent Schrodinger equation. Since in this case the mass of the electron is different inside and outside the potential barrier, the boundary conditions at an interface say, $x = a$, are

$$\psi_1(x = a) = \psi_2(x = a)$$

$$\frac{1}{m_1}\frac{\partial \psi_1}{\partial x}(x = a) = \frac{1}{m_2}\frac{\partial \psi_2}{\partial x}(x = a).$$

If the energy of an electron is E, then for $E > V_0$ the transmission coeffient for an electron is given by

$$T = \frac{1}{\cos^2(2k_2a) + \frac{1}{4}\left(\frac{m_1}{m_2}\frac{k_2}{k_1} + \frac{m_2}{m_1}\frac{k_1}{k_2}\right)^2 \sin^2(2k_2a)}$$

with

$$\hbar k_1 = \sqrt{2m_1E}, \quad \hbar k_2 = \sqrt{2m_2(E - V_0)}.$$

In this case region 2 would be the AlAs and hence m_2 is the effective mass of electrons in the AlAs, m_1 is the effective mass in the GaAs cladding regions.

For energies $E < V_0$, one has

$$\hbar K_2 = i\hbar k_2 = \sqrt{2m_2(V_0 - E)}$$

and the expression for the transmission coefficient is changed appropriately. In Figure 3.14 is presented the transmission coefficient as a function of electron energy for a barrier which is 240 Å wide and 1.35 eV high. The electron energy is merely the photon energy which has been converted here to photon wavelength. Indeed, strong undulations are evident in the transmission coefficient. However, when considering this problem one must try to take into account the three dimensional nature of the structure. This means that the electrons in the conduction band of the GaAs are distributed in a three-dimensional band. In Figure 3.15 is presented a parabolic approximation to the conduction band of the GaAs. The electrons are distributed from the conduction band minimum to the Fermi energy and there is a density of states associated with this distribution which is given by[17]

$$D(\epsilon) = \frac{\sqrt{2m_1^3(\epsilon - \epsilon_c)}}{\hbar^3\pi^2}.$$

When a photon is incident on the GaAs it may excite an electron from any of the occupied electron states. Further, this electron may be excited into a state with any possible $k_\perp$ and $k_{||}$. There is a density of states associated with these k-vectors given by

$$D(k_\perp, k_{||}) = \frac{k_{||}}{2\pi^2}.$$

Neglecting any transition rules which may exist for these excitations, one can nonetheless calculate the transmission coefficient taking these effects into account. For any particular wavelength, hence energy, of photon, one averages the transmission coefficient for all the energies possible from which an electron may be excited and all the $k_\perp$ to which an electron may be excited. It is $k_\perp$ which is important in getting past the barrier and $\vec{k}$ conservation is assumed. The resulting transmission coefficient as a function of photon wavelength is presented

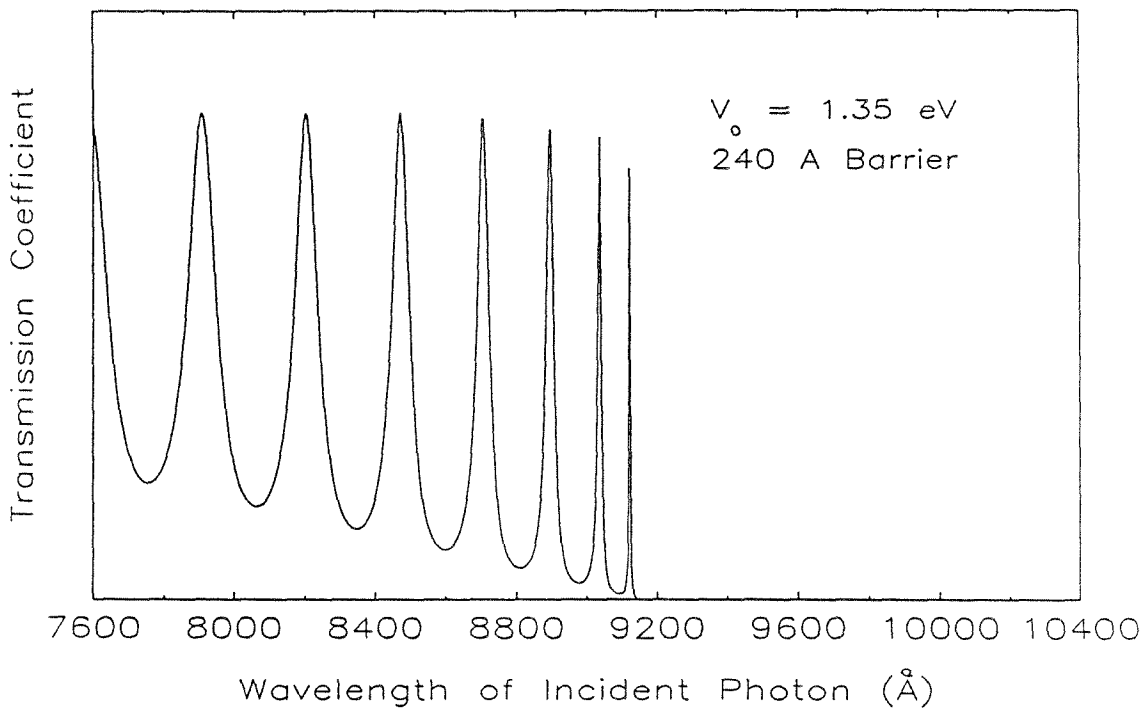

Figure 3.14: Transmission coefficient for an electron incident on a one-dimensional energy barrier. The energy of the electron has been converted into a wavelength for the incident photons. The electron effective mass outside the barrier was taken to be that of GaAs and in the barrier that of AlAs. The transmission coeffiecient oscillates between 1 and values less than 1.

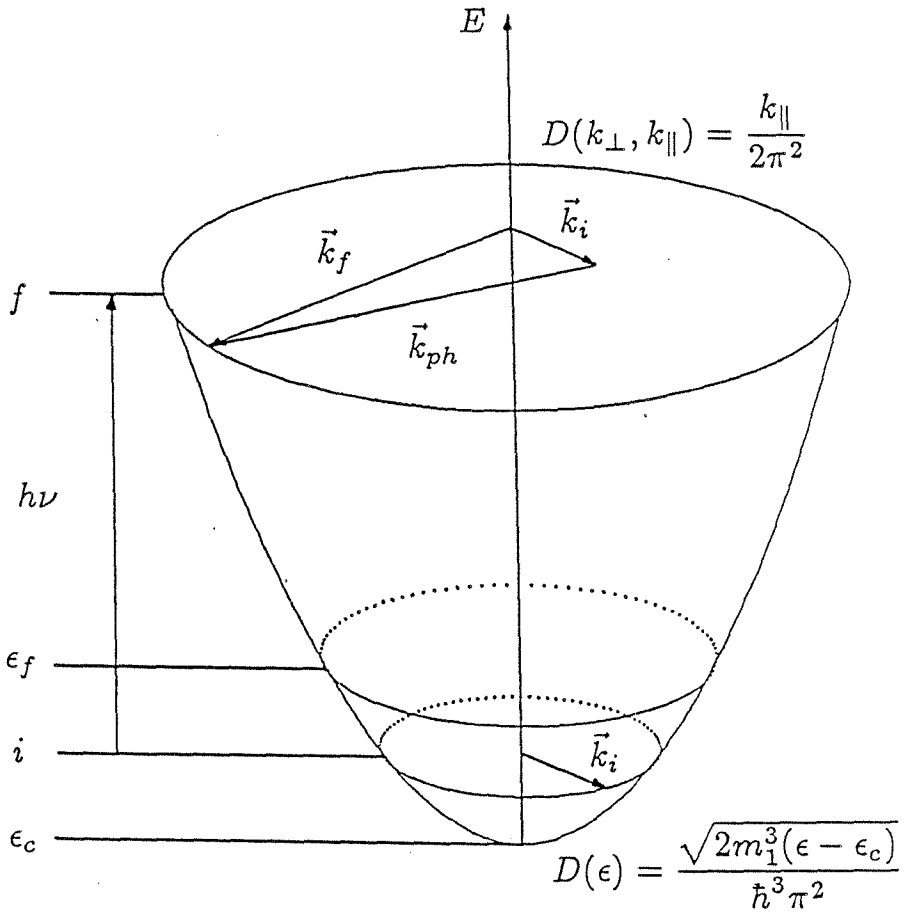

Figure 3.15: Schematic representation of the conduction band of GaAs. A photon of energy $h\nu$ may excite an electron from any state between ϵ_c and ϵ_f weighted by the density of states $D(\epsilon)$. The electron may be excited into a state with some arbitrary $k_\perp$ weighted by the density of states $D(k_\perp, k_\parallel)$.

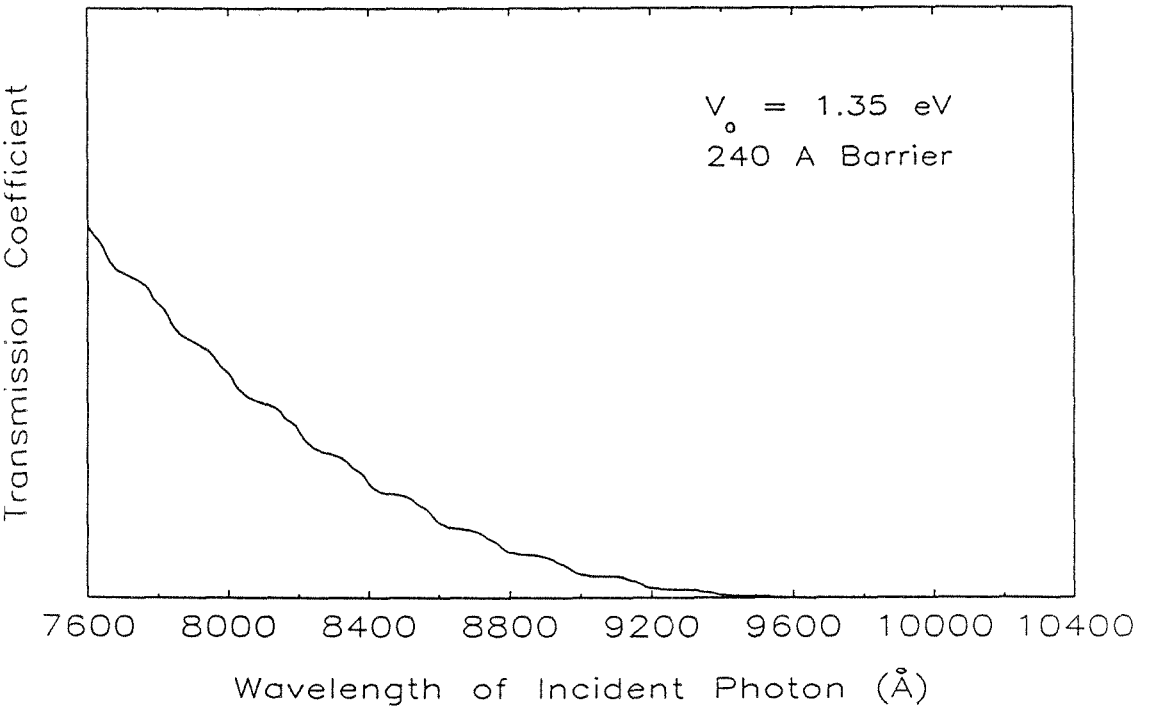

Figure 3.16: Transmission coefficient for an electron incident on a one-dimensional energy barrier. For any given incident photon energy the various states from which and to which an electrom may be excited has been taken into account. The oscillations of Figure 3.14 have clearly been reduced.

in Figure 3.16. It is evident that the undulations are decreased significantly in amplitude compared with those in Figure 3.14. One could also average over the possible variations in barrier thicknesses which may exist in any one device in the samples. This would further reduce the size of these undulations. It seems unlikely, then, that the undulations seen on the spectra are in fact due to transmission coefficient oscillations.

It has also been observed that the undulations disappear when the top layer of GaAs is made thinner. This together with the above argument leads one to conclude that the undulations are in fact due to etalon effects in the structure. These effects could result from nonuniformities in the structure such as variations in doping which in turn change the index of refraction of the material or they could be due to the changes in the index of refraction between the GaAs and AlAs. For a Fabry-Perot etalon the separation between fringes is given by[18]

$$\Delta\lambda = \frac{\lambda^2}{2nd},$$

where d is the thickness of the etalon and n is the index of refraction. In Figure 3.10 the separation of the undulations on the spectrum for Sample 4 is about 80 Å. This would require an etalon thickness of about 12 μm which is characteristically the height of the mesas and comparable also to the total thickness of the growth on the substrate. Reducing the etalon thickness would cause the undulations to separate farther apart and this may explain why they disappear when the top layer of GaAs is made thinner. It is therefore not unreasonable that the origin of the undulations is etalon fringes.

3.6 PHOTOVOLTAGE WITH EXTERNAL BIAS

In Figure 3.17 are presented photovoltage spectra for Sample 6 at 6 K and 300 K with the applied biases noted in the figure. These spectra have been scaled so as to display the relative signal strengths. One notes, first, a large

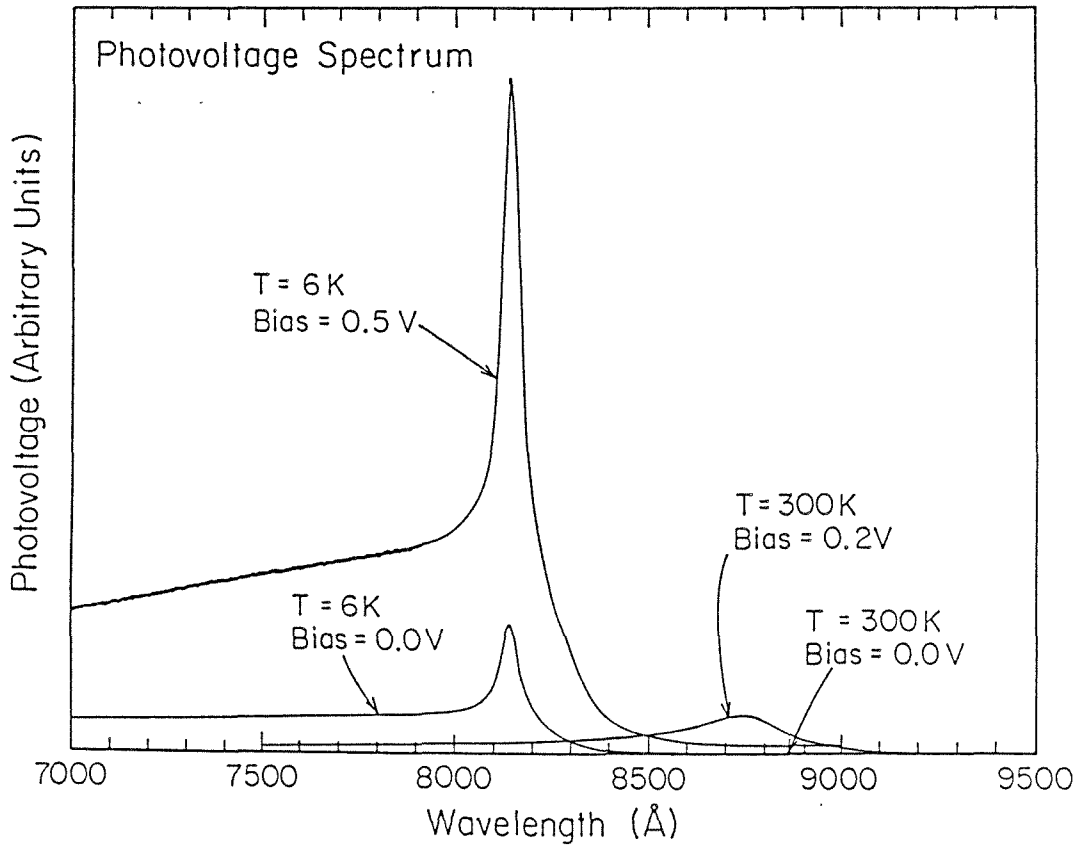

Figure 3.17: Photovoltage spectra for Sample 6 at the temperatures and under the biases indicated. The AlAs layer was 200 Å and the GaAs layers were doped n-type at 5×10^{17} cm^{-3}.

increase in the signal at 6 K (approximately 5 times) with the applied bias as compared to the signal when no bias is applied. At 300 K one sees that with the application of a dc bias, one measures a photovoltage signal which cannot be measured above the noise level without the application of the bias. Note also that in general one observes a greater photovoltage for a greater applied bias. It is unlikely that exciton absorption is the process that creates the charge carriers which produce the photovoltage since the GaAs is degenerately doped. It has been proposed above that the mechanism for the production of the photovoltage is the flow of electrons across the AlAs barrier. These electrons were optically excited to energies greater than that presented by the AlAs barrier. It was proposed that the driving force for the flow of the electrons was the difference in concentration of optically excited electrons on either side of the barrier and that this concentration difference was a result of the integrated light intensity difference on either side of the barrier. To account for the increase in signal under a non-zero applied dc bias the following mechanism is proposed.

The dc bias causes a certain amount of accumulation of electrons to take place on one side of the barrier and causes a depletion of electrons on the other side of the barrier. This charge redistribution takes place very near (within 100 Å) the barrier so that the bulk optical properties of the structure are not greatly affected for small biases (0.5 V or less). However, now, when there is a difference in the integrated light intensity on either side of the barrier, there is an even greater difference in the number of electrons which can be optically excited and then flow across the barrier. This enhanced difference in the number of electrons excited on either side of the barrier causes the enhanced photovoltages which one observes. The conclusion that the bulk optical properties of the samples are not greatly affected by the application of small biases (less than 0.5 V), is a result of the fact that the spectra for samples under bias and not under bias look very much the same except for their relative magnitude. This is seen in the top panel of Figure 3.18. It has been observed that when the sign of the

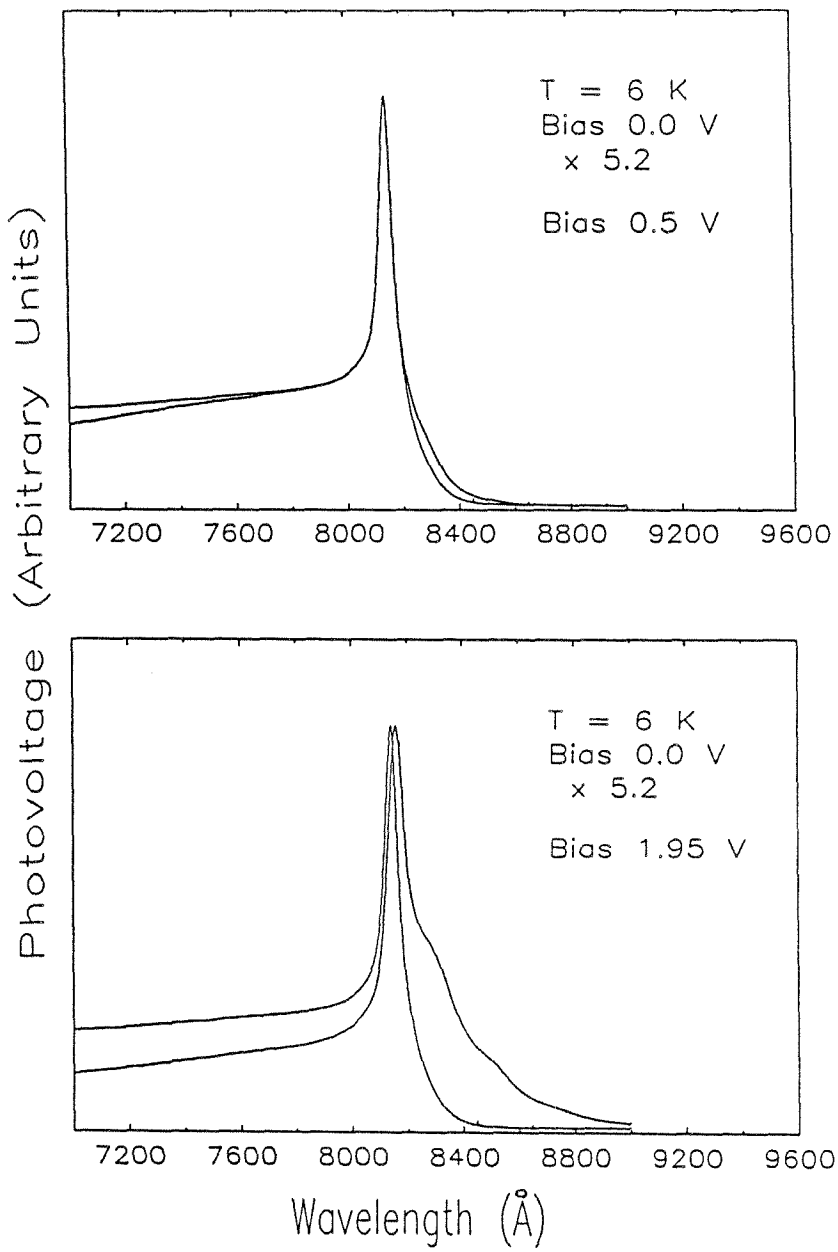

Figure 3.18: Photovoltage spectra for Sample 6 at 6 K. In the top panel the spectrum obtained with no external bias is compared to that obtained with a small, 0.5 V, bias. As can be seen there is not much difference. In the bottom panel the spectum obtained with no bias is compared to that obtained with a large, 1.95 V, bias. As can be seen there is a slight shift of the spectrum to longer wavelengths and a long wavelength tail has developed on the spectrum.

applied dc bias is reversed, the sign of the photovoltage is reversed. It has also been observed that when the samples are biased with the illuminated side of the barrier negative and the back of the barrier positive (accumulation on the illuminated side), a stronger photovoltage is measured than when the sign of the dc bias is reversed. The overall shift of the spectra between 6 K and 300 K results from the change in the band gap of the GaAs which determines its fundamental absorption edge. This, in turn, determines at which wavelength there is the greatest difference in the light intensity in front of and behind the barrier. This has been discussed above.

In Figure 3.19, are presented the photovoltage spectra for Sample 2 at 6 K and 300 K. In this sample, there is no measurable signal above the noise when no bias is applied. Again, these spectra have been plotted so as to represent the relative magnitudes of the signals. One may note in this figure as well as in Figure 3.17 that the peak seen at 300 K is broader than that at 6 K. This is a result of the fact that at higher temperatures the electron distribution in the conduction band of the GaAs is broadened out due to the thermal energy of the electrons. This broadens the fundamental absorption edge of the GaAs. Hence, the wavelengths where there is a maximum difference in the light intensity on either side of the AlAs barrier are spread out.

In the bottom panel of Figure 3.18, are presented two photovoltage spectra for Sample 6 both taken at 6 K, but one for zero applied dc bias and the other for an applied dc bias of 1.95 V. This applied bias is substantially larger than those applied in the spectra presented in the top panel of Figure 3.18 and Figure 3.17. In this figure, the spectra have been normalized so as to have the same apparent magnitude. There are two points of particular interest in this figure. The first is the shift of the peak position to slightly longer wavelengths in the photovoltage spectrum, which was taken with the applied bias as compared to that taken with no applied bias. The second is the very pronounced signal at long wavelengths past the peak that is developed on the spectrum. The signal on

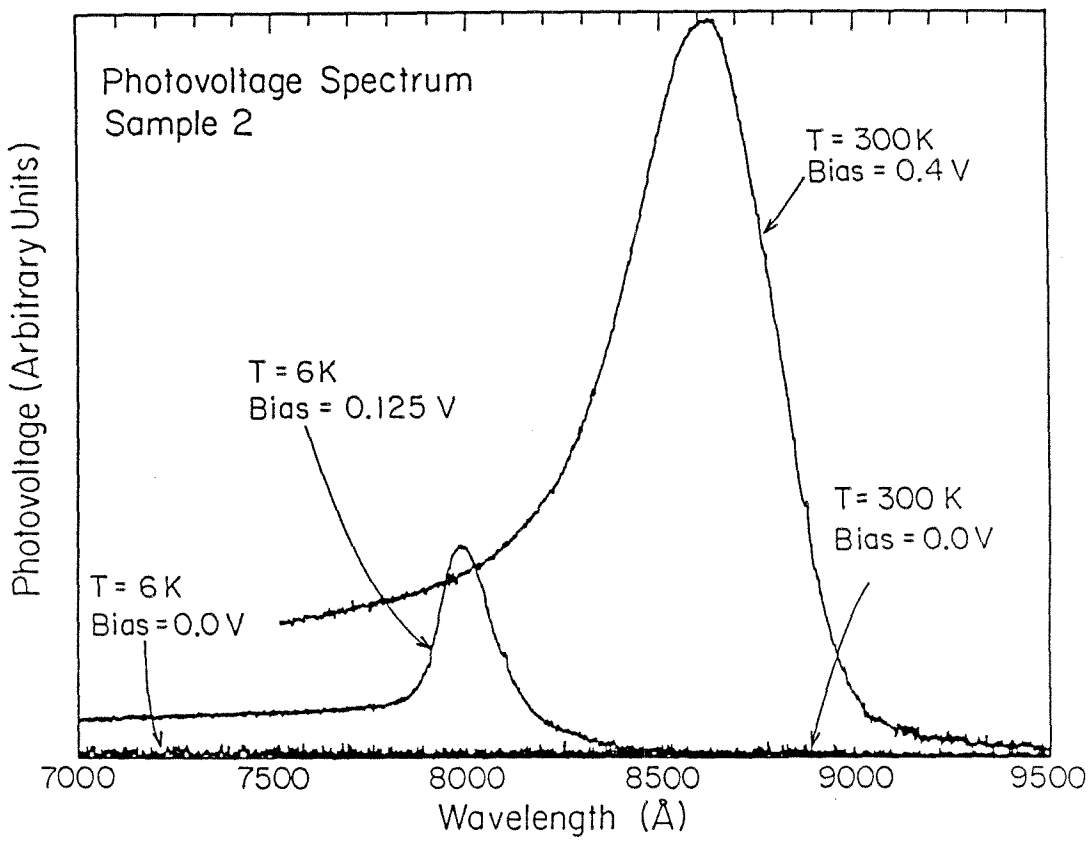

Figure 3.19: Photovoltage spectra obtained for Sample 2 at the temperatures and with the external biases indicated. The AlAs layer thickness was 50 Å with the GaAs doped at about 4×10^{18} cm^{-3}. There is no measureable signal above the noise when no external bias is applied. Note also the increase in the width of the peak for higher temperatures.

this tail is much below the GaAs band gap at 6 K, which is about 8162 Å. Both of these features can be explained in terms of the Franz-Keldysh effect, that is, the band gap narrowing that takes place in the depleted GaAs as a result of the presence of the large electric fields which are present due to the applied bias.[19] This effect is discussed in more detail below. When this happens, the optical absorption edge in this region of the GaAs is moved to longer wavelengths. Thus, the wavelengths at which there is a difference in the number of optically excited electrons on either side of the barrier are shifted to longer wavelengths and so is the resulting photovoltage spectrum which is measured. The long wavelength tail results from the fact that on the side of the AlAs barrier where accumulation takes place, electrons are excited by free-carrier absorption while for the same wavelength on the depleted side of the AlAs barrier band-to-band absorption dominates. One thus has a difference in the number of electrons excited by free-carrier absorption on either side of the barrier at a wavelength where one did not have such a difference at zero bias. As the wavelength is increased further, this effect decreases thus producing the decrease in the signal as seen towards longer wavelengths. The undulations seen on the long wavelength tail of the spectrum in the lower panel of Figure 3.18 for the sample under bias is not predicted by the Franz-Keldysh effect. These undulations are probably the result of the same sort of optical etaloning taking place in the sample that has been discussed previously. The applied external bias creates a charge redistribution as discussed above which contributes to changes in the index of refraction in the sample.

3.7 FRANZ-KELDYSH EFFECT

The Franz-Keldysh effect is the effective band gap narrowing due to very high electric fields. In Figure 3.20 are shown the conduction band edge and valence band edge of a semiconductor with and without the presence of an electric field. In the top half of the figure we see that to take an electron

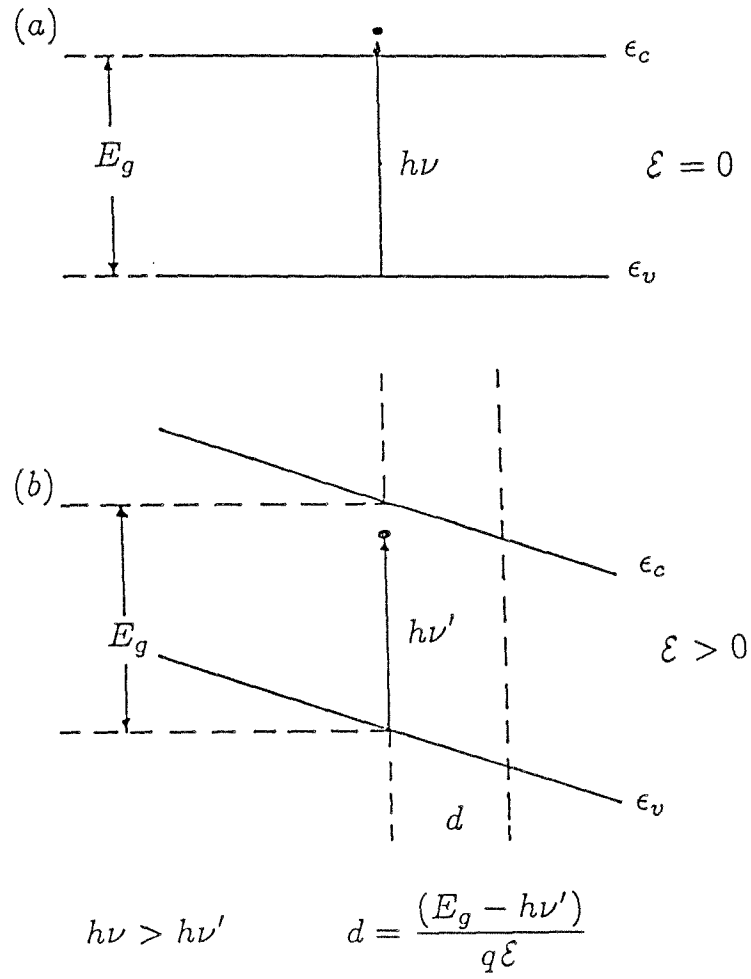

Figure 3.20: Schematic diagram explaining the Franz-Keldysh effect. In (a), with no electric field, a photon of $h\nu \geq E_g$ is required to promote an electron from the valence band into the conduction band. In (b), with the presence of an electric field, a photon of energy $h\nu' < E_g$ is sufficient to excite an electron so that by tunneling in real space through the distance d it may be excited into the conduction band.

from the valence band to the conduction band requires a photon of energy $h\nu$. This, then, is the fundamental absorption edge of the semiconductor. When a very high electric field is applied, a photon of energy $h\nu'$ with $h\nu' < h\nu$ may promote an electron to an energy such that it can tunnel (in real space) into the conduction band. The barrier that this electron must tunnel through is triangular in shape and is of hieght $E_q - h\nu'$ and width d as given in the figure. Thus, the fundamental absorption edge is shifted to lower energies (longer wavelengths). In practice, electric fields of as much as 100kV cm^{-1} are required to observe this effect. When one applies external dc biases on the order of 2 Volts to the heterostructure can one expect such large electric fields to develop in the GaAs?

When a dc bias is applied to a heterostructure, then in general one expects that the voltage is dropped across the AlAs barrier since it is the highest resistance in the structure. To drop a voltage across this layer one must have a certain amount of negative charge on one side of the barrier and a certain amount of positive charge on the other side of the barrier. The negative charge is provided by the accumulation of electrons on one side of the barrier. The positive charge, however, is provided by uncovering positive donors in the depleted GaAs on the other side of the barrier. One could make the assumption that the electrons can accumulate in an infinitely thin sheet of negative charge since they are free to move. The positive donors, however, are fixed in space and so the depletion region has a finite extent.

Suppose one has an AlAs layer 100 Å thick sandwiched between GaAs layers doped at 5×10^{17} cm^{-3}. To drop, say, 0.5 V across this AlAs layer one must have a surface charge density, σ, given by

$$\sigma = \frac{V\epsilon\epsilon_0}{d}$$

on either side of the layer, where d is the thickness of the AlAs layer. For the above parameters $\sigma = 2.8 \times 10^{12}$ cm^{-2} and the depletion region would have to

be $x = 560$ Å wide. The voltage drop across this depletion region can then be calculated from

$$\frac{d^2V}{dx^2} = \frac{\rho}{\epsilon\epsilon_0}.$$

This yields a total voltage drop across the depletion region of 1.4 V. The resulting electric field in this depletion region is over $200kV$ cm-1. In performing this calculation the assumption was made that the electrons can form an infinitely thin sheet of charge. This is not quite true; the electrons will in fact also be spread out spatially and some voltage will be dropped there. Further, the depletion edge is not abrupt but is also spread out. However, this does show that the electric field is large enough to allow one to observe the Franz-Keldysh effect. Another important point brought out here is that a large fraction of the applied dc voltage (in this case, the greater part) is dropped in the GaAs cladding layers and not across the barrier. As the doping in the GaAs is decreased, the external bias increased, or the thickness of the AlAs layer decreased, a greater fraction of the voltage is dropped in the GaAs cladding region.

3.8 OPTICAL DETECTORS

An application to which the photoresponse in these structures may be put is that of a photodetector. A photodetector is a device which can detect light through some electronic process. In general, a photodetector consists of three elements. The first is the generation of charge carriers in the device by the incident light. The second is the transport of these optically generated carriers to provide a current of voltage, and the third is an external circuit to detect this signal. Clearly, in the structures and experiments described above one has all three elements.

There are two broad categories of photodetectors. One is devices known as photodiodes (or photvoltaics). These are devices with a depletion region with a high electric field which serves to separate photogenerated electron-hole pairs

and thus produce a signal. The second class of photodetectors is photoconductors. In these devices the light creates carriers which increase the conductivity of the material. It is probably most correct to regard the structure discussed above as a photoconductor. The model proposed above for the mechanism that produces the photocurrent does not include a depletion region.

To discuss how good a photodetector is one uses quantities known as figures of merit. A figure of merit is a quantity which basically is a measure of the signal-to-noise ratio of the detector and which also may or may not include in it the area of the detector, the band width of the external circuit, etc. There are a few common figures of merit.[20] The responsivity is the ratio of the r.m.s. value of the signal voltage or current to the r.m.s. value of the incident radiation power. The noise equivalent irradiance is the minimum radiant flux density necessary to produce a signal-to-noise ratio of one when the noise is normalized to unit bandwidth. The noise equivalent power is the minimum radiant flux necessary to produce a signal-to-noise ratio of one for unit bandwidth. D^* is the detectivity normalized to unit area and unit bandwidth where the detectivity is the signal-to-noise ratio produced by unit incident radiant flux. D^* is a figure of merit which allows one to compare photodetectors of different areas. One can try to make a very rough estimate of D^* for these structures. To do this one can first write down an expression for the r.m.s. signal current

$$i_s = q\eta \frac{P_{opt}}{\sqrt{2}h\nu}.$$

η is the quantum efficiency which is the number of electron-hole pairs generated per incident photon. This was measured for Sample 4 at room temperature to be about 10^{-2}. One next has to take into account the various sources of noise which may exist in the device.

Noise is the random fluctuations in the measured voltage or current that result from the statistical nature of the processes that produce the signal. A major source of noise in optical detectors is generation recombination noise. This

noise arises from the fact that photons create carriers randomly and that these carriers relax randomly. Thus, the current contributed by one electron lasting τ seconds may be given by

$$i(t) = \begin{cases} \frac{ev}{d}, & \text{if } 0 \leq t \leq \tau, \\ 0, & \text{otherwise.} \end{cases}$$

The Fourier transform of this is the current as a function of frequency, so one averages that over τ to obtain the root mean square noise current associated with this source of noise[21]

$$i_g = (4q^2\eta \frac{P_{opt}}{h\nu}\Delta\nu)^{\frac{1}{2}} \frac{\tau_0}{\tau_d}.$$

In the above expression τ_0 is the average scattering time for a carrier, τ_d is the average time it takes a carrier to travel the distance d in order to produce a signal, and $\Delta\nu$ is the band width of the external circuit. From the mobility of electrons in GaAs at room temperature one can estimate τ_0 to be about 3×10^{-13} sec. A very crude estimate of τ_d can be made as follows. In the structures discussed above an electron is excited typically by a photon of energy 1.5 eV. Now if at each scattering event this electron loses the energy of one optical phonon (about 35 meV), then it would take nearly thirty scattering events to bring the electron down in energy sufficiently so that it could no longer get past the AlAs barrier. In that time the electron could travel a distance on the order of 1 μm so that τ_d is about 4×10^{-13} sec.

Another source of noise, though not the predominant source, is Johnson noise. Johnson noise is the noise that results from the random thermal motion of the charge carriers. The root mean-square noise current associated with this source of noise is given by[21]

$$i_j = (\frac{4kT\Delta\nu}{R})^{\frac{1}{2}}$$

where R is the resistance of the device.

By using these various estimates one arrives at a D^* of about 10^5 at the peak wavelength of about 8700 Å. This value is seven orders of magnitude less than a typical D^* for GaAs photodiodes operating at this wavelength and temperature. However, not only is this estimate a very crude one; no attempt has been made, in this work, in growing the structures above to optimize them as photodetectors. If one were to pursue this aspect of these structures, one would have to design the structure so as to produce an optimum signal-to-noise ratio, and one would would then have to make a serious effort to measure this signal-to-noise ratio. Further, to determine the usefulness of a detector one would also have to take into account other aspects of the device such as its response time.

3.9 SUMMARY

In this chapter results of photoresponse experiments on GaAs/AlAs heterostructures have been discussed. These experiments were employed to study the basic photovoltaic properties of structures consisting of a thin (50 Å to 250 Å) layer of AlAs sandwiched between thick (a few microns) layers of degenerately doped GaAs. It was shown that the photovoltage results from the flow of electrons from the front (the illuminated side) of the AlAs barrier to the back of the AlAs barrier. It was argued that it was the electrons which were excited by free-carrier absorption to an energy greater than the offset between the conduction band of the GaAs and the AlAs which could flow past this barrier. The driving force for the flow of the electrons was the difference in the concentration of optically excited electrons on either side of the AlAs layer and this concentration difference was a result of the light intensity difference on either side of the barrier. It was shown that for decreasing temperature or increasing doping in the GaAs region the peak in the photovoltage spectrum shifted to shorter wavelengths. This shift in the photovoltage spectrum was shown to be a result of the change in the optical properties of the GaAs. The dependence of the

photovoltage spectrum on the thickness of the top layer of GaAs was presented. It was shown that for a thinner top layer of GaAs one could enhance the short wavelength response of the structure. The change in the resistive and capacitive impedance of the structures as a function of wavelength was discussed and explained. The change in the resistive impedance caused a change in the phase of the photovoltage signal. This change of phase had to be overcome in order that the measurement would not give spurious results.

Results were then presented showing the effect of applying an external dc bias to the samples on the photovoltage spectrum. It was shown that the effect of this external bias was to increase the magnitude of the photovoltage signal. In some cases samples which showed no photovoltage signal without an applied external bias displayed a substantial signal when bias was applied. The application of a dc bias causes an accumulation of charge on one side of the barrier and a depletion of charge on the other side of the barrier. Now if there is a difference in the light intensity on either side of the AlAs barrier, there is an enhanced difference in the concentration of optically excited electrons on either side of the barrier and there is thus an enhanced photovoltage signal. It was also shown that for large biases (2 V) the photovoltage spectrum is shifted to slightly longer wavelengths and is enhanced at long wavelengths. This was explained as being due to the Franz-Keldysh effect, that is, the effective band gap narrowing due to the high electric fields that can exist in the depleted GaAs region. At longer wavelengths band-to-band absorption dominates in the depleted GaAs while free-carrier absorption dominates in the other GaAs region.

Finally, the application of these structures and their use as photodetectors was discussed. While it appears that as they stand now these structures would not be very efficient photodetectors, this situation may be improved. The ability to alter the peak wavelength at which they respond may be of some use in this application.

3.10 CONCLUSIONS

This chapter has shown how photoresponse experiments can be used to investigate some of the optical properties of heterostructures. The role of various parameters (doping, temperature, etc.) may be understood through the use of these techniques. Further experiments of this type on heterostructures of varying configurations may lead to observations of fundamental processes such as electron interference effects or may allow one to measure quantities of interest such as band offsets. The role of deep levels or interface states could also be probed using photoresponse experiments of this type. However, it is only through the step-by-step progression from these simple to more complicated structures that one can develop an understanding of the role of the optical and electrical properties of these structures.

REFERENCES

1. R. Chin, N. Holonyak, G. E. Stillman, J. Y. Tang, and K. Hess, *Electron. Lett.* **16**, 467 (1980).

2. F. C. Capasso, W. T. Tsang, and G. Williams, *IEEE Trans. on Electron. Devices* **ED30**, 381 (1981).

3. A. R. Bonnefoi, R. T. Collins, T. C. McGill, and R. D. Burnham , *Appl. Phys. Lett.* **46**, 285 (1985).

4. R. T. Collins, J. Lambe, T. C. McGill, and R. D. Burnham , *Appl. Phys. Lett.* **44**, 532 (1984).

5. H. M. Manasevit, *Appl. Phys. Lett.* **12**, 156 (1968).

6. R. D. Dupuis and P. D. Dapkus, *Appl. Phys. Lett.* **31**, 466 (1977).

7. C. R. Lewis, W. T. Dietze, and M. J. Ludowise, *Electron. Lett.* **18**, 569 (1982).

8. R. D. Burnham, W. Streifer, D. R. Scifres, C. Lindstrom, T. L. Paoli, and N. Holonyak, *Electron. Lett.* **18**, 1095 (1985).

9. G. Y. Robinson, *Solid St. Electron.* **18**, 331 (1975).

10. G. Y. Robinson and N. L. Jarvis, *Appl. Phys. Lett.* **10**, 507 (1972).

11. H. C. Casey, Jr., D. D. Sell, and K. W. Wecht, *J. Appl. Phys.* **46**, 250 (1975).

12. H. C. Casey, Jr. and M. B. Panish, *Heterostructure Lasers* (Academic Press, New York), 1978.

13. H. C. Casey, Jr. and Frank Stern, *J. Appl. Phys.* **47**, 631 (1976).

14. C. Mailhiot, D. L. Smith, and T. C. McGill, *J. Vac. Sci. Technol.* **B1(3)**, 637 (1983).

15. R. C. Miller, D. A. Kleinman, and A. C. Gossard, *Phys. Rev.* **B29**, 7085 (1984).

16. H. C. Casey, Jr. and M. B. Panish, *Heterostructure Lasers* (Academic Press, New York), 1978.

17. N. W. Ashcroft and N. D. Mermin, *Solid State Physics* (Holt, Reinhart and Winston, New York), 1976.

18. E. Hecht and A. Zajac, *Optics* (Addison-Wesley, Reading), 1974.

19. J. I. Pankove, *Optical Processes in Semiconductors* (Dover Publications Inc., New York), 1975.

20. R. K. Willardson and A. C. Beer, Eds. *Semiconductors and Semimetals, Vol. 12, Infrared Detectors II* (Academic Press, New York), 1977.

21. A. Yariv *Introduction to Optical Electronics* (Holt, Rinehart and Winston, New York), 1976.

APPENDIX I

Phase Considerations

It was observed that in some cases the lock-in amplifier would cease to be in phase with the photovoltage signal as the photovoltage spectrum was scanned. This would mean that the fraction of the photovoltage that was actually measured by the lock-in amplifier would change as one scanned the spectrum. The spectrum then would vary artificially as a function of wavelength. This problem can be explained as follows. In Figure A.1(a) is presented a circuit diagram which represents the measuring system. The sample is shown as a current source, i_s, and resistor and capacitor in parallel, r_s, c_s. Also included is a capacitor C, which represents the stray capacitances in the measuring system. The stray capacitance is the sum of the input capacitance of the lock-in amplifier, the capacitance associated with the coaxial cable used, etc. The lock-in amplifier is represented by the resistor R_l. The voltage which is measured across the lock-in amplifier is given by

$$V_m = i_s Z = i_s |Z| e^{i\phi}$$

where Z is the total complex impedance of the system and ϕ is the phase associated with this complex impedance. Now, since all the circuit elements shown in Figure A.1(a) are in parallel the total complex impedance is given by

$$\frac{R_{||}}{1 + i\omega R_{||}(c_s + C)} = \frac{R_{||}}{1 + [\omega R_{||}(c_s + C)]^2}[1 - i\omega R_{||}(c_s + C)]$$

where $R_{||} = \frac{R_l r_s}{R_l + r_s}$ and $\frac{\omega}{2\pi}$ is the frequency of the measurement. Then one has that

$$\phi = \tan^{-1}(-\omega R_{||}(c_s + C)).$$

As discussed earlier, when the sample is illuminated at a wavelength that produces a photovoltage, this photovoltage biases the sample. The sample resistance is lower at this bias and hence this changes the phase angle ϕ. As this phase angle changes, the lock-in amplifier is no longer in phase with the photovoltage and hence does not measure the full value of the photovoltage. This change

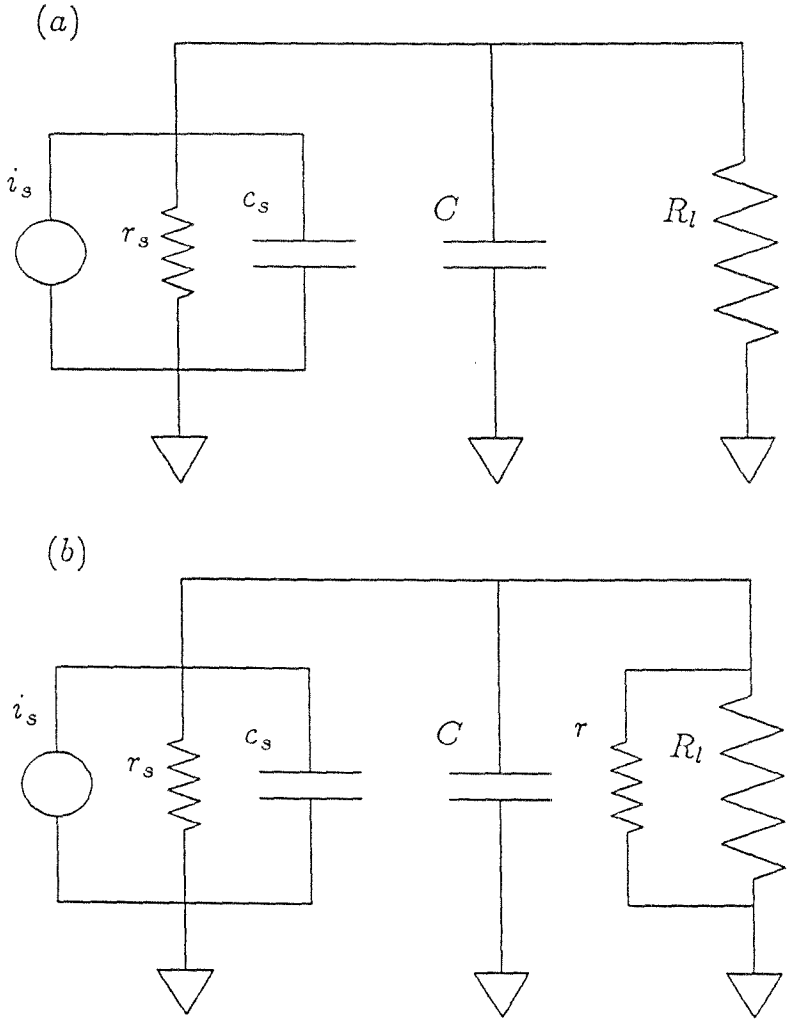

Figure A.1: In (a) the circuit used to measure the photovoltage is presented. The sample is represented by the current source, i_s, resistance r_s, and capacitance c_s all in parallel. C is any stray capacitance and R_l is the lock-in amplifier. In (b) is shown the small resistor, r, which can eliminate the phase drift which was observed.

in the phase was most dramatic when measurements were made on samples with the greatest zero-bias impedance. In these samples the change in the sample impedance was the greatest when a photovoltage was developed across the sample.

In order to correct this problem a small resistor r was introduced as shown in Figure A.1(b). If $r \ll R_l, r_s$ then $R_{||} \sim r$. Since this resistance does not change as the measurement is made, neither does the phase angle. The introduction of this resistance does decrease the magnitude of the measured signal. One could compensate for this somewhat by amplifying the signal more and collecting data over a longer period of time.